

Tool steels and their additive manufacturing for fabrication and repair via PBF and DED processes: techniques, challenges, and applications

Original

Tool steels and their additive manufacturing for fabrication and repair via PBF and DED processes: techniques, challenges, and applications / Kenevisi, Mohammad Saleh; Gobber, Federico Simone; Fino, Paolo; Lombardi, Mariangela; Bondioli, Federica; Biamino, Sara; Ugues, Daniele. - In: MATERIALS & DESIGN. - ISSN 0264-1275. - 258:(2025). [10.1016/j.matdes.2025.114639]

Availability:

This version is available at: 11583/3002754 since: 2025-09-03T11:51:48Z

Publisher:

Elsevier

Published

DOI:10.1016/j.matdes.2025.114639

Terms of use:

This article is made available under terms and conditions as specified in the corresponding bibliographic description in the repository

Publisher copyright

(Article begins on next page)



Tool steels and their additive manufacturing for fabrication and repair via PBF and DED processes: techniques, challenges, and applications

Mohammad Saleh Kenevisi^{a,b,*}, Federico Simone Gobber^a, Paolo Fino^{a,b,c},
Mariangela Lombardi^{a,b,c}, Federica Bondioli^{a,b,c}, Sara Biamino^{a,b,c}, Daniele Ugues^{a,b,c}

^a Department of Applied Science and Technology (DISAT), Politecnico di Torino, Italy

^b Integrated Additive Manufacturing iAM@PoliT Center, Politecnico di Torino, Italy

^c National Interuniversity Consortium of Materials Science and Technology (INSTM), Italy

ARTICLE INFO

Keywords:

Additive manufacturing
Tool steels
Repair processes
Directed energy deposition
Powder bed fusion

ABSTRACT

This review investigates the state of additive manufacturing (AM) of tool steels with a clear, process-aware scope that centers on two dominant AM routes, direct energy deposition (DED) and powder bed fusion (PBF), and their respective roles in fabrication and repair. First, different categories of tool steels and their common damage mechanisms are introduced. The distinct process mechanisms, material responses, and performance metrics characteristic of each technique is outlined, and then how microstructure, residual stresses, porosity, and carbide chemistry emerge under DED and PBF processes for different type of alloys are explained. By contrasting process-specific challenges, such as larger melt pools and intrinsic tempering in DED versus rapid solidification and fine microstructures in PBF, with end-use requirements, e.g. wear resistance, toughness, and reliability in tooling, we reveal common optimization approaches, preheating strategies, parameter windows, post-processing heat treatments, and robust non-destructive evaluation are delineated in this work. The review also assesses the material compatibility, challenges, and economic and environmental considerations of AM tooling, and highlights gaps where cross-process insights can accelerate industrial adoption and discussed future trends. The aim is to provide a coherent, process-aware framework that connects AM physics, materials science, and engineering performance for tool steels.

1. Introduction

Tool steels represent one of the most strategic material classes in manufacturing, with a global market valued at approximately USD 5.5 billion in 2023 and projected to reach USD 7.3 billion by 2030, driven primarily by the growing demand for high-performance dies and molds in automotive, aerospace, energy and consumer industries [1,2]. More than 70 % of forming and molding tools currently used in high-volume manufacturing are fabricated from hot-work or cold-work tool steels due to their exceptional hardness, wear resistance and thermal stability [3]. According to recent industrial surveys, the average service life of such tooling has decreased by 15–20 % over the last decade due to more demanding process conditions, underscoring the importance of both efficient fabrication and effective repair/remanufacturing strategies [4].

At the same time, additive manufacturing (AM) has seen a rapid and steady uptake in the tooling sector, with the market share of metal AM in tooling applications increasing from ~ 4 % in 2015 to > 11 % in 2023

[2,5]. Within this, powder bed fusion (PBF) and directed energy deposition (DED) account for more than 90 % of tool-steel related AM applications. AM enables not only the fabrication of complex tooling components, such as mold inserts with conformal cooling channels, but also the local repair of worn areas, reducing material waste by up to 80 % and shortening lead times by 30–50 % compared to conventional machining routes [5,6]. These developments clearly demonstrate the industrial relevance and growing adoption of AM for high-strength tool-steel alloys in various areas, such as manufacturing specialized tools with built-in cooling channels, developing structural components optimized for lightweight performance, etc., underscoring AM's potential to enhance production capabilities in the steel sector [7–9].

Therefore, this review paper aims to provide a comprehensive overview of AM technologies applied to fabricate new components and to repair damaged tool steel parts. It will explore the fundamentals of tool steels, damage mechanisms, the principles of AM, the challenges and opportunities associated with this approach, and the potential

* Corresponding author at: Department of Applied Science and Technology (DISAT), Politecnico di Torino, Italy.

E-mail address: saleh.kenevisi@polito.it (M.S. Kenevisi).

<https://doi.org/10.1016/j.matdes.2025.114639>

Received 11 July 2025; Received in revised form 18 August 2025; Accepted 26 August 2025

Available online 27 August 2025

0264-1275/© 2025 Published by Elsevier Ltd. This is an open access article under the CC BY-NC-ND license (<http://creativecommons.org/licenses/by-nc-nd/4.0/>).

future directions in this field.

2. Tool steels and common failures

Tool steels are a family of alloy steels specifically designed for applications that require high hardness, wear resistance, and toughness [10]. They are typically classified based on their composition, which includes carbon, alloying elements, and special additives. The performance of tool steel parts is significantly influenced by their microstructure and mechanical properties [11]. The microstructure, which is determined by the composition and heat treatment, affects the hardness, toughness, and wear resistance. Common types of tool steels include cold-work tool steels, hot-work steels, and high-speed steels [3].

2.1. Cold work tool steels

Cold work tool steels are optimized for applications where operating temperatures remain below 200 °C [12]. Their hardness and wear resistance, along with the ability to maintain these properties at lower temperatures, make them particularly useful in applications involving cutting, stamping, and forming. These steels play a critical role in industries such as automotive, aerospace, construction, and metal fabrication. These materials provide excellent performance in tools that operate under mechanical stress and abrasion at room temperature [11,13]. Due to their extreme hardness, toughness, and wear resistance, cold work tool steels significantly extend the life of tooling equipment, thereby reducing costs and downtime in industrial operations.

Cold work tool steels are alloyed with elements such as carbon, chromium, molybdenum, vanadium, etc. to enhance their performance. The composition varies based on the grade and specific requirements of the tool. Generally, carbon is the primary element controlling hardness. Higher carbon content increases hardness but reduces toughness [14]. Chromium enhances corrosion resistance, wear resistance, and hardenability [15]. The toughness and heat resistance of the alloy can be increased by molybdenum, and vanadium refines the grain structure, which improves wear resistance and toughness [16,17]. Moreover, the addition of other alloying elements such as tungsten and niobium can further increase the hardenability of the steel [18]. O1, D2, and K340 are some cold work steels used in various applications.

These alloys are used in a variety of manufacturing processes, especially where tools need to retain hardness and wear resistance at room temperatures. They are used in the production of stamping dies that shape sheet metal into desired forms. Their hardness and wear resistance make them ideal for repetitive stamping operations. Shearing and cutting tools, such as blades and punches, are often made from cold work tool steels to ensure sharpness, wear resistance, and the ability to withstand high-impact forces [19–21]. Moreover, punches used in forming and cutting are frequently made from alloys such as O1, A2, or D2 to provide a balance between toughness and wear resistance, critical for tools subjected to repeated impact [11,22]. Last but not least, cold work tool steels are also employed in cold forging dies, where metal is shaped under high pressure without the application of heat. The die materials must withstand these high pressures while maintaining structural integrity [13].

The performance of cold work tool steels depends heavily on their heat treatment process, which consists of hardening (typically through quenching) and tempering. Heat treatment optimizes the mechanical properties, achieving the desired balance between hardness, toughness, and dimensional stability.

2.2. Hot work tool steels

Hot work tool steels are a class of alloy steels designed for use in high-temperature applications such as forging, die casting, extrusion, and hot shearing. These steels must retain their hardness, toughness, and resistance to thermal fatigue under extreme conditions [23]. Hot work

tool steels are essential to produce components subjected to high temperatures during manufacturing processes. These steels must maintain their hardness and wear resistance at temperatures typically above 200 °C, along with sufficient toughness to resist cracking or deformation [24]. The ability of these steels to maintain their properties under repeated heating and cooling cycles makes them indispensable in industries like automotive, aerospace, and metal forming.

There are two main categories of hot work steels according to the American Iron and Steel Institute (AISI) that are chromium, tungsten, molybdenum (H series) and tungsten (W series) groups of alloys. Like cold work grades, carbon provides hardness and wear resistance but must be controlled to avoid excessive brittleness. The alloying elements, particularly chromium, tungsten, and molybdenum, contribute to the material's ability to resist softening during high-temperature operations. Additionally, cobalt additions can enhance strength at high temperatures [25,26].

Besides the ability to retain the hardness at elevated temperatures and having good thermal fatigue and wear resistance, hot work tool steels must possess good thermal conductivity to dissipate heat away from the working surface [27]. Effective heat dissipation reduces the risk of thermal softening and deformation, improving the tool's overall lifespan.

Hot work tool steels are utilized across a range of high-temperature manufacturing processes. They are extensively used in die casting dies and molds, where molten metals like aluminum, magnesium, and zinc are injected under pressure [28]. These dies must endure extreme temperatures, thermal cycling, and abrasive wear from molten metal. In hot forging, metal is shaped through compressive forces at elevated temperatures. Forging dies made from hot work tool steels must resist wear, cracking, and deformation under these severe conditions [29]. Steels like H11 and H13 are commonly used in forging dies due to their balance of hardness and toughness. Moreover, extrusion dies for hot metals and hot shearing blades are typically made from hot work tool steels [30].

Same as cold work steels, the heat treatment process for hot work tool steels involves hardening and tempering to achieve the desired balance of hardness and toughness. In addition to heat treatment, surface treatments, such as nitriding and hard coating, can be applied to enhance wear and oxidation resistance [31].

2.3. High-Speed tool steels

High-speed tool steels (HSS) are a class of alloy steels designed to maintain hardness and wear resistance at high temperatures, making them indispensable for cutting, drilling, and machining applications. These steels exhibit exceptional performance under high cutting speeds, providing superior hot hardness, toughness, and wear resistance [32]. They are widely used in various industries, including automotive, aerospace, and general manufacturing, where efficiency and tool life at high cutting speeds and temperatures are paramount [33].

HSS are typically divided into two broad categories based on their alloy content. T-series, which are tungsten-based, contain high levels of W, providing excellent hardness retention at high temperatures. A common example is T1, a widely used grade of tungsten-based HSS [34]. The other group is M-series, molybdenum-based, that contain Mo as a primary alloying element, often in combination with W [35]. The M2 grade is the most commonly used one of this group. There are also some other alloying elements, such as Cr, V, and Co, added to achieve the desired combination of hardness, wear resistance, toughness, and hot hardness required for high-speed applications [3].

One of the defining properties of HSS is their ability to maintain high hardness and wear resistance at high temperatures, even at elevated temperatures [36]. In addition to hardness and wear resistance, HSS should possess adequate toughness to resist chipping and cracking during operation and resist softening at high temperatures [37,38]. HSSs are used extensively in applications requiring high cutting speeds and

prolonged tool life under challenging conditions, such as cutting tools, saw blades, punches and dies, end mills, and high-performance drills [11,39,40].

Heat treatment plays a crucial role in optimizing the properties of high-speed tool steels. The process typically involves hardening followed by multiple tempering cycles. Like other grades of tool steels, to further enhance the wear resistance and performance of HSS tools, various surface treatments can be applied [41].

2.4. Damage mechanisms

Abrasive wear is one of the most common wear mechanisms in cold work, hot work, and high-speed applications [42,43]. It occurs when hard particles slide across the steel surface, leading to material loss. High-carbon, high-chromium steels, containing other carbide forming elements, are specifically designed to resist this type of wear due to the presence of hard carbides in the microstructure [44]. However, adhesive wear, or galling, occurs when two surfaces slide against each other and material is transferred from one surface to another. This type of wear is often seen in cutting tools and can lead to a reduction in tool life if not properly managed through lubrication or material selection [45,46].

Fatigue wear occurs due to repeated cyclic loading, causing micro-cracks to form and propagate over time [47,48]. Cold work tool steels must be carefully selected and heat-treated to minimize the occurrence of fatigue-related failures, particularly in punching and shearing applications. Though cold work tool steels are designed for low-temperature applications, they may still experience thermal fatigue due to frictional heating during operation. This type of fatigue leads to crack formation, which can compromise the integrity of the tool. But this wear mechanism is one of the most common failure mechanisms in hot work tool steels [49]. This occurs due to the repeated expansion and contraction of the tool material caused by rapid temperature changes during heating and cooling cycles, leading to the formation of micro-cracks, which can eventually cause failure.

HSS and hot work tool steels are exposed to oxidizing environments due to the high operating temperatures, which can lead to surface degradation [49,50]. Additionally, thermal softening is another phenomenon which should be considered as well for high-speed and hot work applications [51,52].

3. AM for part fabrication

Traditional manufacturing of tool steels involves casting, forging, and machining processes. While these methods produce high-quality components, they present several limitations. As an example, complex geometries and internal features, such as conformal cooling channels in molds, are challenging or impossible to produce with conventional methods [53]. Additionally, subtractive manufacturing processes like machining result in significant material removal and waste, especially for components with intricate designs [54]. With these processes, the tooling development process is time-consuming, delaying product development cycles, and there exist some repair challenges. Damaged or worn tool steel components are often replaced rather than repaired due to difficulties in matching material properties and achieving metallurgical bonding [55]. These limitations drive the need for innovative manufacturing approaches that can overcome these challenges.

Metal AM processes relevant to tool-steel applications fall into two main families: Powder Bed Fusion (PBF) and Directed Energy Deposition (DED). The distinction arises from the form of the feedstock and the heat source used to melt the material. PBF processes, such as laser powder bed fusion (LPBF) and electron-beam powder bed fusion (EB-PBF), employ a high-energy beam to selectively melt a bed of gas-atomized metal powder that is spread in thin layers. In contrast, DED processes, including laser-based DED (DED-LB) and arc-based DED, feed either powder or wire directly into a melt pool generated by a laser, electron beam, or electric arc.

These processes by having benefits including design freedom, material efficiency, customization, and repair capabilities have shown promise in processing tool steels for both fabrication and repair applications. Table 1 and Table 2 compare the benefits and limitations of the main additive manufacturing techniques used for tool steels processing, and provide some benefits and challenges in processing tool steels by AM. Commonly, DED is suitable for larger, simpler applications, while LPBF is more appropriate for producing smaller, complex geometries, often requiring support structures during fabrication.

However, AM processing of tool materials faces several difficulties, including poor processability, crack formation, and anisotropic microstructure caused by localized heat effects [7,60]. Other challenges arise from lack-of-fusion defects, porosity, and evaporation of alloying elements [7,61]. Moreover, the process is limited in terms of geometrical accuracy and surface quality, often necessitating further subtractive post-processing [62]. These factors hinder the widespread fabrication of tool materials through AM. Despite all these challenges, in recent years, significant progress has been made and different tool steels like H13 (hot work) [63–65], D2 (cold work) [66–68], and M2 (high-speed) [69–71] have been studied and successfully processed by AM. Different components of tool steels, such as impeller, drill, and injection molding dies, that are made by AM processes are depicted in Fig. 1.

During metal solidification in AM, grain growth typically follows the heat flow direction, which is often perpendicular to the boundary of melt pool. However, this behavior slightly differs between LPBF and DED due to variations in melt pool geometry. In LPBF, the generally high scanning speed creates a long, shallow melt pool (Fig. 2a and b), resulting in nearly vertical grain growth, closely aligned with the building direction. Conversely, the larger power and lower scanning speed in DED produce a deeper melt pool, leading to grain growth that deviates from the building direction due to the curvature of the solid/liquid interface (Fig. 2c). Additionally, during the early stages of solidification, competitive grain growth occurs, where grains with orientations aligned with the heat flow direction are more likely to survive. This results in differing grain orientations between components fabricated by LPBF and DED.

Generally, the microstructure of the additive manufactured tool steel parts is composed of martensite, retained austenite, and carbides [63,69,76–78]. Different micro-sized and nano-sized carbides, including MC, M₂C, M₂₃C₆, and M₇C₃, are formed in the tool steels processed by AM techniques. However, the type of the carbides formed is highly affected by processing parameters and the process itself. Fig. 3 is a schematic overview of the microstructures of tool steels, in general, that are processed by conventional and AM techniques.

Retained austenite is commonly observed in AMed tool steels, such as cold work [79], hot work [80,81], and HSS [70,71], due to their high carbon and alloying element content. As a result, the hardness of AM parts in the as-printed state is often lower than that of conventionally

Table 1
Comparing two different fusion-based AM processes [56–59].

Feature	DED	LPBF
Feedstock material	Powder/wire	Powder
Heat source	Laser / arc / electron beam	Laser / electron beam
Material consumption	Low	Medium
Part complexity	Low	High
Part size (build volume)	Big	Medium
Build rate	High (0.5 – 1 kg/h)	Low (0.1 – 0.2 kg/h)
Dimensional accuracy/resolution	Medium	High
Applications in tooling	Repairs, large molds, near-net-shape repair and fabrication	Complex inserts, lattices, conformal cooling
Cost	\$\$	\$\$\$

Table 2
Benefits and challenges of processing tool steels by AM processes in different aspects.

Aspect	Benefits	Limits
Technical	<ul style="list-style-type: none"> – Capability of fabricating complex-shaped components. – Possibility of fabricating parts with enhanced mechanical performance. 	<ul style="list-style-type: none"> – Not all materials are suitable for processing. – Internal defects such as porosity and cracks. – Inhomogeneous microstructure. – Need for post-processing treatments. – Limitation in build volume.
Environmental	<ul style="list-style-type: none"> – Reducing material waste – Reducing greenhouse gas emissions – Possibility to recycle damaged parts to use as feedstock material. 	<ul style="list-style-type: none"> – Relatively energy-intensive
Economical	<ul style="list-style-type: none"> – Assemblies can be fabricated at once, reducing the assembly time. – Possibility to repair parts and reuse them 	<ul style="list-style-type: none"> – Initial cost is relatively high.

manufactured counterparts. For example, a D2 cold work tool steel part produced by DED exhibited a hardness of only 43–45 HRC, compared to 58 HRC typically seen in wrought D2 steel [82,83].

Regarding maraging steels, AM of these steels, especially the 18Ni-300 alloy, has become increasingly studied [84–86], with fewer instances reported for other alloys like 18Ni-250 [87] and 14Ni-200 [88]. It has been shown in the literature that LPBF and DED are capable of producing high-density, crack-free maraging steel parts with densities above 99 % [85,89,90]. These AM-produced steels have a significantly different microstructure compared to traditional wrought maraging

steels, characterized by a cellular or dendritic solidification structure (Fig. 4a). In LPBF, cell sizes range between 0.3–2 μm [85,86,90], while in DED, they are around 5 μm [91–93]. Martensitic transformation occurs within these solidification cells, resulting in martensite laths often surrounded by retained austenite along cell boundaries, caused by the microsegregation of alloying elements during solidification (Fig. 4b). This retained austenite, enriched in nickel, is stabilized at room temperature, leading to an austenite content of 6–11 %, depending on the AM process parameters [92,94,95].

Post-processing heat treatments are normally required for AM tool steel components. Tempering typically reduces the hardness and strength of as-quenched tool steels due to dislocation recovery and the

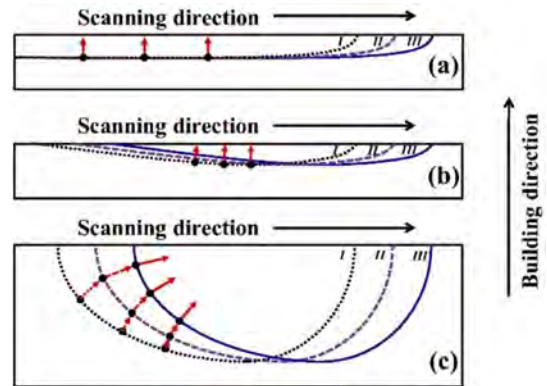


Fig. 2. Schematic representation of the melting pool and growth direction in a, b) vertical and nearly vertical grain growth in PBF and c) typical inclined grain orientation in DED [75] (Reproduced with permission from © Elsevier, all rights reserved).

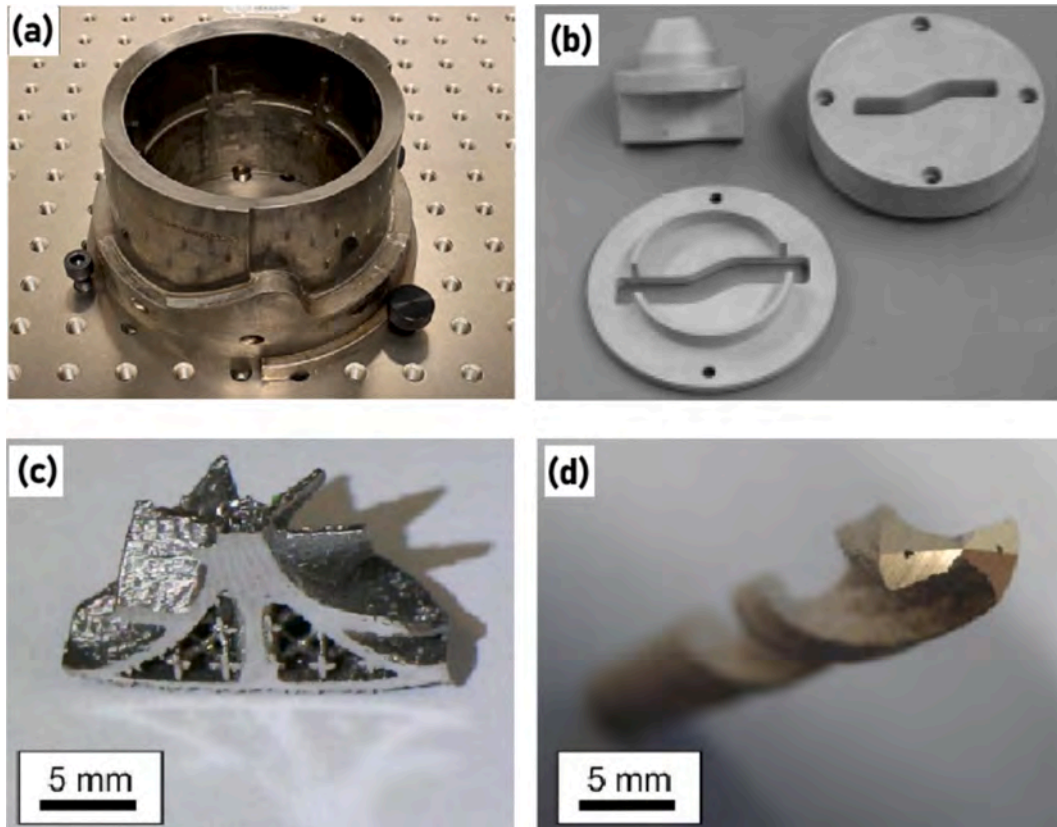


Fig. 1. Components of tool steels made by AM processes: a) cooling insert, b) die set of sheet metal stamping, c) impeller with lattice structure, and d) drill having integrated cooling channels [72–74] (Reproduced with permission from © Elsevier, all rights reserved).

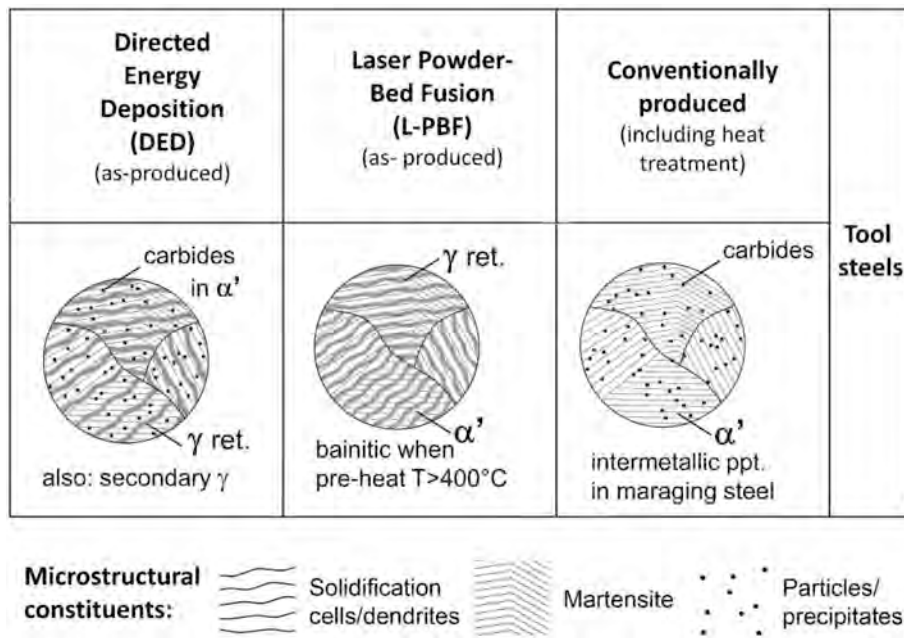


Fig. 3. Schematic representation of the microstructure of tool steels resulted by different processes [60] (Reproduced with permission from © Elsevier, all rights reserved).

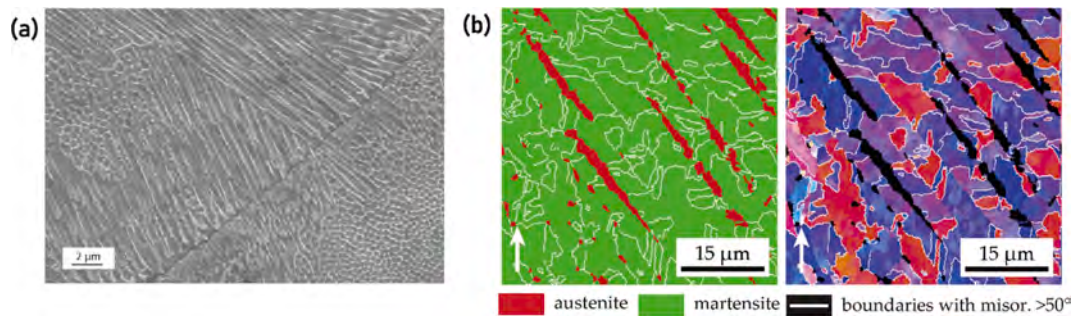


Fig. 4. A) SEM micrograph of the solidification structure (cellular/dendritic) of 18Ni300 alloy fabricated by LPBF[95] and b) EBSD analysis of the same material processed by DED [92] (Reproduced under CC BY licence).

relaxation of distorted supersaturated martensite. However, direct tempering of tool steel samples at temperatures between 300–550 °C has demonstrated a significant secondary hardening effect, similar to that observed in wrought materials [65,96]. This phenomenon is primarily attributed to the decomposition of retained austenite and formation of secondary carbides. Additionally, solid solution strengthening from the dissolution of elements such as vanadium, molybdenum, or silicon within the cellular structure contributes to this hardening behavior. Conversely, tempering at temperatures exceeding 600 °C leads to the decomposition of martensite into ferrite and spheroidized nano-sized carbides, resulting in decreased hardness but improved toughness [65,96].

Post-processing heat treatment of maraging steels has also been shown to have significant effect on the microstructure of these alloys. The cellular microstructure of the as-built samples is reported to be preserved during aging at typical temperatures lower than 530 °C [86,90]. However, at higher aging temperatures significant austenite reversion occurs at solute rich cell boundaries [97]. Following solutioning treatment, where the microstructure becomes fully austenitic, the cellular microstructure is completely eliminated, and upon quenching, the material forms a coarser, fully martensitic structure, which results in reduced hardness and strength compared to its as-produced state [86,95,98].

Due to different factors, such as the presence of some internal defects and inhomogeneity of the microstructure in some cases, the mechanical properties of the AM parts can vary significantly from one research to another. Table 3 summarizes the mechanical properties of some parts made by DED and PBF processes.

Tool steels produced by AM exhibit pronounced variability in key mechanical properties, such as hardness, yield and ultimate tensile strength, and elongation, even when the same alloy composition is used. This spread reflects a mix of process- and material-driven factors. First, the thermal histories associated with different AM approaches diverge. PBF processes typically yield very small melting pools with extremely rapid cooling, whereas DED processes involve larger melt pools and repeated remelting events. Second, choices around energy density and scanning strategies influence porosity, microsegregation, and microstructure evolution. Third, feedstock quality matters. Particle size distribution, morphology, dissolved gases, and how spent powder is reused can all shift outcomes. Fourth, build orientation and component geometry shape thermal gradients and anisotropy within the part. Fifth, post-processing steps, for example hot isostatic pressing, tempering, solution treatments, and aging, are not applied uniformly across studies, introducing additional variability. Collectively, these factors help explain why, for instance, reported H13 hardness spans roughly 450 to 700 HV depending on processing and heat treatment, while higher-carbon alloys

Table 3

Mechanical properties of tool steel parts made by AM processes (AB: as-built, HT: heat treated, DT: direct tempering, QT: quench tempering, HIP: hot isostatic pressing).

Material	Process	Condition	Hardness	Yield Strength	Tensile Strength (MPa)	Elongation (%)	Ref.
H13	DED	AB	630 ± 6 HV	–	–	–	[99]
		HT	535 ± 5 HV	–	–	–	
H13	LPBF	AB	585 ± 6	1342 ± 67	1704 ± 30	1.55 ± 0.05	[77]
H13	DED	AB	581 – 700 HV	–	–	–	[100]
		HT	495 – 500 HV	–	–	–	
	Ultrasound Assisted DED	AB	640 – 649 HV	–	–	–	
		HT	450 – 460 HV	–	–	–	
Modified H13	LPBF	DT	527 HV	1568 – 1610	1736 – 1745	9.9 – 10.3	[101]
		QT	–	1465 – 1514	1688 – 1735	10.4 – 11.0	
		AB	56 HRC	–	1808	2.0	[102]
W360	LPBF	HT	55 – 57 HRC	1500 – 1670	1970 – 2010	6.6 – 8.1	[103]
W360	DED	AB	633 – 662 HV	–	–	–	[104]
		HT	634 HV	–	–	–	
X45CrMnMoNiSi6-3-3-1-1	LPBF	AB	542 HV	–	–	–	[105]
		HT	≈ 700 HV	–	–	–	
	DED	AB	623 HV	–	–	–	
		HT	≈ 700 HV	–	–	–	
Cr-Mo-V HSS	DED	HT	750 – 850 HV	–	926	≈ 0.7	[106]
Cr-Mo-V-W HSS	DED	AB	800 – 850 HV	–	1017	≈ 0.65	
M4	DED	AB	818 HV	–	–	–	[107]
HWS	DED	AB	644 HV	–	–	–	
		HT	737 HV	–	–	–	
		AB	57 HRC	–	≈1280	0.5	[71]
M2	LPBF	AB	789 ± 10 HV	–	–	–	[108]
		HT	783 ± 2 HV	–	–	–	
		HIP + HT	803 ± 4 HV	–	–	–	
D2	DED	AB	33 – 47 HRC	–	–	–	[66]
		HT	42 – 60 HRC	–	–	–	
D2	DED	AB	470 ± 10 HV	–	–	–	[99]
		HT	745 ± 3 HV	–	–	–	
D2	DED	AB	347 – 433 HV	1922 ± 77 (compression test)	–	–	[68]
		HT	551 – 698 HV	2217 ± 53 (compression test)	–	–	
D2	DED	AB	486.2 ± 10.6 HV	784 ± 7	1054 ± 2	2.4 ± 0.2	[67]
		HT	720.1 ± 10.0 HV	1480 ± 43	1794 ± 69	0.8 ± 0.1	
Nb-alloyed tool steel	DED	AB	729 ± 19	–	–	–	[109]
		HT	828 ± 8	–	–	–	
ASP2030	LPBF	AB	654 – 817 HV	–	–	–	[110]
Cr-Si-Mn tool steel	DED	AB	550 – 720 HV	–	1809 – 1828	8.4 – 8.9	[111]
Cr-Mo-Si-Mn tool steel	DED	AB	500 – 720 HV	–	1653 – 1670	6.9 – 7.3	[111]

such as D2 and M2 can show even larger spreads in ductility due to crack susceptibility, carbide distribution, and internal stresses. For example, one of the key reasons for the high brittleness can be the high levels of residual stresses in the AM parts, which is reported to be as high as 1400 MPa in some parts [80,112,113]. To enable meaningful cross-study comparisons, explicit reporting of parameters, standardized test coupons, and consistent powder handling are essential.

In the following sections the major AM processes that are used for processing and fabricating tool steels are presented and discussed in more detail.

3.1. Directed energy deposition (DED)

DED is an AM process where focused thermal energy (e.g., laser, electron beam, or plasma arc) melts materials as they are deposited. It is particularly suitable for repair applications due to its ability to add material to existing components. It provides precise control over the deposition area, minimal heat-affected zones (HAZ), and the ability to repair complex geometries [75,114,115].

The nozzle travel speed, laser power, and feeding rate are some of the main processing parameters of DED. As a general trend, increasing the travel speed decreases both the width and the height of the single-track depositions, while an increase in the laser powder and feeding rate results in wider depositions with higher heights [116]. This occurs because increasing the laser power and feeding rate and decreasing the scanning speed supply more energy and material to the substrate, causing more

powder to melt. Consequently, this leads to the formation of larger melt pools. In a recent study, Kenevisi et al. [117] demonstrated the viability of processing K340 cold-work tool steel using DED through a structured design-of-experiments approach. It identified clear process–geometry relationships, with laser power chiefly controlling track width and surface quality while nozzle travel speed governs track height, and shows that higher energy density can worsen surface roughness yet reduce certain defects.

Research shows that nearly fully dense and crack-free tool steel samples can be fabricated using DED with optimized parameters [118–120]. Generally, the fabricated components of tool steels consist of four different regions: fully annealed and HAZ regions corresponding to the substrate, and untampered and tempered regions corresponding to the deposition [117,121–123]. The microstructure of the deposited material generally consists of martensite, carbides, and retained austenite. In a recent study, M4 and HWS steels were also deposited on a D2 substrate, and the volume fraction of retained austenite was 22 % in M4 deposited material, which was more than 60 % in the HWS alloy [107]. Regarding its structure, the DED tool steel components mostly possess a fine dendritic or cellular structure, which is generally a bit coarser compared to the LPBF built counterpart. This is due to the lower cooling rates of the DED process ($\sim 10^4 \text{ K s}^{-1}$) in comparison to that of the LPBF ($\sim 10^6 \text{ K s}^{-1}$) [75]. Additionally, the formation of eutectic carbides network and chains of interdendritic carbides are widely reported in processed cold work tool steels where there are higher amounts of carbide forming elements [69,70,124]. This feature, Fig. 5,

has been clearly shown in a research study by Bartels et al. [125].

The applied thermal cycles during AM processes can modify the microstructure of the material. It is shown that in H13 thin wall deposited by DED, the retained austenite in the microstructure tends to slightly increase in the first deposited layer as the next layers are deposited [126], as shown in Fig. 6. Pinkerton and Li [121] also reported that by moving along the building direction the volume fraction of retained austenite tends to increase.

However, as more layers are deposited, the amplitude of the thermal cycles gradually diminishes. The initial layer undergoes remelting up to the addition of the third layer, resulting in complete decomposition of the formed martensite and the formation of new martensite during subsequent cooling. From layer 3 to layer 7, only partial re-austenitization occurs. Beyond this point, the maximum temperature in the first layer is insufficient to trigger the martensite-to-austenite transformation.

The effect of this intrinsic heat treatment is not only on the austenite to martensite transformation. It is shown that by moving from the bottom to the top of the samples along the building direction, the grain structure can change from dendritic to cellular, due to the higher cooling rate and thermal gradient at the top [96].

Additionally, the aforementioned thermal processes involved in DED result in a microstructure that differs significantly from that of traditionally wrought materials. This variation influences the approach to post-processing heat treatments to achieve the desired mechanical properties for tools. Junker et al. [127] explored the impact of additive manufacturing on the performance of hot work tool steel X37CrMoV5-1 and examined how the material responds to various heat treatments, as the results are depicted in Fig. 7a. Their findings show that in-situ hardening occurs during additive manufacturing due to the rapid cooling from the molten to the solid state, which creates a fine-grained martensitic and dendritic structure, Fig. 7b, contributing to relatively high hardness. However, this also leads to low yield strength. When subjected to conventional heat treatment involving austenitizing, quenching, and triple tempering, the mechanical properties of the additively manufactured material were found to be comparable to those of conventionally produced material. Interestingly, it was demonstrated that tempering the additively manufactured material without prior austenitizing preserves the fine-grained structure (Fig. 7c). This heat treatment approach has the potential to enhance the mechanical properties beyond those of conventionally produced materials, offering a promising opportunity to extend the tool's lifespan.

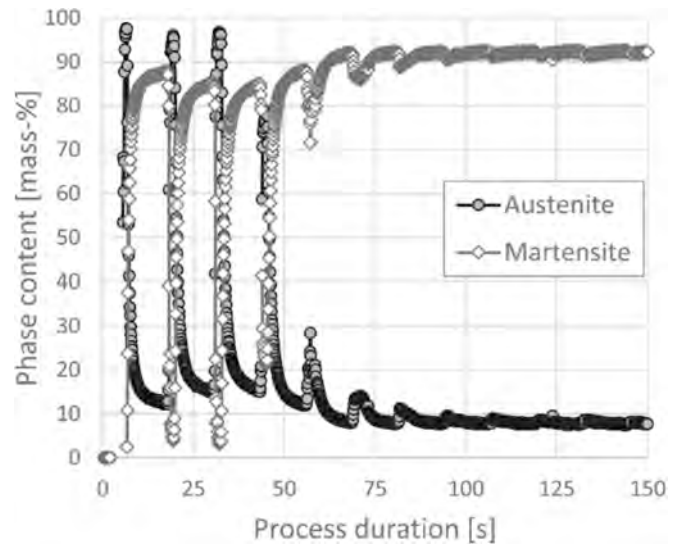


Fig. 6. Time-resolved evolution of phase content in the first deposited year of H13 [126] (Reproduced with permission from © Elsevier, all rights reserved).

In DED, typical cooling rates fall within roughly 10^3 to 10^5 K/s across common process windows, which are generally lower than those seen in powder bed fusion (PBF). This contrast tends to produce coarser dendritic or columnar grains and larger melt pools in DED builds. As a result, the as-built hardness of DED parts is frequently lower than that of LPBF components, unless particular strategies to accelerate cooling or post-build heat treatments are employed. Nevertheless, with careful control of track overlap and energy input, DED can reach near-full densification. Reported hardness profiles for DED-hardened steels often reveal clear gradients along the build height, with bottom regions being tens to a few hundred HV harder or softer than the top regions in multilayer deposits, a consequence of the intrinsic tempering effect caused by successive layers. To optimize outcomes, researchers have used finite-element and melt-pool simulations to relate laser power and travel speed to predicted melt-pool dimensions and to the orders of magnitude difference in cooling rate. These models support parameter tuning aimed at achieving a more uniform microstructure and reduced hardness variability.

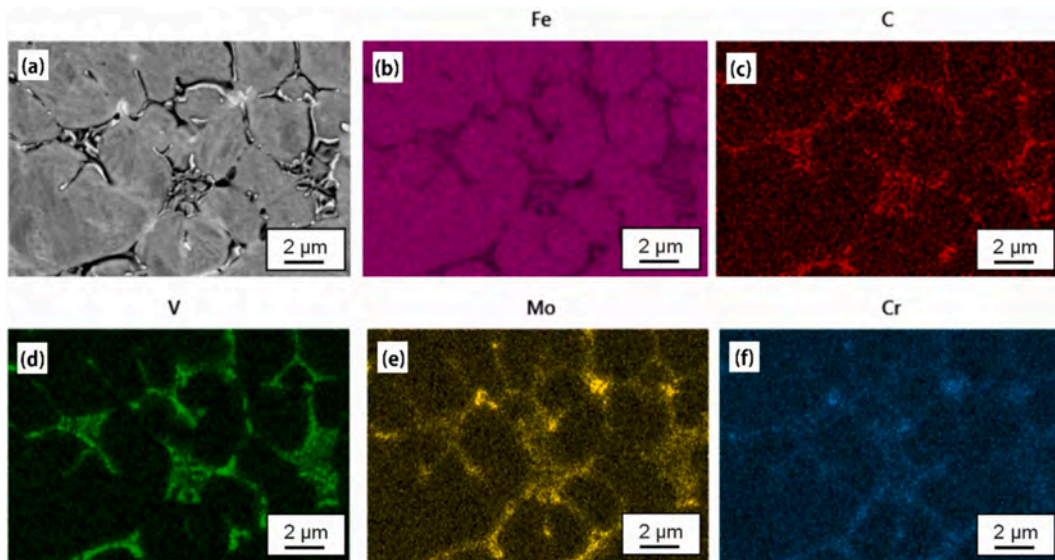


Fig. 5. a) Sem micrograph of the cross-section microstructure of Vanadis 4 Extra sample showing the interdendritic carbides and b-f) the EDS mapping of a corresponding region [125] (Reproduced under CC BY licence).

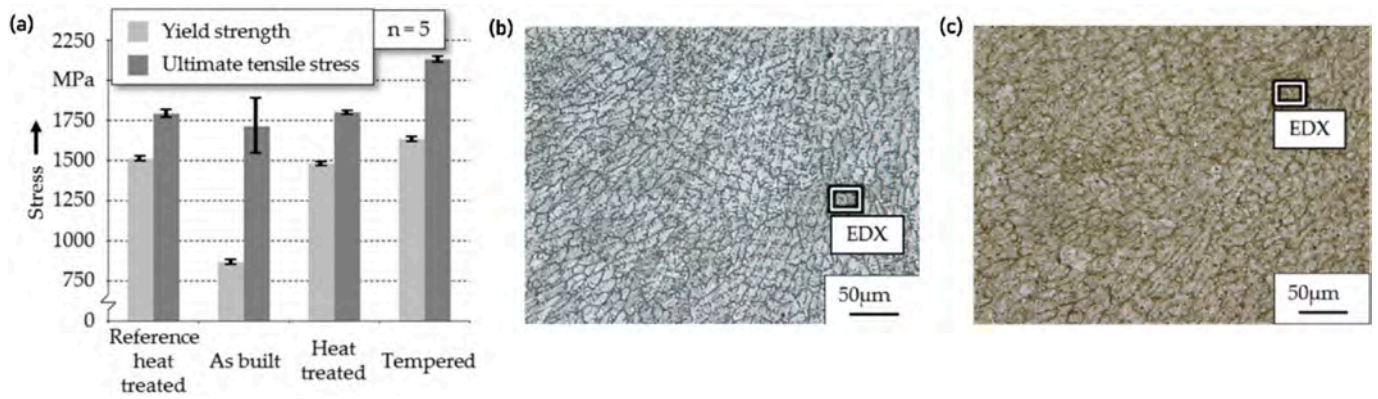


Fig. 7. a) Tensile test results of the tool steel at different conditions and the microstructure of DED material in b) as-built and c) tempered conditions [127] (Reproduced under CC BY licence).

As stated, hardness of the material is also affected by this intrinsic heat treatment, as tempered martensite is generally reported in the as-built tool steel components [121]. As a result, the last deposited layers exhibit higher hardness values than those of the first deposited layers, as shown in Fig. 8.

The successive layer deposition in AM techniques can result in a formation of a heat affected zone (HAZ) in the substrate material close to the interface region. The microstructural evolution in this region can negatively affect the hardness of the material. However, as depicted in Fig. 9, it is shown that by applying a post-processing HT the reduction in the hardness value can be controlled [107].

Generally, higher laser powers, which provide higher energy densities, can result in lower hardness values due to the microstructure coarsening occurred as a result of decreased cooling rates [82]. In a study, Junker et al. [128] investigated the correlation between hardness variation and specimen deformation during upsetting testing. Hardness measurements revealed that areas with lower hardness, which correlate with lower yield strength, are more easily deformed, resulting in an irregular specimen shape (Fig. 10). Specimens produced with higher laser power demonstrated a more homogeneous hardness distribution and more optimal shape after testing, confirming that laser power plays a key role in mechanical uniformity and deformation behavior.

A finite element model of the DED process was developed by Jardin et al. [129] to predict the thermal history during the manufacturing of high-speed steel AISI M4 samples. By integrating the simulations within an optimization loop, variable laser power functions were identified to

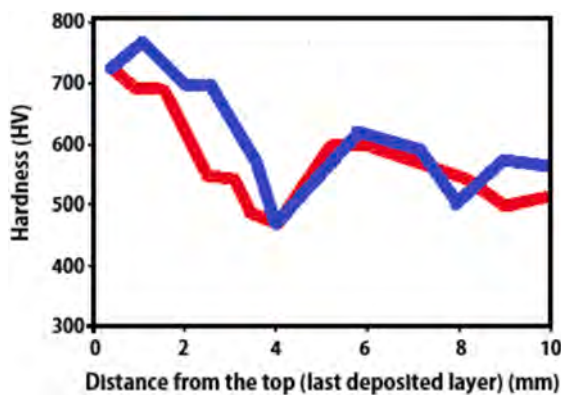


Fig. 8. Variation in the microhardness values along the building direction of DED-fabricated H13 alloy (at gas flow rates of 0.22 g/sec (red) and 0.34 g/sec (blue)). Relatively higher hardness values in the last deposited layers is observed, where the intrinsic heat treatment is negligible [121]. (For interpretation of the references to colour in this figure legend, the reader is referred to the web version of this article.)

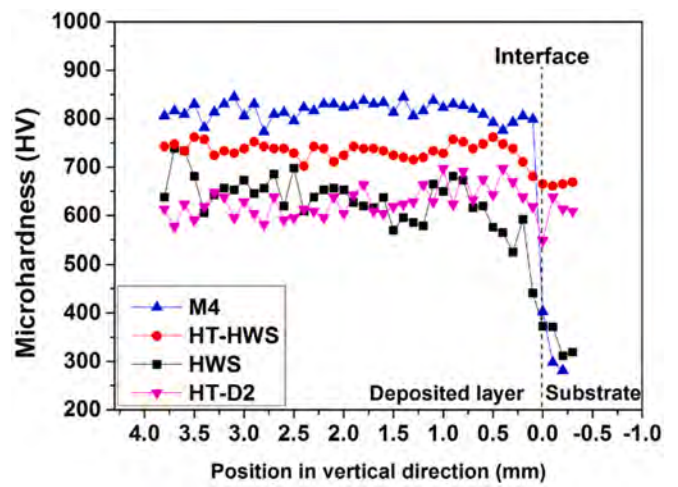


Fig. 9. Hardness values of different deposited materials from the deposited region to the substrate in as-built and heat treated conditions [107] (Reproduced under CC BY licence).

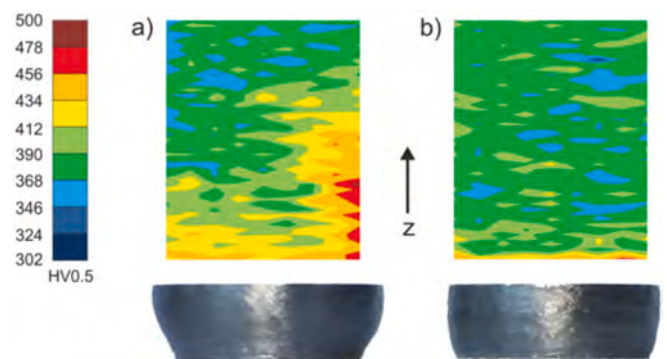


Fig. 10. Microhardness distribution and the geometry (after performing upsetting test) of 18Ni300 alloy processed by DED using a) 700 W and b) 800 W of laser beam [128] (Reproduced under CC BY licence).

achieve a constant melt pool size, aiming for a homogeneous microstructure throughout the deposited layers. Their results demonstrated that while optimized laser power functions improved microhardness homogeneity compared to a constant laser power (Fig. 11a), complete microstructural uniformity was not fully achieved as indicated by nanohardness mapping (Fig. 11b).

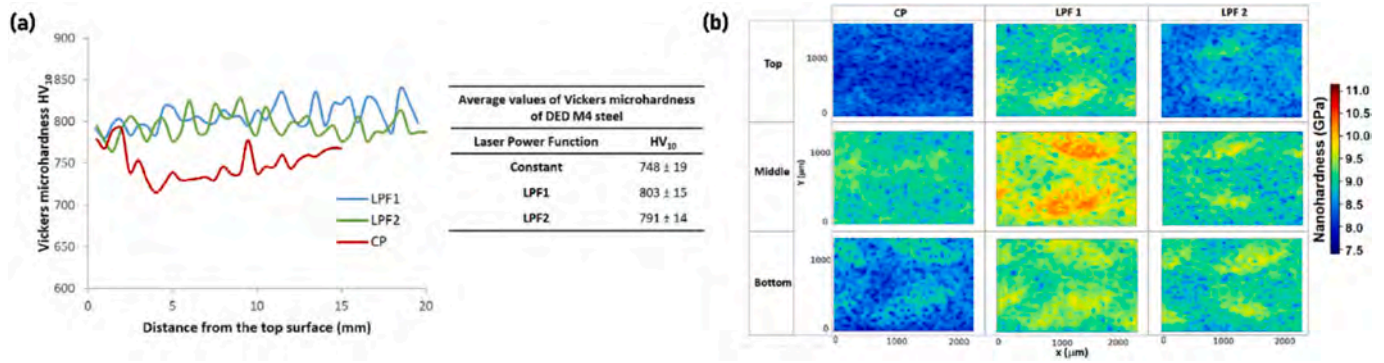


Fig. 11. Variations of the a) microhardness and b) nanohardness values along the building direction of M4 sample fabricated by DED process by using three different laser power functions: constant power value (CP) and two time-dependant power functions (LPF1 and LPF2) identified by FE simulation [129] (Reproduced with permission from © Elsevier, all rights reserved).

Post-processing heat treatment can modify the microstructure, such as austenite to martensite transformation, carbide formation, etc. [107]. By performing a heat treatment (Fig. 12) the cellular dendritic structure of the M4 deposition disappeared and a network of eutectic chromium-rich carbides was formed [107].

Tawfik Abdollah Omar [66] also investigated the effects of post-processing heat treatment on the microstructure of DED processed D2 samples, and reported that following heat treatment, fine secondary carbides precipitated within the matrix (Fig. 13b). This precipitation is attributed to the substitutional diffusion of chromium into the matrix, which leads to the formation of chromium carbides at the expense of cementite. In contrast, the DED sample in its as-processed state showed that chromium carbides were predominantly formed at the grain boundaries (Fig. 13a).

Moreover, the upper half of the as-processed sample (Fig. 13c) exhibited a dendritic morphology characterized by columnar grains. After applying a two-step tempering process—initially at 400 °C and subsequently at 500 °C—this dendritic morphology transformed into a markedly more equiaxed microstructure (Fig. 13d). This change is due to homogenization during heat treatment, where new, equiaxed, strain-free grains replace the deformed dendritic grains. This replacement occurs because of the differences in stored strain energy between the deformed and undeformed material. New nuclei formed in the interdendritic regions grow through diffusion, consuming the original dendritic structure.

Post-processing heat treatment is generally beneficial in making the microstructure more homogeneous. However, in some cases, it has shown to have some detrimental effects. In HWS deposited alloy, heat treatment was observed to have a negative effect on the impact properties of the material [107]. The martensite fraction increased significantly after heat treatment. Additionally, in the interface region, quenching and tempering caused the precipitation of primary rod-like carbides along the grain boundaries. This microstructural change led to a reduction in toughness.

The mechanical properties of components made by DED are reported

to be mostly comparable to those found in quenched and tempered wrought materials, indicating that the DED-produced material is naturally tempered during the production process [113,118,122,131]. However, in applications like hot stamping, understanding the thermal properties of materials is crucial for the effective functioning of the produced components. Therefore, it is important to assess the material's effective thermal diffusivity of an AM component, which can be different from the conventionally made material. In a research study, Arrizubieta et al. [132] experimentally measured the thermal diffusivity of DED-deposited AISI H13 using flash and lock-in thermography techniques. Due to the rapid cooling rates typical of the additive manufacturing process and the resulting grain refinement, the effective thermal diffusivity of the laser-deposited H13 was found to be roughly 15 % lower than the standard value for cast H13. This lower thermal diffusivity resulted in an increased number of cycles that are needed to lower the temperature of the blank to specific temperatures, as shown in Fig. 14. However, despite the unidirectional characteristics of the process, the thermal diffusivity of the laser-deposited material exhibited isotropic behavior.

As already mentioned, the majority of the research studies are on hot work and cold work tool steels. Nonetheless, there are also some works on maraging alloys. Maraging steels, such as M300 are commonly processed using AM processes for different industrial applications. Compared to hot work tool steels, maraging steels have higher nickel content and lower carbon content, reducing their susceptibility to cracking during AM [133]. Research has shown that AM processed M300 exhibits comparable strength to conventional M300 when proper heat treatments are applied [134,135]. This steel often undergoes solutioning and aging treatments to enhance strength, though these treatments typically do not improve ductility [136]. However, Liu et al. [137] demonstrated a novel solutioning-isothermal heat treatment, where DED-fabricated samples were cooled to 320 °C after solutioning at 870 °C. A holding time of 80 min resulted in a 33 % increase in ductility.

In the DED-fabricated maraging steel some precipitations of the

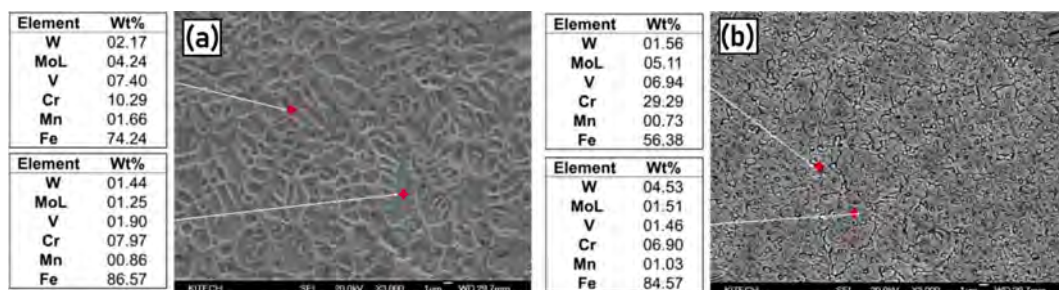


Fig. 12. SEM micrographs and EDS analysis of HWS deposition in a) as-built and b) heat treated conditions [107] (Reproduced under CC BY licence).

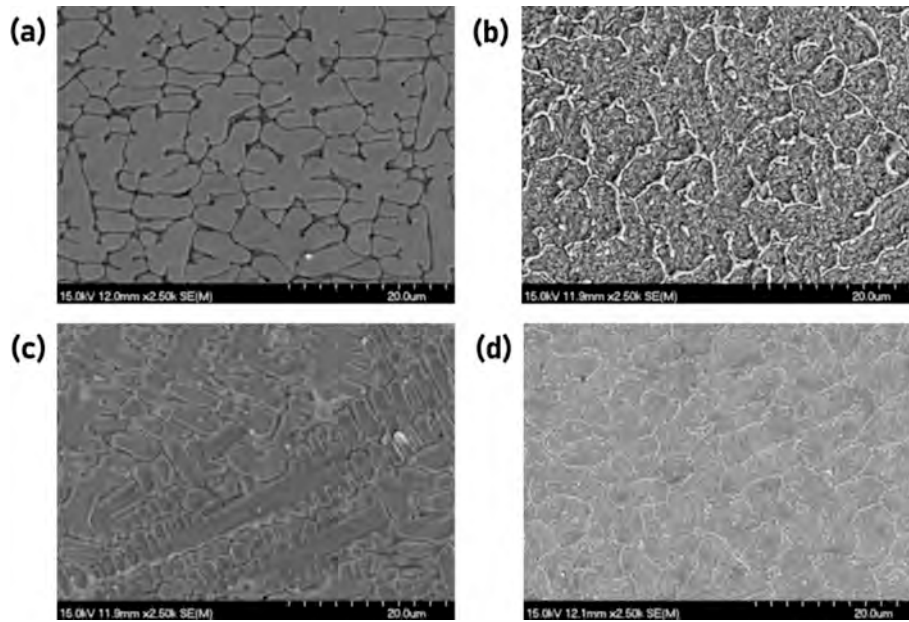


Fig. 13. SEM micrographs of DED fabricated D2 samples at a,b) lower half and c,d) upper half of the sample in a,c) as-built and b,d) heat treated conditions [130] (Reproduced with permission from © Elsevier, all rights reserved).

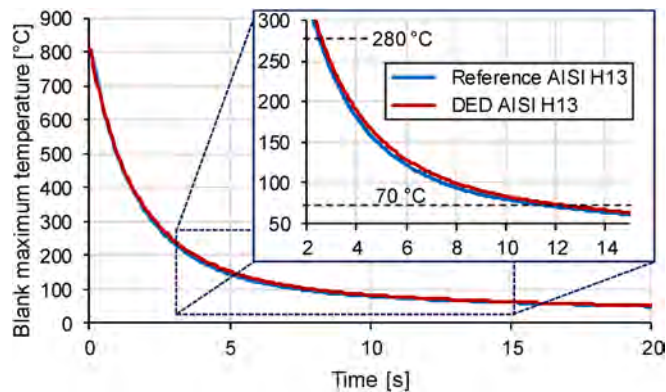


Fig. 14. Temperature changes in the blank made by casting and AM during the hot stamping process [132] (Reproduced under CC BY licence).

hardening phases in the as-built condition have been observed [92], as illustrated in Fig. 15, which was not found in the LPBF manufactured parts [90,138]. This demonstrates that the cooling rate in LPBF process is higher than that of DED, which can suppress the precipitation of

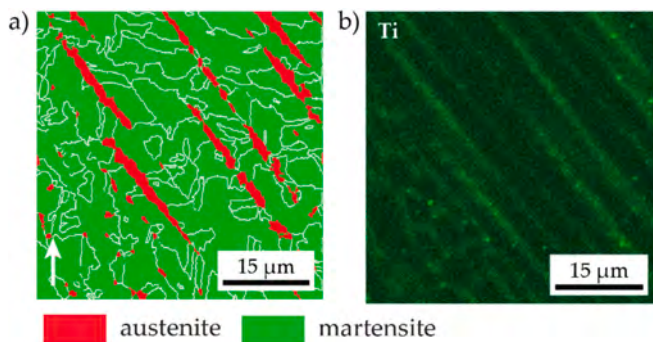


Fig. 15. High magnification EBSD result of the as-built M300 material processed by DED: a) phase distribution and b) EDS mapping showing the presence of nano-sized Ti-rich particles [92] (Reproduced under CC BY licence).

carbides.

3.2. Powder bed fusion (PBF)

Unlike DED, in PBF processes the energy source selectively scans and melts a thin layer of powder material which is layered on a platform. In these processes, laser or electron beam can be used for fabrication. Both laser powder bed fusion (LPBF) and electron beam powder bed fusion (EB-PBF) techniques can produce fine, dendritic microstructures. LPBF results in high amounts of retained austenite and martensitic phases [6]. In contrast, EB-PBF allows for better control over the microstructure due to slower cooling rates, forming more stable bainitic structures in some tool steels [139].

Like DED, tool steels produced using PBF methods generally exhibit high hardness due to fine cellular substructures formed during rapid cooling. For instance, LPBF fabricated steels like H13 can reach hardness levels of 600 HV [6]. In a carbon-martensitic tool steel, post-processing like supersolidus liquid phase heat-treatment (SLPHT) and hot isostatic pressing (HIP) can further enhance hardness and homogenize the microstructure by dissolving carbides, with SLPHT-treated specimens achieving hardness around 650 HV [140].

In this section, the characteristics of tool steels processes by both LPBF and EB-PBF techniques are discussed in detail.

3.2.1. Laser beam powder bed fusion (LPBF)

LPBF is a powder bed fusion process where a high-energy laser selectively melts metallic powders to build parts layer by layer. It allows for high-resolution fabrication of complex geometries with good mechanical properties. High precision, excellent surface finish, and ability to process fine features are some of the advantages of this technique, while imposing some levels of residual stresses, cracking due to high cooling rates, and limitations in part size are challenges of processing materials with LPBF.

Different types of tool steels, such as hot work [80,141], cold work [142], and high speed [108] steels have been processed by LPBF. H13 is one of the tool steel alloys that has been extensively processed by AM. The microstructure of the fabricated parts is generally characterized by a mix of martensitic matrix, bainite, retained austenite, and carbides precipitates [63,143–146], with an ultrafine dendritic or cellular structure, as shown in Fig. 16. Like H13, the microstructure of H11 also

consists of a fine cellular or dendritic structure and retained austenite at the intercellular or interdendritic regions, with some M23C6 carbides in the tempered condition [127,141,147–149].

Typical LPBF cooling rates and their microstructural consequences are reported in the order of 10^5 – 10^6 K·s⁻¹ for typical scan speeds and melt-pool geometries, producing ultrafine cellular/dendritic structures with sub-micron cell sizes and high dislocation density. These processing conditions produce high as-built hardness and strength but also elevated residual stresses and retained austenite fractions unless controlled by preheating or post heat treatment. As an example, high-power LPBF studies of H13 report as-built yield strengths exceeding ~ 1500 MPa and UTS approaching ~ 2200 MPa in optimized conditions (with high energy density and post-treatment), but ductility remains limited in some reports (~1–5 %) without tempering. These quantitative process–structure–property relationships emphasize the role of energy density, scan strategy, and bed/substrate preheat in defining both strength and toughness [2,151].

The presence of retained austenite is commonly reported in the microstructure of the as-fabricated components. The retained austenite in a H13 alloy processed by LPBF was reported to be around 11.5 % [152]. As EBSD phase map in Fig. 17 shows, due to the microsegregation of the alloying elements, such as C, Cr, V, etc., at inter-cellular or interdendritic regions, which are mostly austenite stabilizer, the austenite remains stable at room temperature when the material is rapidly cooled from high temperatures. This microsegregation is also reported in other works [153].

Additionally, alternative explanations for austenite formation, such as carbon diffusion or mixed solidification mechanisms, have also been

proposed [155,156]. Similar to DED, the subsequent deposition of material in LPBF process introduces an intrinsic heat treatment, which can modify the microstructure. Apart from austenite transformation, a partial decomposition of martensite to ferrite and cementite has been observed by Yan et al. [80].

As discussed, the repeated thermal cycles inherent to layer-by-layer AM can act as an intrinsic heat treatment. These different thermal histories result in different degrees of in-situ tempering and precipitation. For example, high-carbon steels may stabilize retained austenite that requires post-HT to obtain target hardness levels. Experimental measurements of thermal diffusivity in laser-deposited H13 report reductions (e.g., ~10–20 % lower effective thermal diffusivity compared to cast H13 in some studies), which has practical consequences for cycle times in hot-stamping and for heat dissipation in service [132].

In the as-build state, hardness values for H13 steel range from 570HV to 680HV, and up to 728 HV in heat treated condition, which are comparable to or exceed those found in quenched and hardened wrought H13, indicating the material's fully martensitic microstructure [76,156–158]. However, yield and tensile strengths in the as-built state are often significantly lower than those of conventionally manufactured and heat-treated H13 [146,155,159]. This is likely due to the extreme brittleness of the material. After tempering, the mechanical properties of the material become similar to those of wrought and heat-treated H13. Nevertheless, elongation to fracture remains lower in both conditions, probably because of residual defects from the manufacturing process, such as porosity [155,157,159–162].

Lack of fusion and porosity are some common internal defects that can lead to lower values of relative densities and negatively affect the

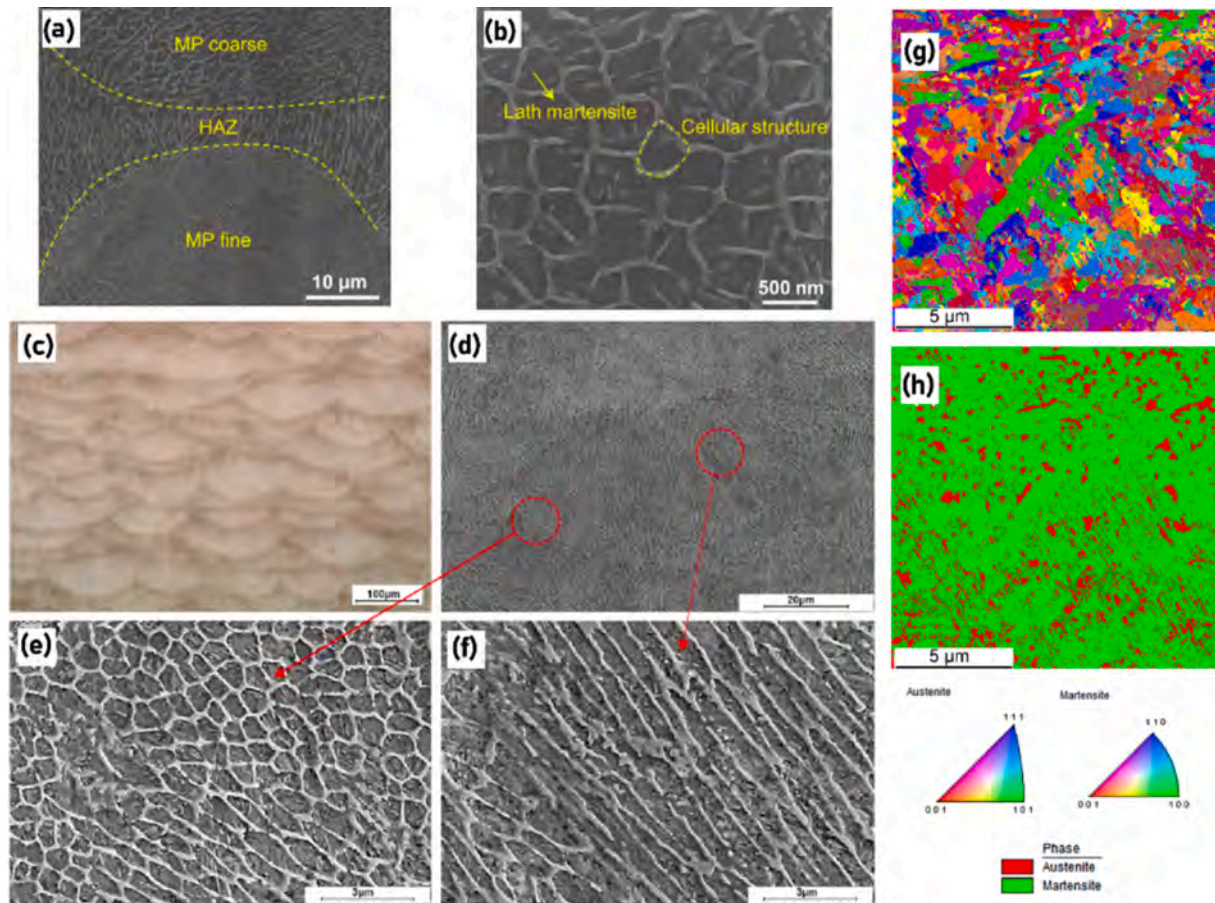


Fig. 16. SEM micrographs of as-built H13 processed by LPBF showing a,b) melt pool structure and cellular structure and lath martensite in the equiaxed zone [150], c-f) Micrographs illustrating both the equiaxed and columnar dendrites, and g,h) EBSD grain orientation map and distribution of phases showing the martensitic microstructure with the presence of retained austenite [63] (Reproduced under CC BY licence).

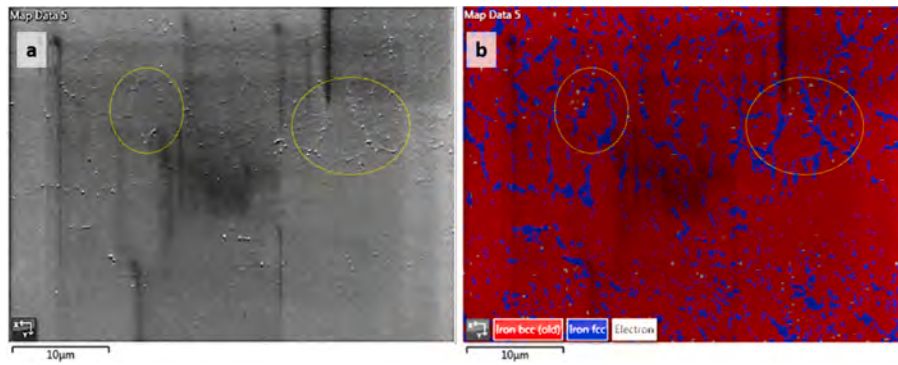


Fig. 17. SEM micrograph and corresponding EBSD layered image showing retained austenite at the cellular boundaries in as-built condition [154] (Reproduced with permission from © Elsevier, all rights reserved).

mechanical properties of the material. Narvan et al. [63] studied the effect of energy density and platform preheating on the densification of the LPBF-processed H13 alloy (Fig. 18). Their results showed that at low volumetric energy densities, e.g. 50 J/mm³) significant amounts of internal defects are formed, resulted in low values of relative density. Additionally, it was observed that samples with higher relative densities were achieved when the platform was preheated to 200 °C, compared to the condition when no preheating was applied.

Regarding the optimum energy density, there is no exact value that can be chosen for manufacturing defect-free samples. Mazur et al. [160] suggested that in processing H13 alloy by having an energy density of 80 J/mm³ a proper balance between the dimensional accuracy and relative density of the samples can be made. However, as shown in Fig. 18, near full-dense samples with a relative density of 99.7 % could be made by having an energy density of at least 60 J/mm³ [63].

Another factor affecting the soundness of the deposited material, in terms of internal defects, is the scanning strategy. Currently, the traditional line scan is still the most commonly used scan strategy in LPBF process, which is also named alternating scan. Beal et al. [143] claimed that different scan strategies can greatly affect the relative density of the AM samples. It was shown that in H13 processing by filling, sequential, alternated, and refill scan strategies the volume fraction of porosity can be decreased from 8 % to 6 %, 5 %, and 4 %, respectively, as presented in Fig. 19.

Asberg et al. [142] processed a high-alloy (Cr-Mo-V) cold-work tool steel by LPBF focusing on the correlation between the manufacturing

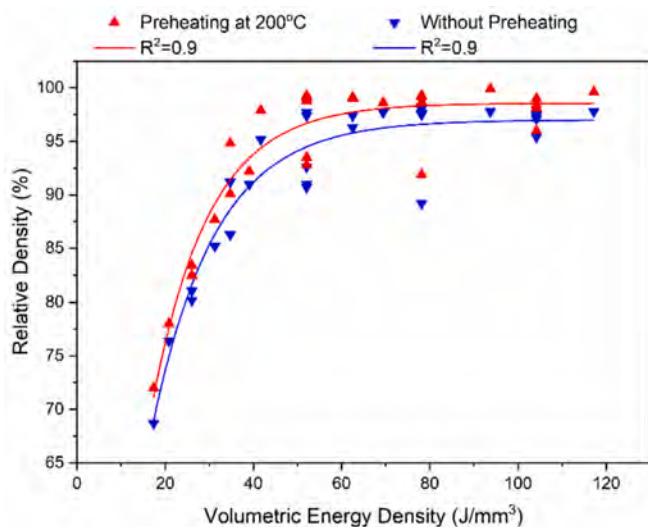


Fig. 18. Effect of platform preheating and energy density on densification of H13 in LPBF process [63] (Reproduced under CC BY licence).

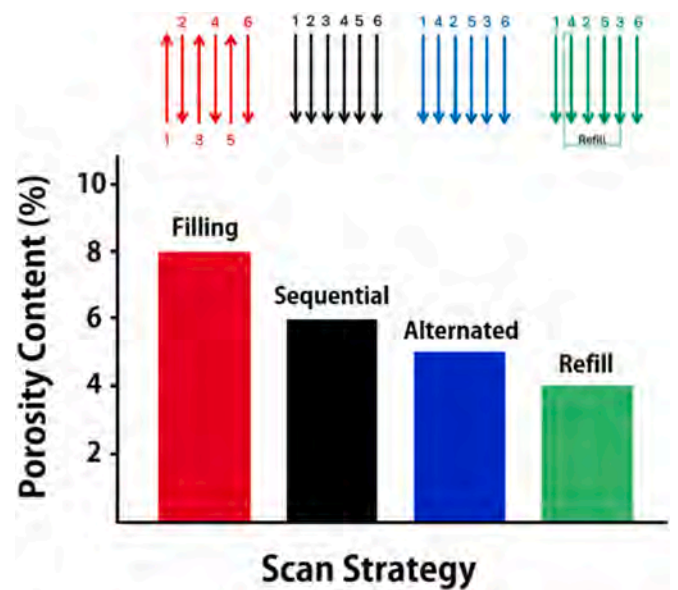


Fig. 19. Different scan strategies and the resulting cross-section of H13 processed by LPBF [143].

process, thermal history, and the resulting microstructure. Like LPBF-processed H13 alloy [163], a fine cellular-dendritic structure was obtained due to rapid cooling, resulting in martensitic microstructure with high amounts of retained austenite (64 %). The hardness of the material was lower than expected at 597 ± 38 HV due to the high retained austenite content.

HSSs have also been processed by LPBF. The microstructure of M2 alloy, like hot work tool steels, shows a dendritic structure with retained austenite. In addition to stabilizing austenite, the microsegregation that occurs during solidification also promotes the formation of carbides and eutectic structures in the areas between the dendrites [70,71,164].

The hardness of M2 material is reported to be highly affected by the scanning strategy. Samples with a hardness value of 57 HRC were produced by using an island scanning strategy [71]. However, when a remelting scanning strategy was applied, the hardness increased to 64 HRC, as depicted in Table 4. However, the tensile strength of the as-built sample, reaching 1300 MPa, fell somewhere between those of the conventionally cast alloy with and without heat treatment. Additionally, the surface roughness of the fabricated sample was improved by 47 % when the top layer was remelted.

Kunz et al. [108] claimed that for M50 steel, LPBF processing avoids coarse carbides and produces a fine martensitic structure with high hardness, comparable to conventionally produced steel after quenching

Table 4

Mechanical properties of M2 alloy processed by LPBF, displaying the changes in hardness, surface roughness, and tensile strength of the material in different conditions [71].

	Hardness (HRC)	R _a surface roughness (μm)	Tensile strength (MPa)
Conventional	19	–	~ 800
Conventional + HT	65	–	~ 1600
LPBF	57	18.3	~1280
LPBF + Remelting	64	8.6	–

and tempering. While Hot Isostatic Pressing (HIP) improves hardness and fatigue strength by reducing porosity, the LPBF samples exhibit lower fatigue strength and bending toughness than the reference material.

Maraging steel produced by LPBF often exhibits equal or slightly higher yield and ultimate tensile strength in its non-aged state, attributed to its finer microstructure [85,86,165]. Various research works have investigated processing different maraging steels fabricated by LPBF and studying the effect of processing parameters [166] and post-processing techniques such as heat treatment [167,168] and surface modification [169] on the microstructure and performance of the material. Additionally, the mechanical properties of the fabricated parts have been studied [170,171].

Following aging heat treatment, with or without prior solution treatment, a substantial increase in hardness (e.g., from 381 to 645 HV) and tensile strength is observed, accompanied by a corresponding reduction in ductility, consistent with expected material behavior [85,94,95,98]. However, regarding the post-processing heat treatment, there are two different views. Casati et al. [95] determined that solution treatment is unnecessary for samples produced by LPBF, as they can be directly aged. Their findings indicate that retained austenite does not significantly influence fracture processes. However, other researchers present a contrasting view, arguing that solution treatment followed by aging leads to a more favorable fracture mechanism, and therefore recommend performing a solution treatment before aging [86].

3.2.2. Electron beam powder bed fusion (EB-PBF)

In EB-PBF an electron beam is used to melt layered metal powders in a vacuum environment [172]. It offers advantages in processing materials with high thermal conductivity but is less common for tool steels due to equipment costs and material limitations. However, the vacuum environment and preheating of the powder bed help minimize residual stresses and it provides high building rates.

Therefore, compared to DED and LPBF, less research studies have

been done on fabricating tool steel components by EB-PBF. Nonetheless, as Asberg et al. [142] studied the processability of a high-chromium cold work tool steel by LPBF, the same material was processed by EB-PBF to fill knowledge gaps regarding how different additive manufacturing techniques influence the microstructure and properties of tool steel. As visible in Fig. 20, it was observed that, in the last deposited layers, dendrites with well-developed secondary arms and a carbide network in the interdendritic space were formed, reflecting a slower solidification rate. They also found that this process led to a more stable bainitic structure with higher hardness (701 ± 17 HV).

Moreover, in the inner regions, compared to LPBF, they claimed that coarser dendrites were formed in the EB-PBF processed material. This is due to the lower cooling that is achieved in this process. They reported the cooling rates to be within the range of $2.0 - 2.5 \times 10^6$ °C/s and $0.5 - 3.8 \times 10^4$ °C/s for LPBF and EB-PBF processes, respectively. Additionally, this can lead to the formation of martensitic and bainitic microstructure considering the applied thermal cycles during the manufacturing process. Based on Fig. 21, in LPBF, each layer undergoes cooling below the austenitization temperature with oscillations around critical points. Partial remelting of previous layers introduces deeper thermal cycling, leading to austenitization and the formation of martensitic microstructures in a few previously deposited layers. Subsequent cycles promote partial martensite decomposition.

In contrast, EB-PBF, with a preheating temperature of 850 °C, involves maintaining higher internal temperatures, which supports in situ heat treatment. It should be noted that while CCT diagrams provide insights into the potential transformations, they cannot fully predict the final microstructure due to the complex cooling dynamics of the process.

In EB-PBF the combination of high preheating and cooling rates resulted in the aforementioned in-situ heat treatment effects, reducing residual stresses and minimizing cracking [173]. Cormier et al. [174] could make samples having complete interlayer bonding and minimal porosity. A noteworthy finding of the work was the presence of localized non-homogeneities at the boundary between the exterior contours and interior squares of the part, which were only visible after etching, although their chemical composition and hardness were similar to the surrounding martensite. Their experiments revealed that processing conditions greatly influence both the build speed and mechanical properties, with faster build speeds leading to a decline in mechanical properties when sintering replaces melting.

Microstructural evolution in EB-PBF is a feature that needs to be understood. Cormier et al. [174] could obtain fully martensitic samples exhibiting a hardness range of 48–50 HRC, when the material was rapidly air-cooled immediately after finishing the fabrication process. However, a mix of martensitic and bainitic microstructure containing retained austenite was found when the material is normally cooled in the building chamber [173] (Fig. 22). Generally, in H13 alloy, the slower

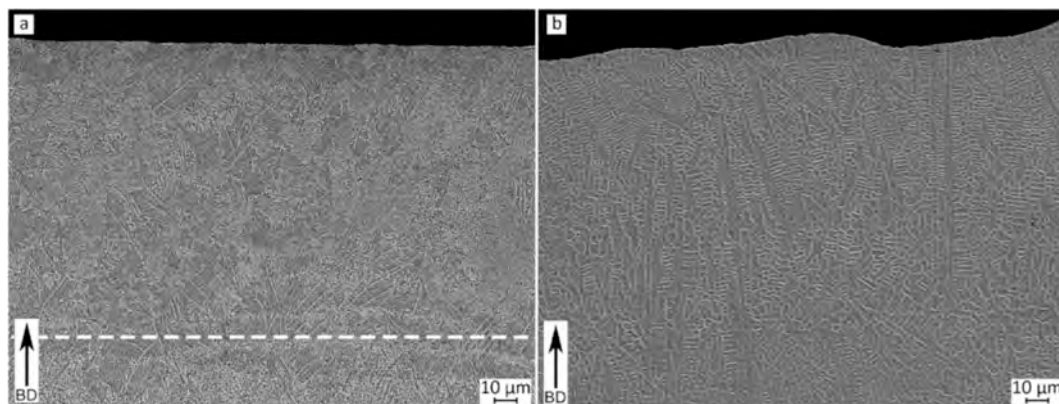


Fig. 20. SEM micrographs of the last deposited layers of Vanadis 4 cold work tool steel processed by a) LPBF and b) EB-PBF showing the differences in the resulting microstructure [142] (Reproduced under CC BY licence).

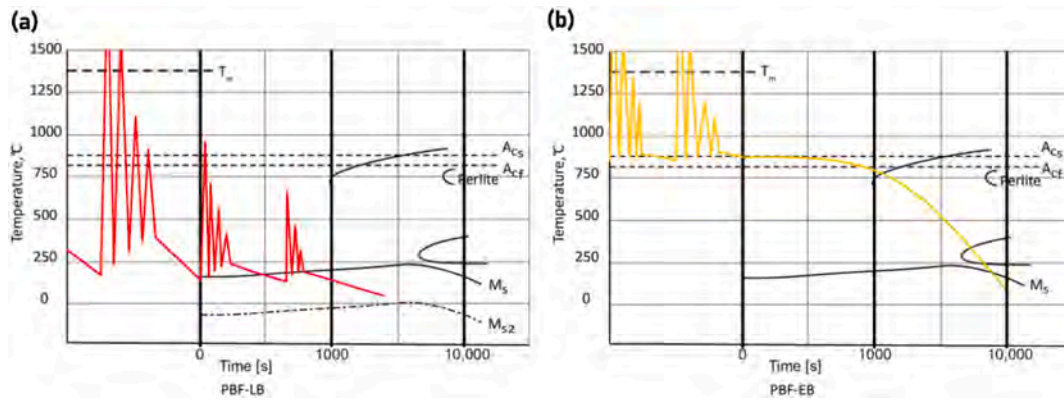


Fig. 21. Schematic representation of the applied thermal cycles during a) LPBF and b) EB-PBF processes combined with the CCT diagram of Vanadis 4 cold work tool steel [142] (Reproduced under CC BY licence).

cooling near the bottom allows for bainite formation, while faster cooling near the top promotes martensite formation.

Yang et al. [173] provided a hypothetical model (Fig. 23) of the microstructural evolution of H13 alloy by using both the thermal history during fabrication and simulations.

The predicted solidification process of H13 steel during EB-PBF follows the sequence: Liquid (L) \rightarrow L + δ \rightarrow L + δ + γ \rightarrow L + γ , which is then followed by the formation of primary carbides. During the fast cooling from the liquid state to the preheating temperature, a cellular structure forms, consisting of low-alloyed γ -Fe surrounded by higher-alloyed γ -Fe, both with closely matching chemical compositions. As a result, primary carbides develop by consuming the alloying elements present in the high-alloyed γ -Fe at the preheating temperature, which explains the gradual breakdown of the cellular structure as the height decreases. As cooling continues, γ -Fe and γ '-Fe transform directly into α -Fe, leading to the formation of thin lamellar carbide precipitates. The formation of the cellular structure is linked to the initial solidification of δ -Fe and γ -Fe, accompanied by segregation, a phenomenon previously described in LPBF by Casati et al. [148]. Their simulation results revealed the precipitation of three primary carbides—MC, M_2C , and M_7C_3 —at temperatures between 1216 °C to 1283 °C, aligning with experimental data. It is worth mentioning that due to the rapid cooling rate during solidification, which restricts back-diffusion in the solid phase, a strong correlation between Scheil module calculations and the experimental findings was achieved.

With regard to the mechanical properties of H13 alloy, a gradient in hardness was observed, with the highest values near the top surface (565.6 HV) and decreasing with depth, while tensile testing revealed tensile strength values of 1470 MPa with elongation reaching 5 %,

highlighting significant mechanical performance [173].

Wei et al. investigates the production of crack-free M2 alloy samples under various processing parameters, focusing on volumetric energy density (VED) and powder bed preheating temperature. Optimized conditions achieving high relative density (99.7 %) were identified, where a VED of 43.6–47.9 J/mm³ and powder bed preheating of 820 °C yield ultra-high hardness (~70 HRC) and exceptional wear resistance, with a wear rate 13.7 % lower than that of conventional wrought M2 HSS in quenched and tempered condition. Discussing this high wear resistance in AM processed part, a schematic illustration is provided in Fig. 24. Regarding the abrasion process mechanisms, the wrought M2, with a martensitic matrix and coarse eutectic carbides, exhibits local plastic deformation and abrasive wear caused by fragmented carbides during friction (Fig. 24a). In contrast, AM processed material, characterized by finer grains and fewer carbides, shows reduced plastic deformation and carbide fragmentation, leading to less abrasive and adhesive wear (Fig. 24b). However, AM processed samples with structural defects suffer from increased plastic deformation, severe adhesive wear, and higher friction, exacerbating wear through oxide layer rupture and minimal carbide content (Fig. 24c).

Cooling is a crucial step in the injection molding process, significantly impacting productivity and profitability. Efficient cooling reduces cooling time, thereby increasing production rates. Traditionally, cooling channels are drilled as straight bores around the tool cavity, but conformal cooling channels, which maintain an equidistant distance from the surface to be cooled, have been shown to improve product quality and reduce cycle time [176–178]. Rännar et al. [179] performed a preliminary investigation on the fabrication of conformal cooling channels of H13 by EB-PBF and compared them to conventional,

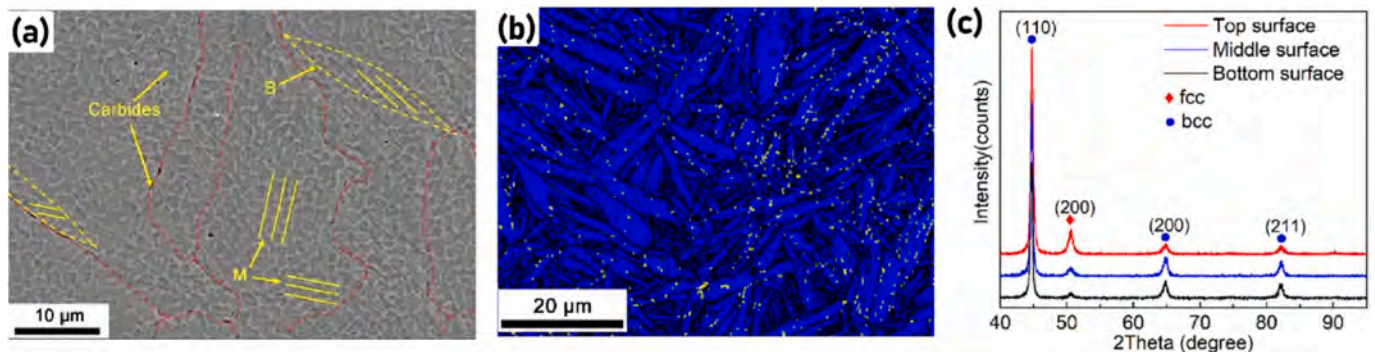


Fig. 22. Microstructure of H13 alloy showing a) bainite formation and the presence of carbides mainly at grain boundaries, b) EBSD phase distribution map showing a martensitic microstructure with small amount of retained austenite (yellow regions) and c) XRD results confirming the presence of retained austenite mainly at the last deposited layers [173]. (For interpretation of the references to colour in this figure legend, the reader is referred to the web version of this article.) (Reproduced with permission from © Elsevier, all rights reserved)

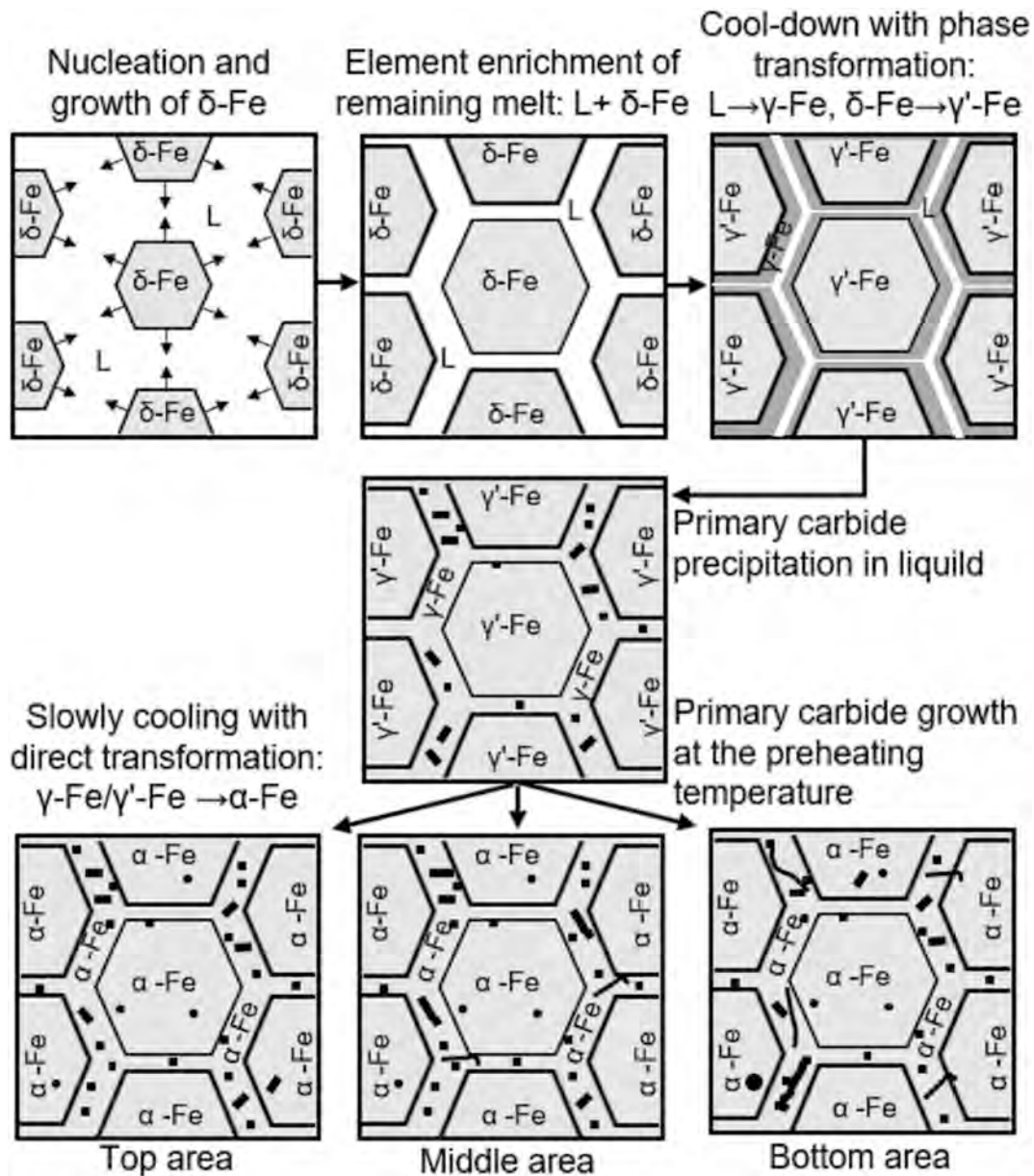


Fig. 23. A proposed model, based on thermal history and simulations, of the microstructural evolution in H13 processing by EB-PBF [173] (Reproduced with permission from © Elsevier, all rights reserved).

machined inserts, focusing on their impact on cooling efficiency and overall process performance. They reported that this approach can provide a significant advantage in terms of dimensional accuracy and cooling time compared to conventional machined cooling systems.

In summary, PBF provides excellent geometric precision and fine microstructures but is more prone to internal porosity and residual thermal stresses due to rapid solidification within a powder bed. In contrast, DED allows high-deposition-rate fabrication and are particularly suited for repairing large tools, but they generally produce coarser, weld-like microstructures with a higher risk of dilution and defect propagation if process control is inadequate. An appropriate choice between PBF and DED therefore depends on the required fidelity, part size and the acceptable trade-off between process speed and part quality.

4. AM for component repair

Many engineering components, such as industrial machinery, molds and dies, are routinely exposed to severe conditions like extreme heat,

overloading, high impacts, rapid thermal cycling, erosion, friction, and dynamic contacts [180]. As a result, numerous components and machines suffer damage annually, losing functionality due to scratches, pits, cracks, peeling, and partial fractures [181]. Different factors that affect the lifecycle of tools are depicted in Fig. 25. This leads to the yearly acquisition of new machinery and equipment, as damaged ones are discarded after losing their functionality, contributing to material loss and waste generation.

In the industrial sector, Tungsten Inert Gas (TIG) welding was among the first methods adopted for repairing damaged components. While TIG welding is easy to implement, it generates a large amount of heat in the repaired part, which results in high residual stresses and distortions [183,184]. Alternatively, Plasma Transferred Arc Welding (PTAW) and Electron Beam Welding (EBW) provide the advantage of lower heat input, minimizing these problems [185,186]. However, these methods require more complex and expensive equipment.

As a result, the capability of repairing damaged parts using AM plays a crucial role in modern engineering and industry for several reasons.

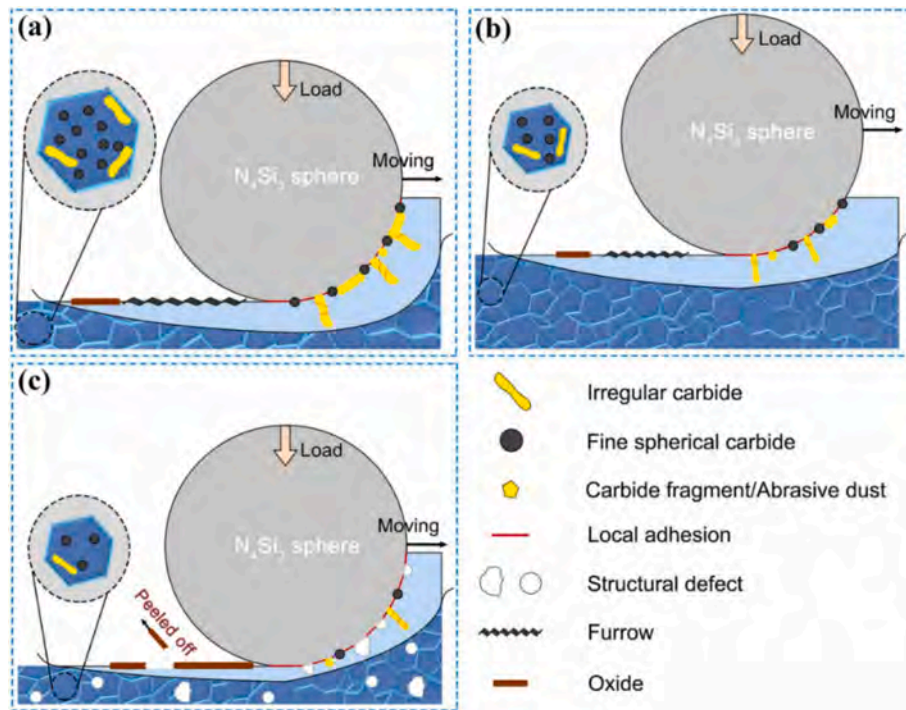


Fig. 24. The abrasion mechanisms in different conditions of a sample HSS alloy: a) wrought material b,c) EB-PBF processed material with different processing parameters (b: 43.6 J mm^{-3} and powder bed preheating of $820 \text{ }^\circ\text{C}$ and c: 43.6 J mm^{-3} with preheating of $750 \text{ }^\circ\text{C}$ or 40 J mm^{-3} with a preheating of $820 \text{ }^\circ\text{C}$) [175] (Reproduced with permission from © Elsevier, all rights reserved).

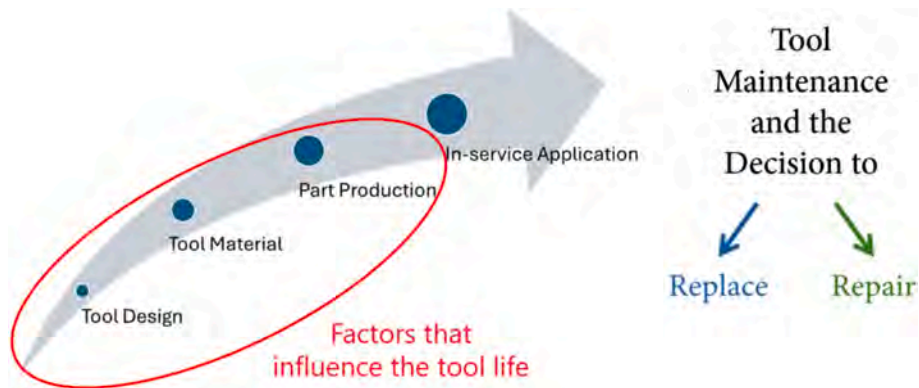


Fig. 25. The affecting factors that determine the lifecycle of tools.

AM enables the restoration of damaged parts to their original functionality, effectively extending their operational life. Instead of discarding a component due to wear or minor damage, AM allows for precise repairs that can bring the part back to serviceable condition. Repairing parts through AM is often more cost-effective than manufacturing new ones [131]. It reduces the need for raw materials and decreases manufacturing costs. Moreover, by repairing instead of replacing, AM contributes to waste reduction and resource conservation. It minimizes the environmental impact by lowering the demand for new materials and reducing the energy consumption associated with full-scale production processes.

Asnafi [182] has made a comparison focuses on production costs and revenues for a part that requires manufacturing tools, considering two approaches: traditional manufacturing and a process incorporating AM (Fig. 26). In the conventional approach, the tool is entirely replaced with a new one. In contrast, the AM-based process involves repairing or remanufacturing the damaged tool, as the original tool is no longer usable due to wear or damage. It is shown that design for AM leads to a tool

that decreases cycle time, thereby lowering production costs. As a result, the breakeven point is reached more quickly with a tool made using AM. The costs associated with traditional toolmaking and tool remanufacturing through AM, along with projected revenue levels, are important factors that need to be identified.

Therefore, repairing damaged tools using additive manufacturing is important because it offers a sustainable, cost-effective, and efficient alternative to part replacement. It extends the useful life of components, reduces environmental impact, and leverages advanced manufacturing technologies to meet the needs of modern industry.

Different processes have been used to repair various tool steels. Parts made from H13 [187], Vanadis 4 Extra [188], and X155CrMo12-1 [189] have been repaired by laser cladding. Repair of tool steels has been carried out by other AM processes such as arc-based DED [190] and LPBF [102]. As DED, in general, allows direct deposition onto existing geometry, requires minimal disassembly for large parts, and offers relatively high deposition rates that minimize downtime, it has become the most commonly adopted industrial AM route for repairing heavy and

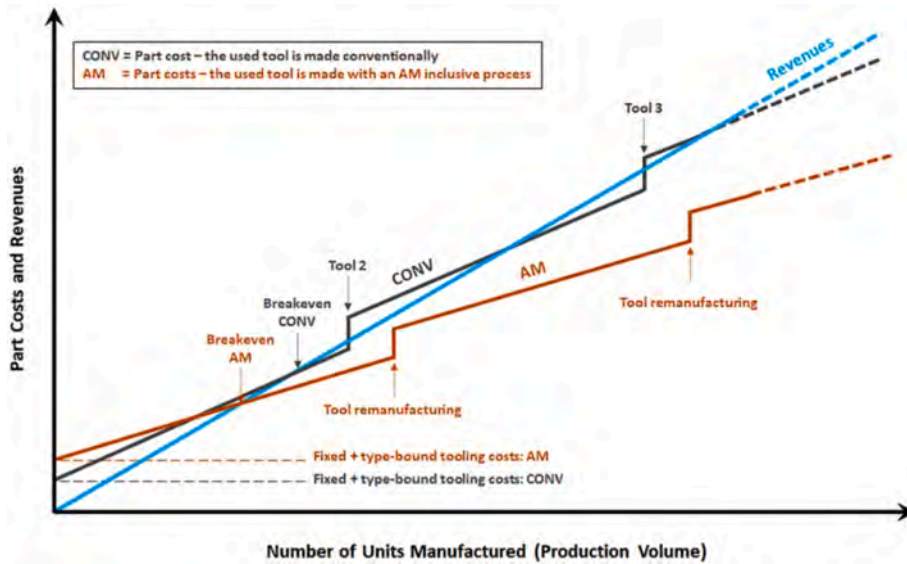


Fig. 26. Comparing the part costs and revenue considering conventional manufacturing and AM technology [182] (Reproduced under CC BY licence).

medium-sized tooling. As shown in Fig. 27, as of 2019, DED has been the major AM process for repair and restoration of industrial components [191].

Like any other manufacturing and repair processes, this technique also has some limitations and advantages. The strengths and weaknesses of DED and conventional repair processes are provided in Table 5.

In general, DED is typically favored for repairing large tool components because it can add material directly onto existing geometries without the constraints of a powder-bed setup, and it offers high deposition rates at the damage site. LPBF repairs can be performed as well, but are usually better suited to smaller inserts or features that demand fine detail, given the limited build volume and reliance on a powder bed. From an economic perspective, publicly reported case studies and techno-economic analyses show that AM repair often reaches a favorable break-even point for high-value tooling. The approach can lower material and processing costs, shorten downtime compared with ordering a new tool, and extend tool life by substantial margins, often by two to three times, depending on the specific case. Environmentally, life-cycle assessments generally indicate that repair via DED reduces material consumption and embodied CO₂ relative to full replacement, primarily by avoiding casting and reducing scrap, though factors such as machine energy use and the environmental footprint of powder production must be included in a comprehensive life-cycle view. Recently developed decision-support frameworks combine techno-economic and life-cycle assessment metrics to guide repair-versus-replace choices. These tools highlight critical factors such as part importance, remaining useful life, and the economic impact of downtime as decisive inputs in

the decision process [5].

Kattire et al. [187] investigated the tool repair using CPM9V alloy, identifying laser power, travel speed, and powder feed rate as critical factors affecting track geometry, while dilution was mainly influenced by powder feed rate and gas flow rate. The process also produced compressive residual stresses in the deposited layer. Leunda et al. [188] successfully repaired heat cracks on Vanadis 4 Extra dies using DED with the same material, achieving defect-free metallurgical bonding with a hardness value comparable to the substrate.

The deposition of H13 steel powders on the wrought material, with a powder feeding rate of 0.057 g/s, a travel speed of 14.17 mm/s, and a laser beam diameter of 0.50 mm [82]. The researchers discovered that raising the energy input throughout the process led to a minor decrease in hardness. This reduction was attributed to several factors, including the increased height of the deposited layers, higher secondary dendritic arm spacing, and a slower cooling rate.

Petruse and Langa [192] studied the repairing of a hot forging mold, which encountered wear and tear, by DED process. The repair process was first designed, simulated, and the surface milling and material deposition were carried out on the mold. Fig. 28 Shows the different steps of the repair.

In a case study, it was shown that the forging tool which was repaired by DED process had an increased lifespan of more than 300 % compared to the conventional repaired tool [192]. The same trend was also observed for the repaired forging mold.

Repairing tools and dies are not always done by depositing the same material of the damaged component. Foster et al. [193] deposited

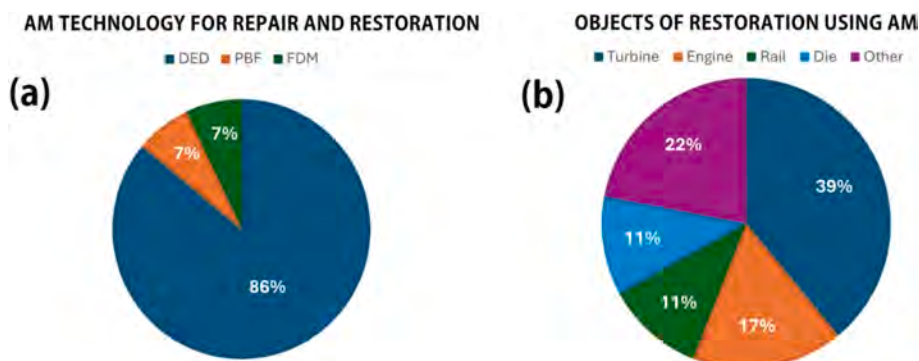


Fig. 27. a) AM technology for repair and restoration and b) object of restoration using AM [191].

Table 5
Strengths and weaknesses of DED and conventional repair processes.

	Advantages	Limits
DED process	<ul style="list-style-type: none"> - Enables targeted, accurate material deposition, which minimizes waste and allows for complex shapes to be restored accurately. - Adds material only where necessary. - Increases material recycling rates by minimizing scrap. - Supports a wide variety of materials and alloys, making it adaptable for diverse tools and molds, allowing custom repairs tailored to specific needs. - Capable of rapid replacement, which minimizes operational delays, improves buy-to-fly ratio, and decreases energy consumption and CO₂ emissions. - Being cost-effective for complex repairs or low-volume, high-value parts. - Possibility of wear-resistant layer design and fabrication. 	<ul style="list-style-type: none"> - Often requires additional machining to achieve the desired finish and tolerances. - Parameter optimization demands expertise and fine-tuning. - Potential issues with inter-layer adhesion and microstructural inhomogeneities. - Material processability
Conventional techniques	<ul style="list-style-type: none"> - Easy to implement various techniques. - More experienced technicians, easing adoption and reducing training needs. - Generally low-cost techniques. 	<ul style="list-style-type: none"> - Tends to involve substantial material removal, which can lead to waste and may weaken the repaired component. - Achieving high precision for complex or hard-to-access areas is challenging. - Applied thermal cycles may alter the microstructure of the component.

Stellite 21 cobalt-based alloy on a damaged AFRC die insert made of H13 (Fig. 29a and b), and they claimed that this approach provides the repaired component with excellent toughness, wear resistance, and

machinability.

In Fig. 29c and d, abrasive wear, which involves the removal of metal, is represented by negative values, while adhesive wear, which leads to metal accumulation, is indicated by positive values. The results revealed a 49 % improvement in reducing abrasive wear and a 67 % improvement in mitigating adhesive wear in the repaired die insert. Stellite 21 alloy exhibit exceptional wear resistance at high temperatures, alongside superior corrosion, erosion, abrasion, and galling resistance, which are critical in hot forging applications [193]. Unlike H13 tool steel, whose tensile strength diminishes at forging temperatures (200–250 °C), Stellite 21 maintains its tensile integrity, further highlighting its suitability for demanding industrial processes [193–195]. These factors led to superior wear properties in the repaired component.

LPBF has also been used to repair tools and dies made of tool steels. Generally, preheating the substrate is highly suggested to avoid cracking. However, Megahed et al. [102] developed a process window with no preheating for H11 alloy and statistically provided a relationship between surface roughness and process parameters. The researchers claimed that the repair of a volume of ~ 2000 cm³ was successfully performed with an energy density of 70 J/mm³ with no pores or cracks, as can be seen in Fig. 30. They suggested using high scan speeds and small hatch spacing combined with high laser powers providing an energy density of 50 – 150 J/mm³ to achieve high relative densities.

Overall, the case studies presented highlight the transformative impact of AM processes in repair applications, demonstrating significant improvements in efficiency and material sustainability. By enabling tailored repairs and extending the life of critical components, these technologies offer substantial advantages over conventional methods, particularly in environmental impacts. Despite certain challenges, such as material compatibility and microstructural inhomogeneities, the ongoing advancements in AM hold great promise for overcoming these limitations.

5. Challenges and limitations

5.1. Technical challenges

Repairing dies and tools presents significant challenges, primarily

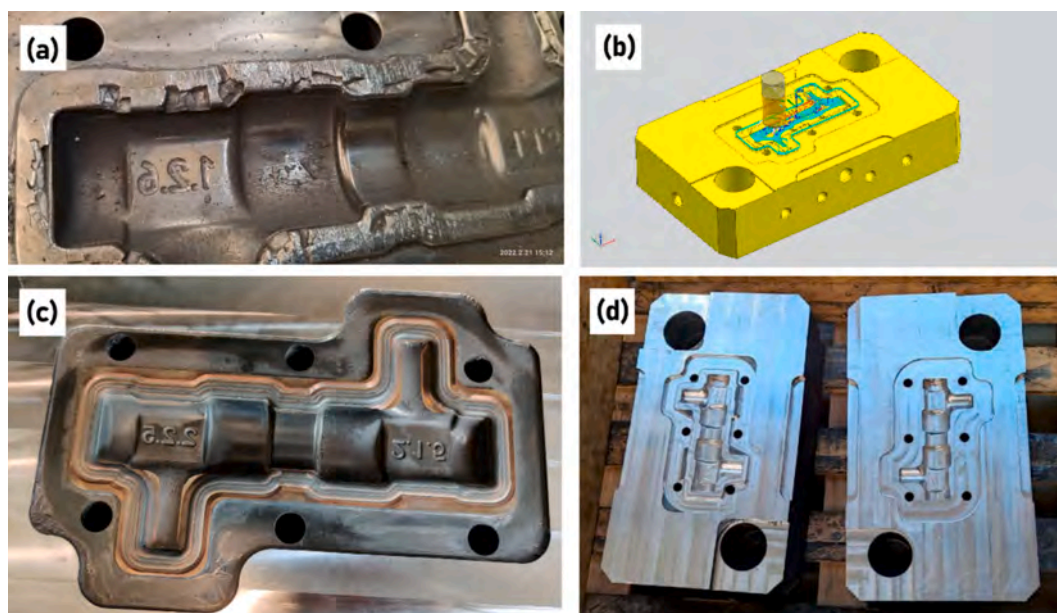


Fig. 28. a) Defected mould after numerous forging cycles, b) simulating the machining and milling process, c) as-deposited mould, and d) final product [192] (Reproduced under CC BY licence).

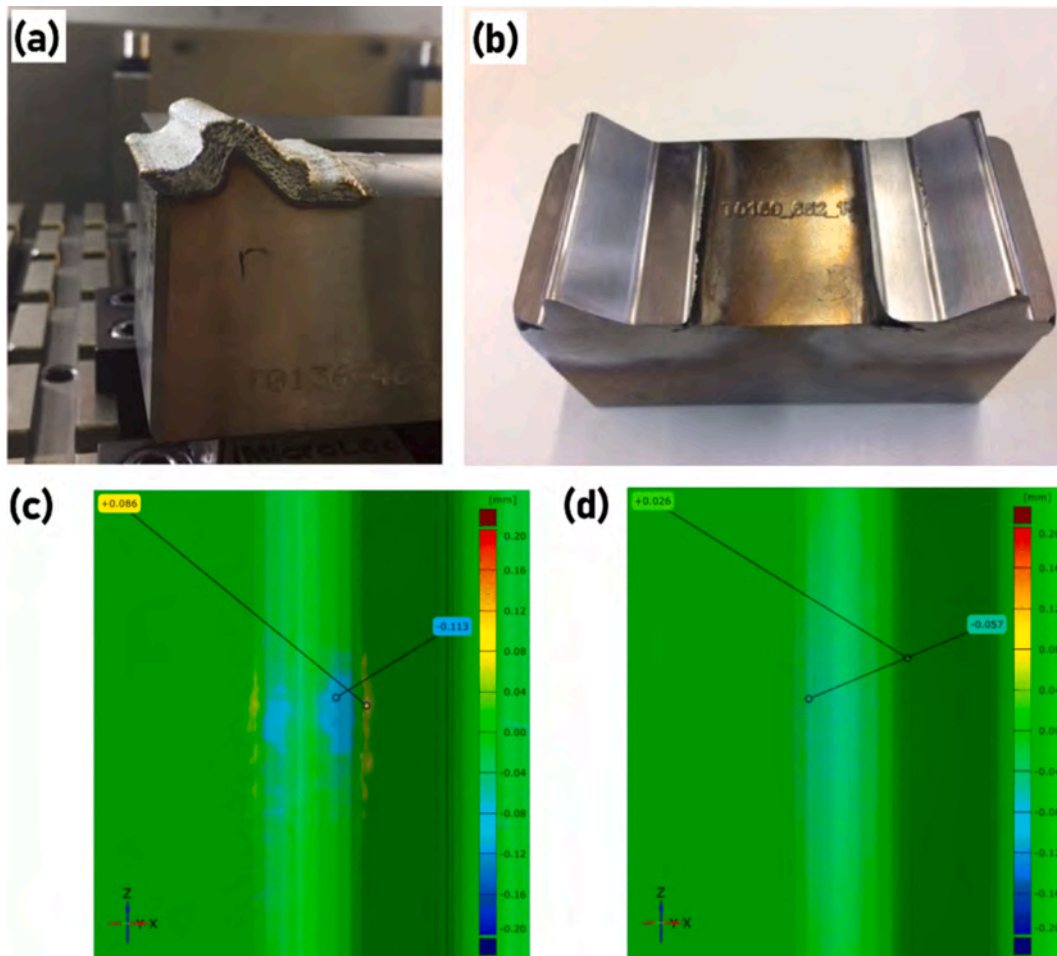


Fig. 29. Repaired die insert in a) as-deposited and b) machined condition. CMM surface profiles corresponding to the abrasive and adhesive wear performance of the c) original H13 and d) DED repaired die insert [193] (Reproduced under CC BY licence).

due to the low weldability of the materials commonly used in their production. These materials often contain high levels of carbon and alloying elements, which contribute to the formation of brittle phases, complicating the repair process [196].

Regarding internal defects, porosity is a common issue in AM parts and negatively impacts mechanical properties. It can be categorized into three main types: lack of fusion, keyhole voids, and trapped gas pores [197]. Lack of fusion occurs due to insufficient melting, leading to poor adhesion between layers or tracks, often resulting in irregularly shaped voids. Keyhole porosity originates from unstable keyhole tips formed by high-power melting, and its size depends on keyhole geometry. Trapped gas pores, typically spherical, are caused by inert gases (argon, helium) or shielding gases (such as nitrogen), which may remain in the solidified material. Another significant issue in AM is the formation of cracks due to high residual stresses induced by rapid cooling and thermal gradients. Proper control of processing conditions, such as processing parameters, preheating condition, melt pool dynamics, alloy modification, etc., can mitigate these defects.

As mentioned, AM provides a higher cooling rate than conventional processes, leading to unique microstructures that exhibit enhanced hardness and wear resistance. However, the high temperature gradients often lead to microcracks and porosity, especially in high-carbon tool steels [7]. In Fig. 31 both pores and cracks can be observed in the cross-section of a V4E sample processed by DED. In the study by Yuan et al. [198] on multilayer deposition, a 1-layer sample showed no cracks and few pores, achieving a relative density of $99.44 \pm 0.45\%$. In the 2-layer sample, both pores and cracks were present, but the density ($99.65 \pm 0.33\%$) remained similar to the 1-layer sample. Notably, cracks

appeared only in the second layer, while the first layer was nearly crack-free. In the 4-layer sample, significantly more pores and cracks were observed, particularly in the third and fourth layers, with the density slightly decreasing to $98.73 \pm 0.72\%$.

Defects, especially large pores, were concentrated at the layer interfaces, while cracks typically formed in the upper parts of the layers, sometimes extending into adjacent layers. Crack propagation generally followed the build direction, and there are formed as a result of internal stresses. It must be noted that the depositions were made on a hot work tool steel substrate. Therefore, while the first layer was deposited on a hot work steel, subsequent layers were deposited on a cold work deposited layer. This situation mirrors the challenges in DED on cold work tool steel.

In a high-alloy (Cr-Mo-V) cold-work tool steel defects included pores, about $50\text{--}100\ \mu\text{m}$ in diameter, was found close to the surface of LPBF specimens [142]. However, compared to these samples, the EB-PBF fabricated parts showed fewer defects (no pores or cracks). It is known that tensile strength is highly affected by the internal porosity. In a H13 LPBF material, the tensile strength experienced a significant decrease of more than 20% when the volume fraction of porosity slightly increased from 0.2% to 0.4% [77]. Additionally, ductility remains a challenge in as-built AM-produced tool steels in both DED and PBF processes [67,71,106].

In multilayer deposition, the microstructure transitions from a fine cellular structure in the bottom layer to a columnar dendrite structure in the top layer, which significantly affects hot cracking susceptibility [199–201]. The fine cellular structure has short backfill channels during the final stages of solidification, allowing liquid metal to easily fill

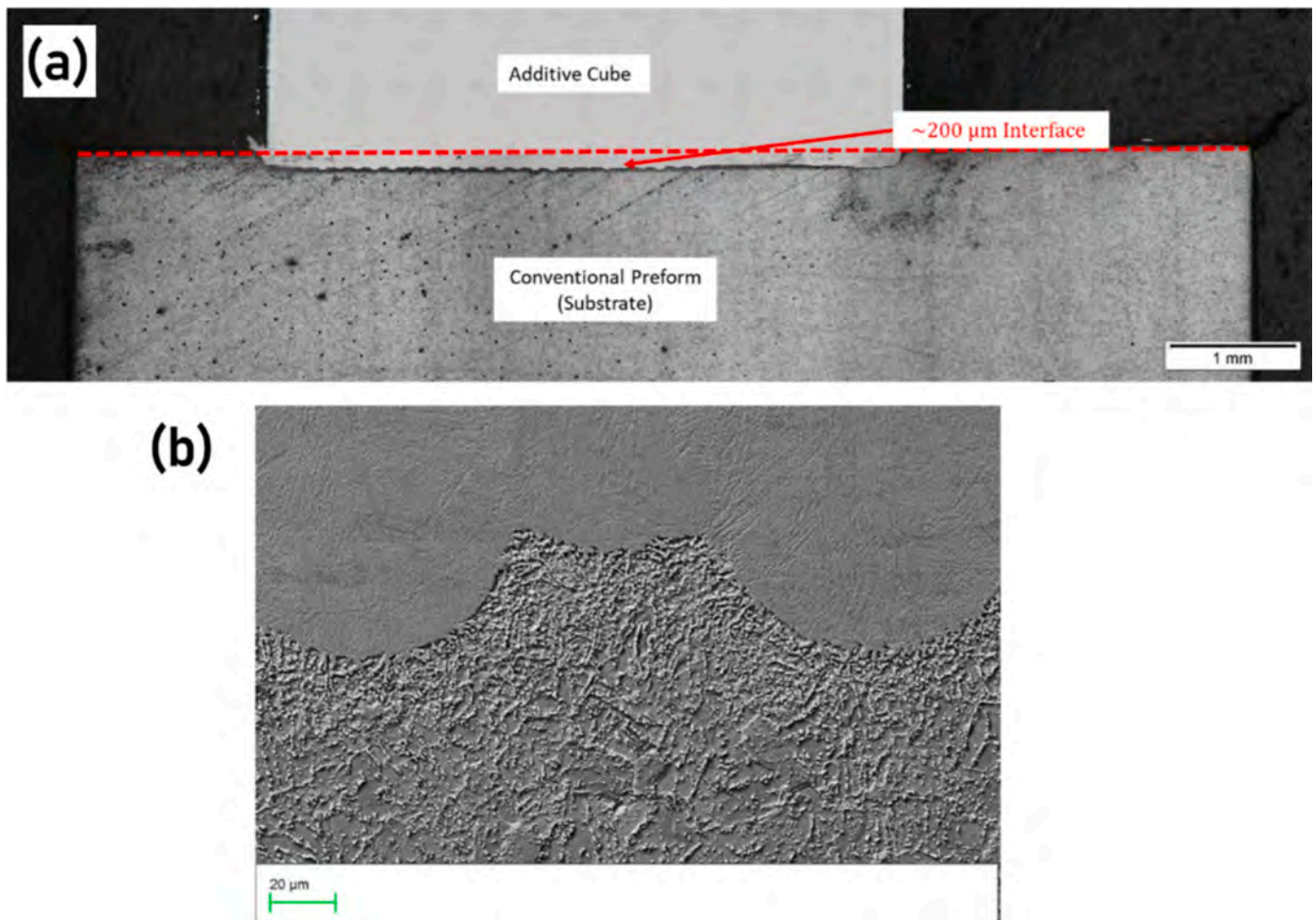


Fig. 30. a) Cross-section of a repaired *H11* component and b) the microstructure of the interface [102] (Reproduced under CC BY licence).

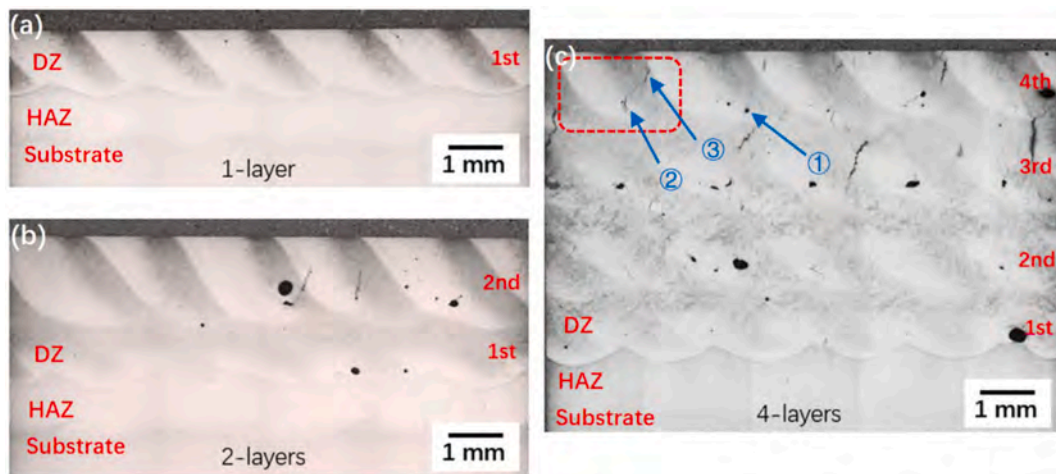


Fig. 31. LOM micrographs of cross-sections of V4E tool steel processed by DED: a) few pores in 1-layer deposition, b) both pores and cracks in 2-layer deposition, and c) higher amounts of cracks and pores [198] (Reproduced under CC BY licence).

cavities caused by solidification shrinkage and thermal contraction. In contrast, columnar dendrites have longer channels that can close prematurely, trapping liquid in the interdendritic regions and forming cavities, increasing the likelihood of cracking. Therefore, coarser microstructures and columnar dendrites generally have a higher susceptibility to cracking, especially in the upper layers during solidification. Preheating can reduce the thermal gradient (G) and cooling rate, which

reduces the susceptibility to hot cracking during AM processes [60,141]. It should be noted that high preheating temperatures above the martensite start temperature (M_s) can lead to the transformation of austenite into upper bainite.

The separation of the deposited material from the baseplate and warpage has been reported (see Fig. 32). Preheating the build plate to temperatures between 300 °C and 500 °C has been shown to reduce

these stresses but can also lead to unwanted phase transformations and microstructural defects [7,139]. Kempen et al. [71] also showed that by preheating the substrate to 200 °C, crack-free samples of M2 alloy could be produced by LPBF. The same beneficial effect is also stated by Megahed et al. for H11 steel [102].

Additionally, Krell et al. [156] reported that crack density decreases as the base plate preheating temperature increases. This reduction in crack density is not due to the suppression of the martensitic phase transformation. Instead, preheating lowers the maximum temperature gradients and the material's elastic modulus, leading to reduced thermal stresses. Additionally, preheating lowers the material's yield stress, enabling thermal stresses to be relieved more effectively through plastic deformation.

Delamination and cracking were also detected in the repairing process of a tool by DED. As shown in Fig. 33, delamination of first deposited layer and cracking in subsequent layers happened after cooling.

Concerning the microstructure, carbide distribution is often a challenge, with molybdenum-rich and vanadium carbides forming at grain boundaries, which affect the material's toughness and wear resistance [6,139]. Post-process heat treatments play a role in controlling the distribution and dissolution of carbides, which directly impacts the wear resistance and hardness of the final product [6,139,140].

Surface quality is another feature which should be considered when fabricating new components or performing repair on tool steels. In a LPBF fabricated M2 part, the measured arithmetic mean surface roughness was around 18 μm [71]. It should be noted that the surface roughness obtained by DED fabricated parts are generally higher than those components processed by LPBF.

To summarize (as also provided in Table 6), internal defects common to AM tool steels can be grouped into a few key categories: lack-of-fusion porosity, which appears as irregular voids created when energy input or track overlap is insufficient; keyhole porosity, gas-filled voids arising from unstable deep-penetration melt pools; spherical pores due to trapped shielding or atomization gas; and solidification or hot cracking, typically interdendritic or at grain boundaries, driven by limited liquid feeding during solidification and the presence of low-melting films. The prevalence of each defect type depends on the specific AM process and the processing conditions. For instance, lack-of-fusion porosity is most often linked to low volumetric energy density in powder-bed fusion, whereas hot cracking becomes a prominent concern for high-carbon, high-alloy tool steels like D2 and M2 that exhibit wide freezing ranges and carbide-forming elements.

Practical mitigation strategies that have demonstrated effectiveness in the literature include preheating the build bed or substrate to reduce

thermal gradients and suppress excessive martensite formation; careful tuning of energy density and scanning strategy, such as adopting remelting passes, island patterns, or rotated scans, to promote deeper fusion and reduce porosity; rigorous powder quality control, favoring spherical, gas-atomized powders with a narrow particle-size distribution and tight oxygen content control; post-build densification steps such as HIP to close residual pores; tailored post-processing heat treatments (solution treatment followed by tempering, aging, and possibly HIP) to relieve residual stresses, homogenize segregations, and optimize carbide precipitation; and material or process choices, including using EB-PBF or alternative routes like binder-jet plus sintering for steels prone to cracking. When considering repair scenarios with DED, additional precautions are advised: maintaining appropriate track overlap, controlling dilution when depositing on existing substrates, and managing interpass temperatures to minimize delamination and interlayer cracking. Tailoring these mitigations to the specific alloy chemistry and the intended part function is essential for effectiveness.

5.2. Material compatibility

Material compatibility is a key factor when using AM for repairing components. It is vital that the repair material is the same or closely matches the base material. Variations in material composition, thermal expansion rates, or mechanical properties between the original component and repair material can result in poor bonding, cracks, or reduced structural strength. As an example, differences in thermal properties may introduce residual stresses, potentially causing material failure. Therefore, choosing the right alloy or material for the repair process can be particularly challenging, especially given the diverse materials used in forging tools and molds. The repair material must closely resemble the original in terms of mechanical, thermal, and chemical properties to preserve the tool's performance and longevity.

As known, H13 is widely used for dies and molds but poses AM challenges because its high hardenability and carbide-forming elements promote retained austenite and high residual stresses after fast cooling. Reported strategies to improve processability include bed/substrate preheating, energy-density optimization, and tailored post-HT (tempering) to reduce brittleness. For example, recent high-power LPBF work has shown that, with careful energy-density control and post processing, H13 can reach very high strengths in as-built or heat-treated states, but variability remains if process controls are loose [151]. With regard to cold work steels, these steels contain high carbon and strong carbide formers (Cr, V, W), giving excellent wear resistance but also a large solidification range and strong segregation that promotes hot cracking and embrittlement in melting-based AM. Successful

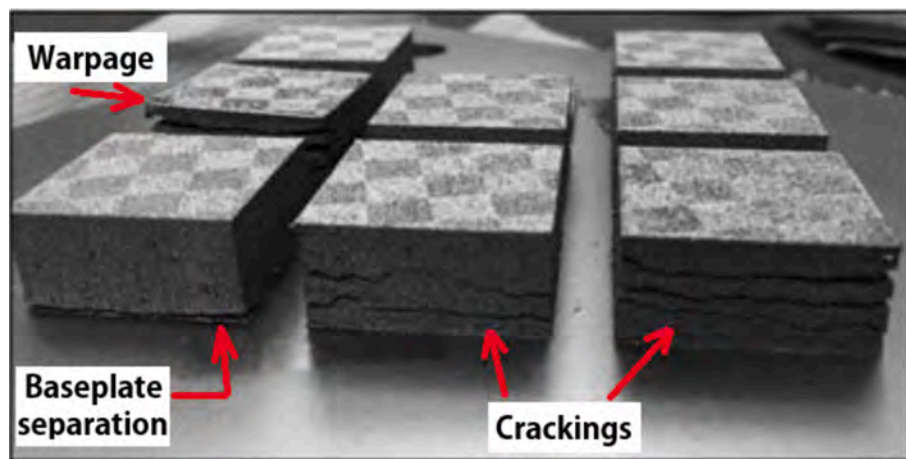


Fig. 32. Fabricated M2 steel part showing cracks, delamination and separation, and warpage [202] (Reproduced with permission from © Informa UK Limited, all rights reserved).

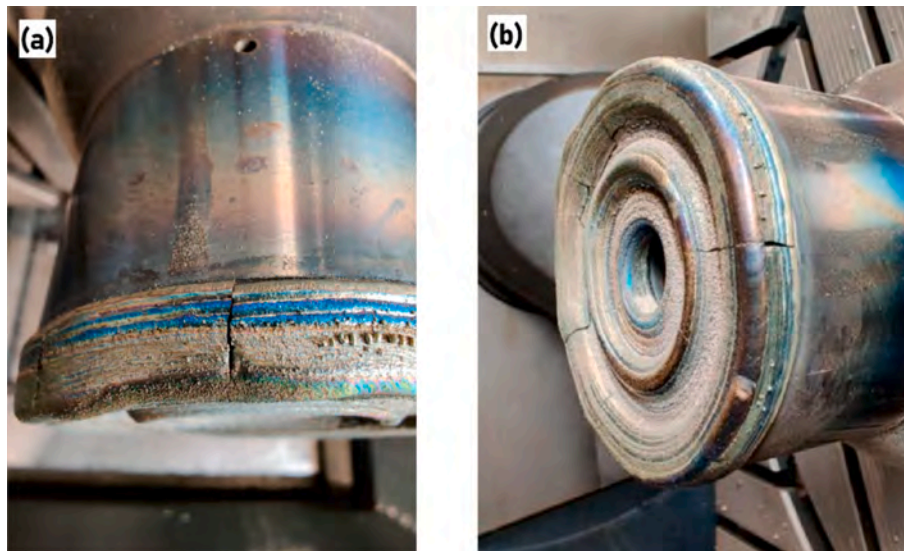


Fig. 33. a) Delamination happened in the first deposited layer and b) cracking in different layers [192] (Reproduced under CC BY licence).

Table 6
Defects, root causes and mitigation strategies (summary).

Defect	Root cause(s)	Practical mitigation(s)
Lack-of-fusion porosity	Low energy density, poor hatch overlap, high scan speed	Increase energy density / decrease scan speed, optimize hatch/overlap, remelting passes
Keyhole/gas porosity	Unstable keyhole, trapped gas	Adjust focus, reduce excessive power, adjust gas flow, optimize powder quality
Solidification/hot cracking	Wide solidification range, segregation (high C, Cr, V), high thermal gradient	Preheat substrate/bed, use EB-PBF (vacuum + preheat), use modified chemistries or alternative AM route
Delamination / interlayer adhesion issues	Poor track overlap, excessive dilution, insufficient interpass temperature control	Optimize bead overlap, control powder feed and laser parameters, use interpass temperature control, employ in-situ monitoring

processing strategies are fewer and often depend on either (i) alternative AM routes (e.g., EB-PBF under high preheat) or (ii) alloy modifications to reduce crack susceptibility. Moreover, when DED is used for repair, matching chemistry and controlling dilution are critical to avoid brittle interfaces. The literature increasingly explores partial alloy redesign or multi-step thermal cycles to manage carbide distribution [4,203]. However, maraging steels are relatively AM-friendly due to low carbon and strengthening by precipitation. Both LPBF and DED produce high-strength maraging parts; in many cases, inherent thermal cycles induce some precipitation and can reduce the need for full solution + aging cycles, though final aging is often applied to reach the highest strengths. Maraging alloys can be therefore potential candidates for AM tooling elements when very high strength-to-ductility performance is required without excessive cracking risk.

Therefore, it is of great importance to perform a comprehensive assessment before part fabrication or repair (to analyze and understand the material), define the optimized set of processing parameters according to the material and conditions, perform a real-time assessment, designing a proper post-process procedures, and also post-process quality controls.

Recently, number of works have been done to tackle the internal defects issue and also material performance improvement. Alloy

development using in situ alloying with pure elemental powders has been a technique. However, the process faces challenges due to differences in melting points and other thermal properties. Hantke et al. [204] demonstrated successful processing of low-stress H13 steel specimens from pre-alloyed powders without preheating. Other techniques, such as mechanical alloying, were explored, with Narvan et al. [63] improving H13 properties through VC particle incorporation, and Köhler et al. [205] enhancing microstructure and hardness by blending TiC carbides with H13 powder. These approaches offer promising improvements in alloy performance.

6. Economic considerations

Research on repair operations has not only explored their feasibility but also examined their sustainability and environmental impact. Various factors, including energy consumption, pollution, material waste, lead time, and cost, have been used to measure the environmental effects of repair processes [206–208]. These studies highlight the importance of considering both operational efficiency and environmental responsibility in repair methodologies. In other words, tooling decisions, whether to repair or replace a tool, rely on several practical and economic considerations. Key factors include how much life remains after a repair, the repair cost (materials, machine time, and skilled labor), and the relative lead times for repairing versus producing a new tool. The cost of downtime while the tool is unavailable and the environmental footprint, such as embodied energy and CO₂, also play a role when choosing between repair and replacement. Decision-support approaches bring these inputs together to estimate break-even points between repairing and replacing. In many cases, particularly for high-value tools, DED repair can be financially advantageous due to material savings and shorter lead times. Recent work in this area, including life-cycle assessment and decision-support studies, offers frameworks and concrete numbers to evaluate these trade-offs in real industrial settings [5].

Morrow et al. [207] quantitatively evaluated the energy consumption and emissions associated with producing mold and die tooling through DED and CNC milling. The study revealed complex trade-offs between economic and environmental impacts, with CNC milling being more sustainable for simple molds with a high solid-to-cavity volume ratio, while DED was more efficient for molds with a low solid-to-cavity volume ratio.

Fig. 34a and b illustrate the raw material (H13) production processes for DED using powder and conventional manufacturing using plate,

alongside the specific energy consumption for these respective material production pathways. This comparison highlights the energy requirements associated with each method.

The direct atomization route requires approximately 20 % less energy than plate production, while the indirect route consumes around 25 % more. Additionally, the direct atomization method results in reduced air emissions with reductions ranging from 3 % to 27 %. These results highlight potential energy and environmental advantages of producing tool steel powder over traditional steel plate production.

Rather than manufacturing a new tool entirely, the remanufacturing process focused on surface modifications, with 10 % of the tool mass removed via CNC machining, 10 % re-deposited using DED, and 10 % finish-machined. Fig. 34c shows that while the remanufacturing process consumed 12 GJ of energy, this is less than half the energy required to produce the tool steel for a new tool. This approach offers both environmental savings and substantial economic advantages.

Regarding an automotive engine producing die, Bennett et al. [209] applied a hybrid repair process to overcome the limitations of traditional TIG welding repairs, which restore dies to only 20.8 % of their original operational life before necessitating further repair. The process involves machining away damaged die areas and reconstructing them by DED. The DED-repaired dies exhibit lifespans equivalent to the original dies, effectively eliminating the need for emergency repairs and reducing unscheduled production downtime. Comparative life cycle analyses between the traditional TIG welding repair and the DED repair process demonstrate that the DED method significantly decreases environmental impacts across most evaluated categories. The significant potential of DED for reducing energy consumption, emissions, and costs by enabling tooling repair and remanufacturing has been also noted by other researchers [207].

7. Recent Advances and future trends

7.1. Approaches and innovations in tool steel AM

The use of AM for producing steel parts remains still limited due to some concerns about the properties, particularly ductility, along with variability in material properties and anisotropy. These challenges stem from internal defects, inhomogeneity of the microstructure, residual stresses, and the presence of brittle phases such as carbide networks and martensite containing high amounts of C. To address these issues, several methods have been suggested, including optimization of processing parameters, real-time monitoring, preheating the substrate, as well as utilizing hybrid techniques and applying post-processing processes.

To enhance the quality of steel parts, optimizing processing parameters is the initial approach. In addition to parameter optimization, process monitoring and control play a crucial role in ensuring dimensional accuracy and part quality. However, challenges such as residual stress, part deformation, micro-pores, cracks, and anisotropic properties cannot be entirely resolved through parameter adjustments alone. To address these issues, various techniques, including substrate and powder preheating, post-processing, and hybrid methods, have been developed [140,146,181,192,210,211].

One of the key advantages of AM in the tooling industry is its capability of fabricating conformal cooling molds. They are designed with curved cooling channels that closely follow the shape of the part being molded. This design can decrease injection molding cycle times by 10 % to 40 % [212]. Cortina [213] explored the use of DED to improve hot stamping tools by enhancing heat transfer and cooling efficiency. Conformal cooling channels manufactured via DED were compared with conventional straight channels, showing improved performance and reduced cycle times, with more uniform temperature distribution. Additionally, the research investigated the creation of bimetallic tools

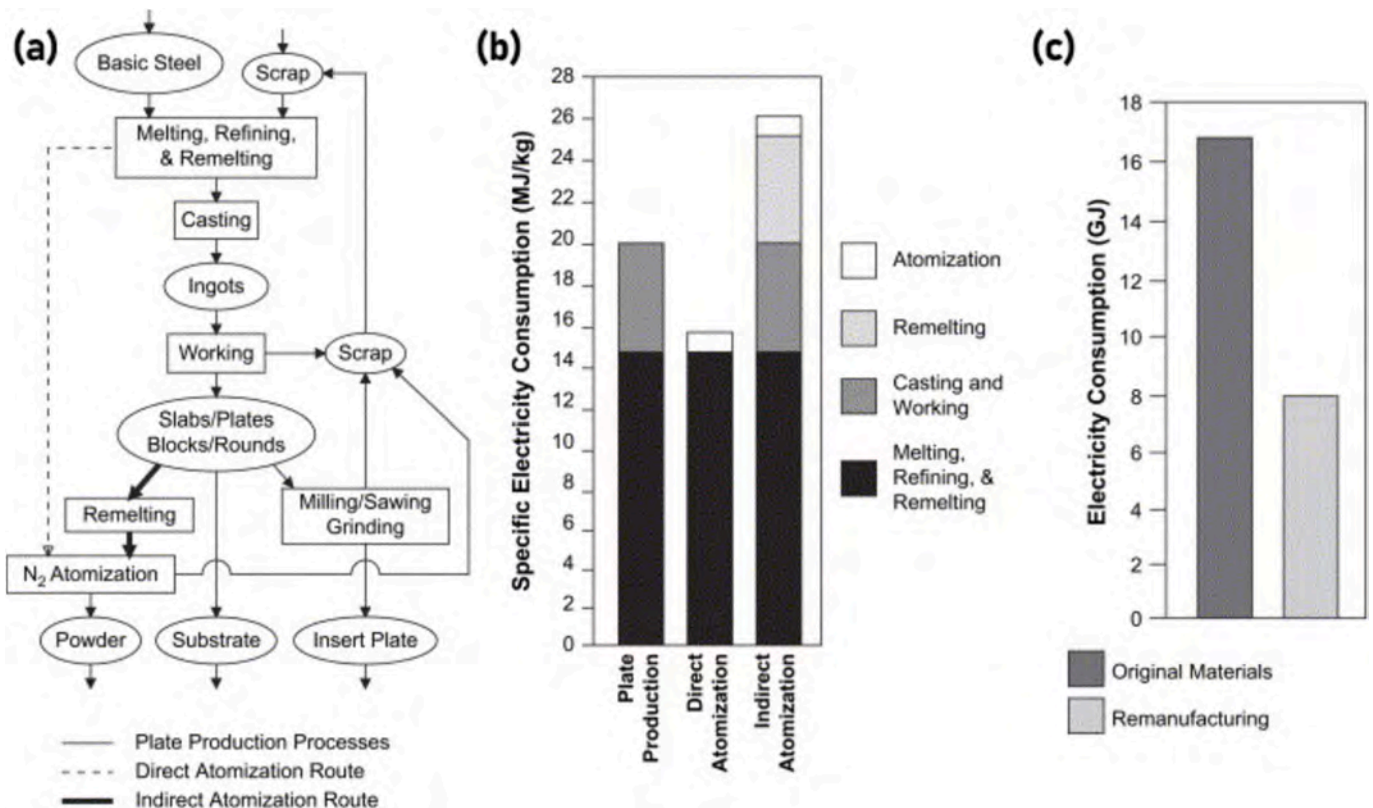


Fig. 34. a) Feedstock material production pathways for conventional manufacturing and ded, b) specific energy consumption of these pathways, and c) energy consumption of remanufacturing and virgin material manufacturing [207] (Reproduced with permission from © Elsevier, all rights reserved).

by coating high thermal conductivity steel with H13 (Fig. 35), resulting in a 44.5 % cycle time reduction compared to conventional H13 tools. However, DED-deposited AISI H13 was found to have lower thermal conductivity than cast H13, affecting the overall efficiency.

This bimetallic approach in the tooling industry has been investigated by other researchers as well. Enhancing the surface properties of H13 tool steel has been the focus of several studies aiming to improve its performance in high-temperature applications. Titanium carbide (TiC) has been widely deposited onto the H13 steel matrix to increase its wear and corrosion resistance [214,215]. It is reported that higher TiC content enhances hardness and wear resistance of the coated steel. However, an increase in TiC content inversely affects the material's ductility, highlighting a trade-off between hardness and ductility [216]. To improve the adhesion between TiC coatings and the steel substrate, the incorporation of nickel/chromium alloys has also been explored [217]. These findings contribute to the development of surface modification techniques for extending the service life of H13 steel components in demanding environments.

Additionally, bimetallic tools have been effectively utilized to enhance energy efficiency, reduce environmental impact, and optimize material usage in the production of mold and dies. While H13 tool steel is commonly used, its low thermal conductivity leads to longer manufacturing cycle times. To mitigate this drawback, highly conductive materials such as copper alloys have been employed as volumetric heat sinks to improve thermal performance [207,218]. The study by Morrow et al. [207] has shown that coating a copper substrate with H13 can decrease injection molding cycle times by about 25 % compared to traditional tool steel molds. Nonetheless, integrating copper with steel substrates presents challenges due to their differing material properties reported by Noecker et al. [219] and Beal et al. [143].

7.2. Hybrid manufacturing techniques

Hybrid manufacturing involves combining multiple processes, such as subtractive and additive techniques, within a single machine. This integrated approach offers an optimal industrial solution for producing or repairing intricate components. By merging different processes with complementary strengths, hybrid manufacturing mitigates the limitations of individual methods, thereby improving overall efficiency and competitiveness [220].

Recently, studies have shown that by combining arc-based DED process with 5-axis CNC machining repairing of different tooling materials, such as H13 [181,209,210,221,222], can be done providing strong bonding along the deposition interface and mechanical properties comparable to the parent material.

One of the other hybrid processes is the combination of AM with rolling deformation, where a micro roller is moved behind the AM energy source and the material is rolled just after being deposited, as shown in Fig. 36.

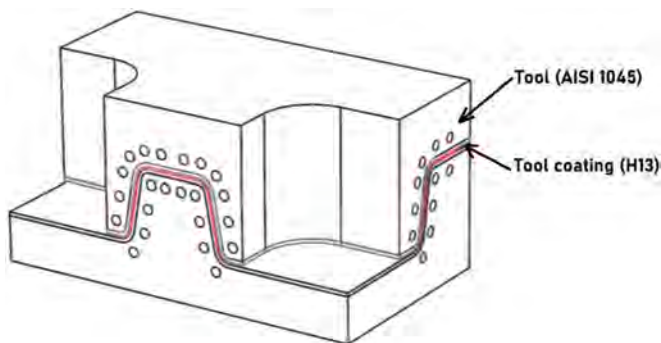


Fig. 35. Schematic illustration of the bimetallic hot stamping tool with conformal cooling channels [213] (Reproduced under CC BY-NC-SA licence).

It is stated that this process can improve the distortion control, provide more control on the dimensional accuracy, help releasing internal stresses, refine grain structure, and reduce the porosity content [224–226]. Although this method has not yet been used for tool steel processing, it shows great potential for advancing this field.

7.3. Automation and in-situ monitoring

The evolution of AM technology has expanded its applications from mere part production to encompassing repair and restoration processes. Researchers advocate for the deployment of automated systems in critical repair tasks to mitigate challenges and enhance remanufacturing efficiency [227–229]. The integration of artificial intelligence (AI) in AM offers significant benefits, including increased efficiency, failure prediction, error detection, reduced processing time, and the ability to handle intricate designs more effectively than traditional methods [230]. The implementation of robotic AM systems for the maintenance and repair has been discussed by French et al. [231], aiming to preserve parts' functionality and long-term reliability. It is mentioned that adaptive robotic systems can adjust to changes in repair processes, resulting in improved quality control and higher success rates.

Additionally, deep learning techniques have been employed to address geometric accuracy challenges in DED process, enabling accurate prediction and correction of distortions during part fabrication [232]. These advancements highlight the transformative potential of AI and automation in optimizing repair and remanufacturing processes in the tooling industry.

8. Summary and outlook

The application of AM, particularly DED and PBF, in the fabrication and repair of tool steels has shown remarkable potential, as highlighted in this review. Tool steels, known for their high hardness and wear resistance, are indispensable in industries requiring high-performance components, such as die-casting, forging, stamping, and machining. This review presented an overview of current research on high-performance steels produced, both production and repair, via AM, emphasizing the interplay between microstructure, mechanical properties, and processing techniques. It has been seen that significant progress has been made over the past decade. For components like molds used in injection molding, conformal cooling channels created through AM provide more efficient heat management than traditional straight channels. Additionally, AM's ability in repairing to reduce material waste, extend component lifespans, and shorten downtime has broad implications for cost savings and environmental impact.

Despite these advantages, AM in tool steel faces challenges, primarily related to variability in mechanical properties, microstructural anisotropy, and limited processability. Issues such as porosity, cracking, and residual stresses remain obstacles, particularly in high-carbon steels where brittleness can be pronounced. Preheating the substrate, refining alloy compositions, and optimizing laser or electron beam parameters are critical strategies to mitigate these issues. However, achieving uniform properties across complex geometries and maintaining consistency in repair quality demand advanced in-situ monitoring and control. Additionally, there is a need to standardize post-processing heat treatments to enhance microstructural homogeneity and improve mechanical properties. The development of real-time, automated monitoring systems is crucial, as it could allow for immediate parameter adjustments, ensuring that the repaired regions meet the required performance standards.

Several trends and research directions are likely to shape the future of AM in tool steel fabrication and repair. The combination of AM with traditional methods such as CNC machining and rolling, as well as bimetallic tool fabrication, are emerging as promising approaches for complex fabrication and repairs. These techniques allow for high-precision post-processing and better surface finish, which can enhance

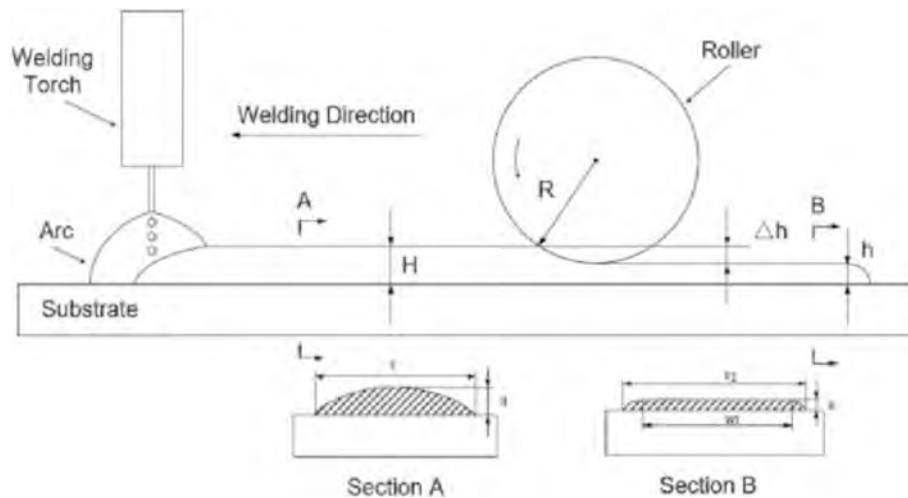


Fig. 36. Schematic setup of the hybrid method combining AM and rolling processes [223] (Reproduced with permission from © Elsevier, all rights reserved).

the durability and functionality of components.

Alloy design for AM should focus on tool-steel chemistries optimized for AM performance, aiming to improve weldability, reduce hot-crack susceptibility, and better control carbide-forming behavior, including the development of low-carbon variants of common tool steels and maraging-inspired compositions. While much published data comes from coupon specimens, there is a pressing need to study large-scale die and mold geometries to understand how scale affects residual stresses and distortion. To ensure comparability across studies, standardized protocols for property qualification are required, including consistent coupon dimensions and orientations, uniform test conditions for tensile, fatigue, and wear, and transparent reporting of powder reuse and oxygen content. Process-aware modeling and closed-loop control strategies should be pursued by coupling melt-pool thermal models with in-situ sensing and machine learning to reduce variability and prevent defect formation.

The adoption of artificial intelligence and machine learning in AM processes is expected to play a pivotal role in optimizing process parameters. Machine learning models can be trained on extensive datasets from AM repairs, helping predict optimal parameter sets for different materials and geometries. This advancement can lead to more consistent results, reducing trial-and-error in parameter selection and enhancing the predictability of outcomes.

Additionally, more comprehensive techno-economic and life-cycle assessments are needed, featuring real-world case studies that compare repair versus replacement while accounting for machine energy, powder and consumables, operator skill, and downtime to support broader industrial adoption. Environmental concerns are driving an increased focus on sustainable manufacturing practices. AM repair processes already contribute to sustainability by extending the lifecycle of parts, but more work may need to be done on the use of recycled powders from damaged or end-of-life components as feedstock material. This approach not only reduces waste but also lowers the overall carbon footprint of manufacturing and repair processes.

In summary, AM for tool steel in fabrication and repair represents a transformative shift in manufacturing and maintenance, offering precision, efficiency, and significant sustainability benefits. While technical challenges remain, the outlook is promising as innovations in hybrid approaches and sustainable practices continue to evolve, enhancing productivity, cost-effectiveness, and environmental stewardship.

CRediT authorship contribution statement

Mohammad Saleh Kenevisi: Writing – original draft, Methodology, Investigation, Conceptualization. **Federico Simone Gobber:** Writing –

original draft, Conceptualization. **Paolo Fino:** Supervision. **Mariangela Lombardi:** Supervision. **Federica Bondioli:** Supervision. **Sara Biamino:** Supervision, Conceptualization. **Daniele Ugues:** Writing – review & editing, Supervision, Conceptualization.

Declaration of competing interest

The authors declare that they have no known competing financial interests or personal relationships that could have appeared to influence the work reported in this paper.

Data availability

No data was used for the research described in the article.

References

- [1] L. Dash, S. Padhan, S.R. Das, Experimental investigations on surface integrity and chip morphology in hard turning of AISI D3 steel under sustainable nanofluid-based minimum quantity lubrication, *J. Braz. Soc. Mech. Sci. Eng.* 42 (2020) 500, <https://doi.org/10.1007/s40430-020-02594-x>.
- [2] P. Stavropoulos, *Additive Manufacturing: Design, Processes and Applications*, Springer International Publishing, Cham, 2023, 10.1007/978-3-031-33793-2.
- [3] J.R. Davis, ed., *Metals Handbook Desk Edition*, ASM International, 1998, 10.31399/asm.hb.mhde.2.9781627081993.
- [4] F.R. Cruz, N. Alves, T. Vieira, Direct additive manufacturing as spring of new tool steels, *J. Mater. Res. Technol.* 26 (2023) 5450–5461, <https://doi.org/10.1016/j.jmrt.2023.08.176>.
- [5] N. Porevopoulos, K. Tzimanis, T. Souflas, H. Bikas, V.C. Panagiotopoulou, P. Stavropoulos, Decision support for repair with DED AM processes based on sustainability and techno-economical evaluation, *Procedia CIRP* 130 (2024) 9–14, <https://doi.org/10.1016/J.PROCIR.2024.10.048>.
- [6] A. Bohlen, H. Freife, M. Hunkel, F. Vollertsen, Additive manufacturing of tool steel by laser metal deposition, in: *Procedia CIRP*, Elsevier B.v., 2018, pp. 192–195, 10.1016/j.procir.2018.08.092.
- [7] A. Vogelpoth, J. Saewe, H.G. Krull, S. Richert, P. Weiland, T. Nerzak, F. Eibl, F. Pastors, Additive manufacturing of tool steels, *Steel Res. Int.* 94 (2023), <https://doi.org/10.1002/srin.202200372>.
- [8] H. Freife, Additive manufacturing of a deep drawing tool by direct laser deposition, *Dry Met. Forming OAJ* (2015) 5–10.
- [9] K. Chantziara, D. Nikas, J. Bergström, M. Grehk, M. Pappa, N. Michailidis, High and very high cycle fatigue behavior of an additive manufactured hot-work tool steel, *Mater. Sci. Eng. A* (2024) 147401, <https://doi.org/10.1016/J.MSEA.2024.147401>.
- [10] M. Kenevisi, P. Martelli, F. Gobber, D. Ugues, S. Biamino, Processability of K340 Cold work tool steel by directed energy deposition technique, *IOP Conf. Ser.: Mater. Sci. Eng.* 1310 (2024) 012021, <https://doi.org/10.1088/1757-899X/1310/1/012021>.
- [11] R.A. Mesquita, ed., *Tool Steels*, CRC Press, 2016, 10.1201/9781315181516.
- [12] A. Kirchner, B. Klöden, M. Franke-Jurisch, L. Inarra Rauh-Hain, T. Weißgärber, Manufacturing of Tool Steels by PBF-EB, *Metals (basel)* 11 (2021), <https://doi.org/10.3390/met11101640>.

- [13] S.A. Elghazaly, Innovations in cold work tool steels- research and development, *Int. J. Mater. Technol. Innov.* 3 (2023) 64–73, <https://doi.org/10.21608/ijmti.2023.198375.1080>.
- [14] X. Wang, Y. Chen, S. Wei, L. Zuo, F. Mao, Effect of carbon content on abrasive impact wear behavior of Cr-Si-Mn low alloy wear resistant cast steels, *Front. Mater.* 6 (2019), <https://doi.org/10.3389/fmats.2019.00153>.
- [15] E. Kocaman, B. Kılınc, M. Durmaz, Ş. Şen, U. Şen, The influence of chromium content on wear and corrosion behavior of surface alloyed steel with Fe(16-x)Cr_x(B,C)4 electrode, *Eng. Sci. Technol., Int. J.* 24 (2021) 533–542, <https://doi.org/10.1016/j.jestech.2020.08.003>.
- [16] X. Wu, P. Xiao, S. Wu, C. Yan, X. Ma, Z. Liu, W. Chen, L. Zhu, Q. Zhang, Effect of molybdenum on the impact toughness of heat-affected zone in high-strength low-alloy steel, *Materials* 14 (2021), <https://doi.org/10.3390/ma14061430>.
- [17] M. Zhuang, Q. Liu, X. Li, Y. Ren, X. Liu, Y. Yan, S. Yuan, P. Lv, Z. Ma, Effect of manganese and vanadium additions on the microstructures and two-body abrasive wear behaviors of Fe-B hardfacing alloys, *Intermetallics (barking)* 169 (2024) 108309, <https://doi.org/10.1016/j.intermet.2024.108309>.
- [18] S. Prifihami, S. Moch, A. Anwar, E.M. Nikitasari, The hardness, microstructure, and pitting resistance of austenitic stainless steel Fe25Ni15Cr with the addition of tungsten, niobium, and vanadium, *AIP Conf. Proc.* 1964 (2018) 020041, <https://doi.org/10.1063/1.5038323>.
- [19] Abdul Rahim Mohd Aidil Shah bin, Minhat Mohamad bin, Hussein Nur Izan Syahriah Binti, Salleh Mohd Shukor bin, A comprehensive review on cold work of AISI D2 tool steel, *Metall. Res. Technol.* 115 (2018) 104, 10.1051/metal/2017048.
- [20] E. Aslan, Experimental investigation of cutting tool performance in high speed cutting of hardened X210 Cr12 cold-work tool steel (62 HRC), *Mater. Des.* 26 (2005) 21–27, <https://doi.org/10.1016/J.MATDES.2004.04.004>.
- [21] P. Niederhofer, K. Eger, P. Schwingenschlögl, M. Merklein, Properties of tool steels for application in hot stamping, *Steel Res. Int.* 91 (2020) 1900422, <https://doi.org/10.1002/srin.201900422>.
- [22] S. Al-qawabah, A. Mostafa, A. Al-Rawajfeh, U. Al-Qawabeha, Effect of heat treatment on the grain size, microhardness and corrosion behavior of the cold-working tool steels AISI D2 and AISI O1, *Materiali in Tehnologije* 54 (2020) 785–790, 10.17222/mit.2020.035.
- [23] L.-Å. Norström, N. Öhrberg, Development of hot-work tool steel for high-temperature applications, *Metals Technol.* 8B (1981) 22–26, <https://doi.org/10.1179/030716981803275857>.
- [24] voestalpine Böhler Edelstahl BmbH & Co KG, BÖHLER Hot Work Tool Steel, 2018.
- [25] M. Shibuya, Y. Toda, K. Sawada, H. Kushima, K. Kimura, Effect of nickel and cobalt addition on the precipitation-strength of 15Cr ferritic steels, *Mater. Sci. Eng. A* 528 (2011) 5387–5393, <https://doi.org/10.1016/J.MSEA.2011.03.088>.
- [26] W.M. Garrison, Cobalt and the toughness of steel, *Mater. Sci. Forum* 710 (2012) 3–10, <https://doi.org/10.4028/www.scientific.net/MSF.710.3>.
- [27] F. Deirmina, L. Quarzago, D. Butcher, E. Bettini, S. Mehraban, J. Hann, N. Holländer Pettersson, N. Lavery, A. Röttger, M. Pellizzari, General investigations on the heat treatment and thermal fatigue behavior of an experimental hot work tool steel tailored for laser powder bed fusion, *Mater. Sci. Eng. A* 901 (2024) 146554, <https://doi.org/10.1016/J.MSEA.2024.146554>.
- [28] S. Naimi, S.M. Hosseini, Tool steels in die-casting utilization and increased mold life, *Adv. Mech. Eng.* 7 (2015) 286071, <https://doi.org/10.1155/2014/286071>.
- [29] K.D. Fuchs, Hot-work tool steels with improved properties for die casting applications, in: *Proceedings of the 6th International Tooling Conference, 2002*, pp. 15–22.
- [30] R. Shivpuri, Dies and Die Materials for Hot Forging, in: S.L. Semiatin (Ed.), *Metalworking: Bulk Forming*, ASM International, 2005, 10.31399/asm.hb.v14a.a0003975.
- [31] C.M.D. Starling, J.R.T. Branco, Thermal fatigue of hot work tool steel with hard coatings, *Thin Solid Films* 308–309 (1997) 436–442, [https://doi.org/10.1016/S0040-6090\(97\)00600-7](https://doi.org/10.1016/S0040-6090(97)00600-7).
- [32] M. Boccacini, H. Goldenstein, Solidification of high speed steels, *Int. Mater. Rev.* 46 (2001) 92–115, <https://doi.org/10.1179/095066001101528411>.
- [33] T. Kvackaj, J. Bidulská, R. Bidulský, Overview of HSS steel grades development and study of reheating condition effects on austenite grain size changes, *Materials* 14 (2021), <https://doi.org/10.3390/ma14081988>.
- [34] M.A. Gomes, C.S. Wright, A.S. Wronski, Strength and toughness of sintered plus forged T1 high speed steel, *J. Mater. Sci.* 32 (1997) 1799–1807, <https://doi.org/10.1023/A:1018592404209>.
- [35] R. Komanduri, Cutting-tool materials, *encyclopedia of materials*, *Sci. Technol.* (2001) 1–13, <https://doi.org/10.1016/B0-08-043152-6/00353-3>.
- [36] Y. Wang, B. Mao, S. Chu, S. Chen, H. Xing, H. Zhao, S. Wang, Y. Wang, J. Zhang, B. Sun, Advanced manufacturing of high-speed steels: a critical review of the process design, microstructural evolution, and engineering performance, *J. Mater. Res. Technol.* 24 (2023) 8198–8240, <https://doi.org/10.1016/j.jmrt.2023.04.269>.
- [37] D. Chen, X. Xu, Y. Zhao, X. Fu, L. Wei, Y. Zhou, Z. Wu, Superior mechanical properties of M35 high-speed steel obtained by controlling carbide precipitation and distribution via electropulsing treatment, *Mater. Sci. Eng. A* 888 (2023) 145691, <https://doi.org/10.1016/J.MSEA.2023.145691>.
- [38] B. Yang, X. Xiong, R. Liu, J. Chen, J. Yang, H. Luan, Effect of yttrium hydride addition on microstructure and properties of powder metallurgy CM2 high speed steel, *J. Mater. Res. Technol.* 14 (2021) 1275–1283, <https://doi.org/10.1016/J.JMRT.2021.07.056>.
- [39] J. Schlegel, Manufacturing Processes, in: J. Schlegel (Ed.), *The World of Steel: On the History, Production and Use of a Basic Material*, Springer Fachmedien Wiesbaden, Wiesbaden, 2023, pp. 297–355, 10.1007/978-3-658-39733-3_8.
- [40] W. Theisen, Tools for processing materials, in: H. Berns, W. Theisen (Eds.), *Ferrous Materials: Steel and Cast Iron*, Springer, Berlin Heidelberg, Berlin, Heidelberg, 2008, pp. 271–305, https://doi.org/10.1007/978-3-540-71848-2_9.
- [41] P. Jovičević-Klug, G. Puš, M. Jovičević-Klug, B. Žužek, B. Podgornik, Influence of heat treatment parameters on effectiveness of deep cryogenic treatment on properties of high-speed steels, *Mater. Sci. Eng. A* 829 (2022) 142157, <https://doi.org/10.1016/j.msea.2021.142157>.
- [42] M. Orečný, P. Frankovský, P. Lacková, M. Bursák, Increase of tool steel durability in abrasion wear conditions, *Appl. Mech. Mater.* 611 (2014) 424–429, <https://doi.org/10.4028/www.scientific.net/AMM.611.424>.
- [43] M. Yuan, L. Nyborg, C. Oikonomou, Y. Fan, L. Liu, J.W. Ye, Y. Cao, Comparison of softening behavior and abrasive wear resistance between conventionally and additively manufactured tool steels, *Steel Res. Int.* 95 (2024) 2300577, <https://doi.org/10.1002/srin.202300577>.
- [44] M. Orečný, M. Bursák, M. Šebek, L. Falat, Influence of hardness, matrix and carbide in combination with nitridation on abrasive wear resistance of X210Cr12 tool steel, *Metals (basel)* 6 (2016), <https://doi.org/10.3390/met6100236>.
- [45] S. Hogmark, O. Vingsbo, Adhesive mechanisms in the wear of some tool steels, *Wear* 38 (1976) 341–359, [https://doi.org/10.1016/0043-1648\(76\)90081-8](https://doi.org/10.1016/0043-1648(76)90081-8).
- [46] G.A. Fontalvo, R. Humer, C. Mitterer, K. Sammt, I. Schemmel, Microstructural aspects determining the adhesive wear of tool steels, *Wear* 260 (2006) 1028–1034, <https://doi.org/10.1016/J.WEAR.2005.07.001>.
- [47] J. Krawczyk, A. Łukaszek-Sotek, T. Śleboda, Ł. Lisiecki, M. Bembenek, J. Cieślak, T. Góral, J. Pawlik, Tool wear issues in hot forging of steel, *Materials* 16 (2023), <https://doi.org/10.3390/ma16020471>.
- [48] K. Fukaura, Y. Yokoyama, D. Yokoi, N. Tsujii, K. Ono, Fatigue of cold-work tool steels: effect of heat treatment and carbide morphology on fatigue crack formation, life, and fracture surface observations, *Metall. Mater. Trans. A* 35 (2004) 1289–1300, <https://doi.org/10.1007/s11661-004-0303-5>.
- [49] Y. An Min, B. Jens, X. Chun Wu, L. Ping Xu, Oxidation and thermal fatigue behaviors of two type hot work steels during thermal cycling, *J. Iron Steel Res. Int.* 20 (2013) 90–97, [https://doi.org/10.1016/S1006-706X\(13\)60202-2](https://doi.org/10.1016/S1006-706X(13)60202-2).
- [50] F. Delaunois, V.I. Stanciu, A. Megret, M. Sinnaeve, Oxidation and wear behavior of high-speed steel and semi-high-speed steel used in hot strip mill, *Int. J. Adv. Manuf. Technol.* 119 (2022) 677–689, <https://doi.org/10.1007/s00170-021-08031-0>.
- [51] A. Medvedeva, J. Bergström, S. Gunnarsson, J. Andersson, High-temperature properties and microstructural stability of hot-work tool steels, *Mater. Sci. Eng. A* 523 (2009) 39–46, <https://doi.org/10.1016/J.MSEA.2009.06.010>.
- [52] C. Imbert, N.D. Ryan, H.J. McQueen, Hot workability of three grades of tool steel, *Metall. Trans. A* 15 (1984) 1855–1864, <https://doi.org/10.1007/BF02664899>.
- [53] S. Feng, A.M. Kamat, Y. Pei, Design and fabrication of conformal cooling channels in molds: Review and progress updates, *Int. J. Heat Mass Transf.* 171 (2021) 121082, <https://doi.org/10.1016/J.IJHEATMASSTRANSFER.2021.121082>.
- [54] G. Agrawal, M.K. Khare, Material and energy wastes minimization in a machining system: a review, *J. Mater. Environ. Sci.* 4 (2013) 251–256.
- [55] A. Aprilia, N. Wu, W. Zhou, Repair and restoration of engineering components by laser directed energy deposition, *Mater. Today Proc.* 70 (2022) 206–211, <https://doi.org/10.1016/J.MATPR.2022.09.022>.
- [56] C.P. Paul, A.N. Jinoop, A. Kumar, K.S. Bindra, Laser-based metal additive manufacturing: technology, global scenario and our experiences, *Trans. Indian Natl. Acad. Eng.* 6 (2021) 895–908, <https://doi.org/10.1007/s41403-021-00228-9>.
- [57] I. Gibson, D. Rosen, B. Stucker, Directed energy deposition processes, in: I. Gibson, D. Rosen, B. Stucker (Eds.), *Additive Manufacturing Technologies: 3D Printing, Rapid Prototyping, and Direct Digital Manufacturing*, Springer New York, New York, NY, 2015, pp. 245–268, https://doi.org/10.1007/978-1-4939-2113-3_10.
- [58] H. Fayazfar, M. Salarian, A. Rogalsky, D. Sarker, P. Russo, V. Paserin, E. Toyserkani, A critical review of powder-based additive manufacturing of ferrous alloys: process parameters, microstructure and mechanical properties, *Mater. Des.* 144 (2018) 98–128, <https://doi.org/10.1016/J.MATDES.2018.02.018>.
- [59] M. Armstrong, H. Mehrabi, N. Naveed, An overview of modern metal additive manufacturing technology, *J. Manuf. Process.* 84 (2022) 1001–1029, <https://doi.org/10.1016/J.JMAPRO.2022.10.060>.
- [60] P. Bajaj, A. Hariharan, A. Kini, P. Kürnsteiner, D. Raabe, E.A. Jäggle, Steels in additive manufacturing: a review of their microstructure and properties, *Mater. Sci. Eng. A* 772 (2020) 138633, <https://doi.org/10.1016/J.MSEA.2019.138633>.
- [61] P. Bidare, A. Jiménez, H. Hassanin, K. Essa, Porosity, cracks, and mechanical properties of additively manufactured tooling alloys: a review, *Adv. Manuf.* 10 (2022) 175–204, <https://doi.org/10.1007/s40436-021-00365-y>.
- [62] T. Kelliger, M. Meurer, T. Bergs, Potentials of additive manufacturing for cutting tools: a review of scientific and industrial applications, *Metals (basel)* 14 (2024), <https://doi.org/10.3390/met14090982>.
- [63] M. Narvan, K.S. Al-Rubaie, M. Elbestawi, Process-structure-property relationships of AISI H13 tool steel processed with selective laser melting, *Materials* 12 (2019), <https://doi.org/10.3390/ma12142284>.
- [64] A.T. Silvestri, P. Bosetti, A. Squillace, Laser-directed energy deposition of H13: processing window and improved characterization procedures, *Mater. Manuf. Process.* 38 (2023) 1770–1784, <https://doi.org/10.1080/10426914.2023.2219302>.

- [65] M. Wang, W. Li, Y. Wu, S. Li, C. Cai, S. Wen, Q. Wei, Y. Shi, F. Ye, Z. Chen, High-temperature properties and microstructural stability of the AISI H13 hot-work tool steel processed by selective laser melting, *Metall. Mater. Trans. B* 50 (2019) 531–542, <https://doi.org/10.1007/s11663-018-1442-1>.
- [66] S.M. Tawfik Abdallah Omar, Additive Manufacturing of AISI D2 Tool Steel Using Directed Energy Deposition, Dalhousie University, 2023.
- [67] J.H. Park, K.S. Kim, J.Y. Kim, J.B. Jeon, Y.M. Koo, K.A. Lee, Microstructure and tensile properties of bulk AISI D2 tool steel fabricated by direct energy deposition, *Mater. Charact.* 194 (2022) 112355, <https://doi.org/10.1016/j.MATCHAR.2022.112355>.
- [68] S. Yadav, K. Dileep, A.N. Jinoop, C.P. Paul, A.K. Rai, R. Singh, K.S. Bindra, Laser directed energy deposition of high-carbon high-chromium D2 tool steel structures: processing, heat treatment and material behavior, *J. Mater. Eng. Perform.* 32 (2023) 4881–4891, <https://doi.org/10.1007/s11665-022-07470-4>.
- [69] M. Zhang, C. Chen, L. Qin, K. Yan, G. Cheng, H. Jing, T. Zou, Laser additive manufacturing of M2 high-speed steel, *Mater. Sci. Technol.* 34 (2018) 69–78, <https://doi.org/10.1080/02670836.2017.1355584>.
- [70] Z.H. Liu, D.Q. Zhang, C.K. Chua, K.F. Leong, Crystal structure analysis of M2 high speed steel parts produced by selective laser melting, *Mater. Charact.* 84 (2013) 72–80, <https://doi.org/10.1016/j.MATCHAR.2013.07.010>.
- [71] K. Kempen, B. Vrancken, S. Buls, L. Thijs, J. Van Humbeeck, J.-P. Kruth, Selective laser melting of crack-free high density M2 high speed steel parts by baseplate preheating, *J. Manuf. Sci. Eng.* 136 (2014), <https://doi.org/10.1115/1.4028513>.
- [72] J. Sander, J. Hufenbach, L. Giebeler, H. Wendrock, U. Kühn, J. Eckert, Microstructure and properties of FeCrMoVC tool steel produced by selective laser melting, *Mater. Des.* 89 (2016) 335–341, <https://doi.org/10.1016/j.MATDES.2015.09.148>.
- [73] G.N. Levy, R. Schindel, P. Schleiss, F. Micari, L. Fratini, On the use of SLS Tools in Sheet Metal Stamping, *CIRP Ann.* 52 (2003) 249–252, [https://doi.org/10.1016/S0007-8506\(07\)60577-0](https://doi.org/10.1016/S0007-8506(07)60577-0).
- [74] J. Minguella-Canela, S. Morales Planas, V.C. de Medina Iglesias, M.A. de los Santos López, Quantitative analysis of the effects of incorporating laser powder bed fusion manufactured conformal cooling inserts in steel moulds over four types of defects of a commercially produced injected part, *J. Mater. Res. Technol.* 23 (2023) 5423–5439, <https://doi.org/10.1016/j.JMRT.2023.02.164>.
- [75] T. DebRoy, H.L. Wei, J.S. Zuback, T. Mukherjee, J.W. Elmer, J.O. Milewski, A. M. Beese, A. Wilson-Heid, A. De, W. Zhang, Additive manufacturing of metallic components – Process, structure and properties, *Prog. Mater. Sci.* 92 (2018) 112–224, <https://doi.org/10.1016/j.pmatsci.2017.10.001>.
- [76] B. Ren, D. Lu, R. Zhou, Z. Li, J. Guan, Preparation and mechanical properties of selective laser melted H13 steel, *J. Mater. Res.* 34 (2019) 1415–1425, <https://doi.org/10.1557/jmr.2019.10>.
- [77] J. Lee, J. Choe, J. Park, J.H. Yu, S. Kim, I.D. Jung, H. Sung, Microstructural effects on the tensile and fracture behavior of selective laser melted H13 tool steel under varying conditions, *Mater. Charact.* 155 (2019) 109817, <https://doi.org/10.1016/j.MATCHAR.2019.109817>.
- [78] A. Simchi, H. Asgharzadeh, Densification and microstructural evaluation during laser sintering of M2 high speed steel powder, *Mater. Sci. Technol.* 20 (2004) 1462–1468, <https://doi.org/10.1179/026708304X3944>.
- [79] J. Boes, A. Röttger, C. Mutke, C. Escher, W. Theisen, Microstructure and mechanical properties of X65MoCrWV3-2 cold-work tool steel produced by selective laser melting, *Addit. Manuf.* 23 (2018) 170–180, <https://doi.org/10.1016/j.addma.2018.08.005>.
- [80] J.J. Yan, D.L. Zheng, H.X. Li, X. Jia, J.F. Sun, Y.L. Li, M. Qian, M. Yan, Selective laser melting of H13: microstructure and residual stress, *J. Mater. Sci.* 52 (2017) 12476–12485, <https://doi.org/10.1007/s10853-017-1380-3>.
- [81] K. Trojan, V. Ocelík, J. Capek, J. Čech, D. Canelo-Yubero, N. Ganev, K. Kolařík, J. T.M. De Hosson, Microstructure and mechanical properties of laser additive manufactured H13 tool steel, *Metals (basel)* 12 (2022), <https://doi.org/10.3390/met12020243>.
- [82] J.S. Park, J.H. Park, M.-G. Lee, J.H. Sung, K.J. Cha, D.H. Kim, Effect of energy input on the characteristic of AISI H13 and D2 tool steels deposited by a directed energy deposition process, *Metall. Mater. Trans. A* 47 (2016) 2529–2535, <https://doi.org/10.1007/s11661-016-3427-5>.
- [83] H. Chandler, *Heat Treater's Guide: Practices and Procedures for Irons and Steels, 2nd ed.*, ASM International, 1995.
- [84] D. Bourell, J.P. Kruth, M. Leu, G. Levy, D. Rosen, A.M. Beese, A. Clare, Materials for additive manufacturing, *CIRP Ann. Manuf. Technol.* 66 (2017) 659–681, <https://doi.org/10.1016/j.cirp.2017.05.009>.
- [85] Y. Bai, Y. Yang, D. Wang, M. Zhang, Influence mechanism of parameters process and mechanical properties evolution mechanism of maraging steel 300 by selective laser melting, *Mater. Sci. Eng. A* 703 (2017) 116–123, <https://doi.org/10.1016/j.MSEA.2017.06.033>.
- [86] C. Tan, K. Zhou, W. Ma, P. Zhang, M. Liu, T. Kuang, Microstructural evolution, nanoprecipitation behavior and mechanical properties of selective laser melted high-performance grade 300 maraging steel, *Mater. Des.* 134 (2017) 23–34, <https://doi.org/10.1016/j.MATDES.2017.08.026>.
- [87] M.A. Kottman, Additive Manufacturing of Maraging 250 Steels for the Rejuvenation and Repurposing of Die Casting Tooling, 2014. http://rave.ohiolink.edu/etdc/view?acc_num=cas1416854466.
- [88] M. Cabeza, G. Castro, P. Merino, G. Pena, M. Román, Laser surface melting: a suitable technique to repair damaged surfaces made in 14 Ni (200 grade) maraging steel, *Surf. Coat. Technol.* 212 (2012) 159–168, <https://doi.org/10.1016/J.SURFcoat.2012.09.039>.
- [89] G. Casalino, S.L. Campanelli, N. Contuzzi, A.D. Ludovico, Experimental investigation and statistical optimisation of the selective laser melting process of a maraging steel, *Opt. Laser Technol.* 65 (2015) 151–158, <https://doi.org/10.1016/J.OPTLASTEC.2014.07.021>.
- [90] C. Tan, K. Zhou, M. Kuang, W. Ma, T. Kuang, Microstructural characterization and properties of selective laser melted maraging steel with different build directions, *Sci. Technol. Adv. Mater.* 19 (2018) 746–758, <https://doi.org/10.1080/14686996.2018.1527645>.
- [91] S.L. Campanelli, A. Angelastro, C.G. Signorile, G. Casalino, Investigation on direct laser powder deposition of 18 Ni (300) marage steel using mathematical model and experimental characterisation, *Int. J. Adv. Manuf. Technol.* 89 (2017) 885–895, <https://doi.org/10.1007/s00170-016-9135-x>.
- [92] E.A. Jägge, Z. Sheng, P. Kürnstner, S. Ocylok, A. Weisheit, D. Raabe, Comparison of maraging steel micro- and nanostructure produced conventionally and by laser additive manufacturing, *Materials* 10 (2017), <https://doi.org/10.3390/ma10010008>.
- [93] P. Kürnstner, M.B. Wilms, A. Weisheit, P. Barriobero-Vila, E.A. Jägge, D. Raabe, Massive nanoprecipitation in an Fe-19Ni-xAl maraging steel triggered by the intrinsic heat treatment during laser metal deposition, *Acta Mater.* 129 (2017) 52–60, <https://doi.org/10.1016/J.ACTAMAT.2017.02.069>.
- [94] K. Kempen, E. Yasa, L. Thijs, J.P. Kruth, J. Van Humbeeck, Microstructure and mechanical properties of Selective Laser Melted 18Ni-300 steel, *Phys. Procedia* 12 (2011) 255–263, <https://doi.org/10.1016/J.PHPPRO.2011.03.033>.
- [95] R. Casati, J.N. Lemke, A. Tuissi, M. Vedani, Aging behaviour and mechanical performance of 18-Ni 300 steel processed by selective laser melting, *Metals (basel)* 6 (2016), <https://doi.org/10.3390/met6090218>.
- [96] C. Chen, K. Yan, L. Qin, M. Zhang, X. Wang, T. Zou, Z. Hu, Effect of heat treatment on microstructure and mechanical properties of laser additively manufactured AISI H13 tool steel, *J. Mater. Eng. Perform.* 26 (2017) 5577–5589, <https://doi.org/10.1007/s11665-017-2992-0>.
- [97] B. Mooney, K.I. Kourousis, R. Raghavendra, Plastic anisotropy of additively manufactured maraging steel: Influence of the build orientation and heat treatments, *Addit. Manuf.* 25 (2019) 19–31, <https://doi.org/10.1016/J.ADDMA.2018.10.032>.
- [98] R. Casati, J. Lemke, M. Vedani, Microstructural and mechanical properties of as built, solution treated and Aged 18 Ni (300 grade) maraging steel produced by selective laser melting, *Metall. Ital.* 109 (2017) 11–20.
- [99] J.S. Park, M.-G. Lee, Y.-J. Cho, J.H. Sung, M.-S. Jeong, S.-K. Lee, Y.-J. Choi, D. H. Kim, Effect of heat treatment on the characteristics of tool steel deposited by the directed energy deposition process, *Met. Mater. Int.* 22 (2016) 143–147, <https://doi.org/10.1007/s12540-016-5372-7>.
- [100] D. Masaylo, S. Igoshin, A. Popovich, A. Orlov, A. Kim, V. Popovich, Microstructural and hardness behavior of H13 tool steel manufactured by ultrasound-assisted laser-directed energy deposition, *Metals (basel)* 12 (2022), <https://doi.org/10.3390/met12030450>.
- [101] M. Yuan, Y. Cao, S. Karamchedu, S. Hosseini, Y. Yao, J. Berglund, L. Liu, L. Nyborg, Characteristics of a modified H13 hot-work tool steel fabricated by means of laser beam powder bed fusion, *Mater. Sci. Eng. A* 831 (2022) 142322, <https://doi.org/10.1016/J.MSEA.2021.142322>.
- [102] S. Megahed, R. Koch, J.H. Schleifenbaum, Laser powder bed fusion tool repair: statistical analysis of 1.2343/H11 tool steel process parameters and microstructural analysis of the repair interface, *J. Manuf. Mater. Process.* 6 (2022), <https://doi.org/10.3390/jmmp6060139>.
- [103] W360 AMPO BOHLER Edelstahl GmbH & Co, <https://www.boehler-edelstahl.com/En/Products/W360-Ampo/> (2024).
- [104] J. Vinić, A. Aversa, M. Lombardi, D. Manfredi, Processability and microstructural evolution of W360 hot work tool steel by directed energy deposition, *Met. Mater. Int.* (2023), <https://doi.org/10.1007/s12540-023-01508-5>.
- [105] J. Boes, A. Röttger, C. Mutke, C. Escher, S. Weber, Microstructure and properties of a novel carbon-martensitic hot work tool steel processed by laser additive manufacturing without preheating, *Steel Res. Int.* 94 (2023), <https://doi.org/10.1002/srin.202200439>.
- [106] N. Ur Rahman, L. Capuano, S. Cabeza, M. Feinaeugle, A. Garcia-Junceda, M.B. de Rooij, D.T.A. Matthews, G. Walmag, I. Gibson, G.R.B.E. Römer, Directed energy deposition and characterization of high-carbon high speed steels, *Addit. Manuf.* 30 (2019), <https://doi.org/10.1016/j.addma.2019.100838>.
- [107] G.Y. Baek, G.Y. Shin, K.Y. Lee, D.S. Shim, Mechanical properties of tool steels with high wear resistance via directed energy deposition, *Metals (basel)* 9 (2019), <https://doi.org/10.3390/met9030282>.
- [108] J. Kunz, J. Saewe, S. Herzog, A. Kaletsch, J.H. Schleifenbaum, C. Broeckmann, Mechanical properties of high-speed steel AISI M50 produced by laser powder bed fusion, *Steel Res. Int.* 91 (2020) 1900562, <https://doi.org/10.1002/srin.201900562>.
- [109] K. Borkovcová, P. Novák, N. Merghem, A. Tsepeleva, P. Salvetr, M. Brázda, D. Rajnovic, Processing of niobium-alloyed high-carbon tool steel via additive manufacturing and modern powder metallurgy, *Materials* 16 (2023), <https://doi.org/10.3390/ma16134760>.
- [110] T. Kelliger, M. Meurer, T. Bergs, Orthogonal cutting with additively manufactured grooving inserts made from HS6-5-3-8 high-speed steel, in: *Materials Research Proceedings, Association of American Publishers*, 2023, pp. 1235–1244, <https://doi.org/10.21741/9781644902479-134>.
- [111] S. Choi, H. Kim, J. Sung, D. Lee, J. Seo, Properties of tool steels printed by directed energy deposition process on s45c base metal, *Materials* 13 (2020) 1–22, <https://doi.org/10.3390/ma13225068>.
- [112] P.-J. Maziasz, E.A. Payzant, M.E. Schlienger, K.M. McHugh, Residual stresses and microstructure of H13 steel formed by combining two different direct fabrication methods, *Scr. Mater.* 39 (1998) 1471–1476, [https://doi.org/10.1016/S1359-6462\(98\)00349-2](https://doi.org/10.1016/S1359-6462(98)00349-2).

- [113] R. Cottam, J. Wang, V. Luzin, Characterization of microstructure and residual stress in a 3D H13 tool steel component produced by additive manufacturing, *J. Mater. Res.* 29 (2014) 1978–1986, <https://doi.org/10.1557/jmr.2014.190>.
- [114] D. Herzog, V. Seyda, E. Wycisk, C. Emmelmann, Additive manufacturing of metals, *Acta Mater.* 117 (2016) 371–392, <https://doi.org/10.1016/j.actamat.2016.07.019>.
- [115] R. Matthieu, H. Jean-Yves, M. Manjaiah, Repairing Ti-6Al-4V aeronautical components with DED additive manufacturing, *MATEC Web Conf.* 321 (2020) 3017, <https://doi.org/10.1051/mateconf/202032103017>.
- [116] M. Song, X. Lin, G. Yang, X. Cui, H. Yang, W. Huang, Influence of forming atmosphere on the deposition characteristics of 2Cr13 stainless steel during laser solid forming, *J. Mater. Process. Technol.* 214 (2014) 701–709, <https://doi.org/10.1016/j.jmatprotec.2013.09.023>.
- [117] M.S. Kenevisi, F.S. Gobber, G. Maculotti, G. Genta, M. Galetto, S. Biamino, D. Ugues, Surface topography and cross-section analysis of K340 cold work tool steel double-tracks deposited by directed energy deposition technique, *CIRP J. Manuf. Sci. Technol.* (2025) 158–169, <https://doi.org/10.1016/j.cirpj.2025.03.011>.
- [118] J. Choi, Y. Chang, Characteristics of laser aided direct metal/material deposition process for tool steel, *Int. J. Mach. Tools Manuf.* 45 (2005) 597–607, <https://doi.org/10.1016/j.jmachtools.2004.08.014>.
- [119] J. Choi, Y. Hua, Dimensional and material characteristics of direct deposited H13 tool steel by CO₂ laser, *J. Laser Appl.* 16 (2004) 245–251, <https://doi.org/10.2351/1.1809638>.
- [120] W. Hofmeister, M. Griffith, Solidification in direct metal deposition by LENS processing, *JOM* 53 (2001) 30–34, <https://doi.org/10.1007/s11837-001-0066-z>.
- [121] A.J. Pinkerton, L. Li, Direct additive laser manufacturing using gas- and water-atomized H13 tool steel powders, *Int. J. Adv. Manuf. Technol.* 25 (2005) 471–479, <https://doi.org/10.1007/s00170-003-1844-2>.
- [122] L. Xue, J. Chen, S.-H. Wang, Freeform laser consolidated H13 and CPM 9V tool steels, *Metall. Microstruct. Anal.* 2 (2013) 67–78, <https://doi.org/10.1007/s13632-013-0061-0>.
- [123] J. Mazumder, J. Choi, K. Nagarathnam, J. Koch, D. Hetzner, The direct metal deposition of H13 tool steel for 3-D components, *JOM* 49 (1997) 55–60, <https://doi.org/10.1007/BF02914687>.
- [124] H.J. Niu, I.T.H. Chang, Selective laser sintering of gas atomized M2 high speed steel powder, *J. Mater. Sci.* 35 (2000) 31–38, <https://doi.org/10.1023/A:1004720011671>.
- [125] D. Bartels, D. Nikas, R. März, M. Marschall, J. Schrauder, M. Merklein, A. Selte, P. Krakhmalev, Directed energy deposition of chromium-molybdenum-vanadium cold work tool steel Vanadis 4 Extra®, *J. Mater. Res. Technol.* 38 (2025) 1573–1580, <https://doi.org/10.1016/j.jmrt.2025.08.036>.
- [126] J. Epp, J. Dong, H. Meyer, A. Bohlen, Analysis of cyclic phase transformations during additive manufacturing of hardenable tool steel by in-situ X-ray diffraction experiments, *Scr. Mater.* 177 (2020) 27–31, <https://doi.org/10.1016/j.scriptamat.2019.09.021>.
- [127] D. Junker, O. Hentschel, M. Schmidt, M. Merklein, Investigation of heat treatment strategies for additively-manufactured tools of X37CrMoV5-1, *Metals (basel)* 8 (2018), <https://doi.org/10.3390/met8100854>.
- [128] J. Daniel, H. Oliver, S. Michael, M. Marion, Qualification of laser based additive production for manufacturing of forging Tools, *MATEC Web Conf.* 21 (2015) 8010, <https://doi.org/10.1051/mateconf/20152108010>.
- [129] R.T. Jardin, V. Tuninetti, J.T. Techuindjang, L. Duchêne, N. Hashemi, H.S. Tran, R. Carrus, A. Mertens, A.M. Habraken, Optimizing laser power of directed energy deposition process for homogeneous AISI M4 steel microstructure, *Opt. Laser Technol.* 163 (2023) 109426, <https://doi.org/10.1016/j.optlastec.2023.109426>.
- [130] S.M.T. Omar, K.P. Plucknett, The influence of DED process parameters and heat-treatment cycle on the microstructure and hardness of AISI D2 tool steel, *J. Manuf. Process.* 81 (2022) 655–671, <https://doi.org/10.1016/j.jmapro.2022.06.069>.
- [131] J. Mazumder, A. Schifferer, J. Choi, Direct materials deposition: designed macro and microstructure, *Mater. Res. Innov.* 3 (1999) 118–131, <https://doi.org/10.1007/s100190050137>.
- [132] J.I. Arrizubieta, M. Cortina, A. Mendioroz, A. Salazar, A. Lamikiz, Thermal diffusivity measurement of laser-deposited AISI H13 tool steel and impact on cooling performance of hot stamping tools, *Metals (basel)* 10 (2020), <https://doi.org/10.3390/met10010154>.
- [133] Z. Xia, J. Xu, J. Shi, T. Shi, C. Sun, D. Qiu, Microstructure evolution and mechanical properties of reduced activation steel manufactured through laser directed energy deposition, *Addit. Manuf.* 33 (2020) 101114, <https://doi.org/10.1016/j.addma.2020.101114>.
- [134] N. Rońda, K. Grzelak, M. Polański, J. Dworecka-Wójcik, The influence of layer thickness on the microstructure and mechanical properties of M300 maraging steel additively manufactured by LENS® technology, *Materials* 15 (2022), <https://doi.org/10.3390/ma15020603>.
- [135] C. Barr, R.A.R. Rashid, S. Da Sun, M. Easton, S. Palanisamy, N. Orchowski, N. Matthews, K. Walker, M. Brandt, Role of deposition strategy and fill depth on the tensile and fatigue performance of 300 M repaired through laser directed energy deposition, *Int. J. Fatigue* 146 (2021) 106135, <https://doi.org/10.1016/j.ijfatigue.2020.106135>.
- [136] L. Kučerová, K. Burdová, Š. Jeníček, I. Chena, Effect of solution annealing and precipitation hardening at 250 °C–550 °C on microstructure and mechanical properties of additively manufactured 1.2709 maraging steel, *Mater. Sci. Eng.: A* 814 (2021) 141195, <https://doi.org/10.1016/j.msea.2021.141195>.
- [137] F. Liu, W. Zhang, X. Lin, C. Huang, Z. Wang, F. Liu, W. Huang, P. Wang, X. Li, Achieving superior ductility for laser directed energy deposition 300 M steel through isothermal bainitic transformation, *J. Manuf. Process.* 60 (2020) 426–434, <https://doi.org/10.1016/j.jmapro.2020.10.077>.
- [138] E.A. Jäggle, P.-P. Choi, J. Van Humbeeck, D. Raabe, Precipitation and austenite reversion behavior of a maraging steel produced by selective laser melting, *J. Mater. Res.* 29 (2014) 2072–2079, <https://doi.org/10.1557/jmr.2014.204>.
- [139] C. Botero, M. Ramsperger, A. Selte, K. Åsvik, A. Koptuyg, P. Skoglund, S. Roos, L. E. Rännar, M. Bäckström, Additive manufacturing of a cold-work tool steel using electron beam melting, *Steel Res. Int.* 91 (2020), <https://doi.org/10.1002/srin.201900448>.
- [140] F. Großwendt, A. Röttger, A. Strauch, A. Chehreh, V. Uhlenwinkel, R. Fichte-Heinen, F. Walther, S. Weber, W. Theisen, Additive manufacturing of a carbon-martensitic hot-work tool steel using a powder mixture – microstructure, post-processing, mechanical properties, *Mater. Sci. Eng. A* 827 (2021), <https://doi.org/10.1016/j.msea.2021.142038>.
- [141] F. Huber, C. Bischof, O. Hentschel, J. Heberle, J. Zettl, K.Y. Nagulin, M. Schmidt, Laser beam melting and heat-treatment of 1.2343 (AISI H11) tool steel – microstructure and mechanical properties, *Mater. Sci. Eng.: A* 742 (2019) 109–115, <https://doi.org/10.1016/j.msea.2018.11.001>.
- [142] M. Åsberg, F. Lin, P. Karlsson, C. Oikonomou, E. Strandh, M. Uhlirsch, P. Krakhmalev, A comparative study of the as-built microstructure of a cold-work tool steel produced by laser and electron-beam powder-bed fusion, *Metals (basel)* 14 (2024), <https://doi.org/10.3390/met14080934>.
- [143] V.E. Beal, P. Erasenthiran, N. Hopkinson, P. Dickens, C.H. Ahrens, The effect of scanning strategy on laser fusion of functionally graded H13/Cu materials, *Int. J. Adv. Manuf. Technol.* 30 (2006) 844–852, <https://doi.org/10.1007/s00170-005-0130-x>.
- [144] S. Shakerin, A. Hadadzadeh, B.S. Amirkhiz, S. Shamsdini, J. Li, M. Mohammadi, Additive manufacturing of maraging steel-H13 bimetal using laser powder bed fusion technique, *Addit. Manuf.* 29 (2019) 100797, <https://doi.org/10.1016/j.addma.2019.100797>.
- [145] G. Huang, K. Wei, X. Zeng, Microstructure and mechanical properties of H13 tool steel fabricated by high power laser powder bed fusion, *Mater. Sci. Eng. A* 858 (2022), <https://doi.org/10.1016/j.msea.2022.144154>.
- [146] R. Mertens, B. Vrancken, N. Holmstock, Y. Kinds, J.P. Kruth, J., Van Humbeeck, Influence of powder bed preheating on microstructure and mechanical properties of H13 tool steel SLM parts, in: *Phys Procedia*, Elsevier B.v., 2016, pp. 882–890, <https://doi.org/10.1016/j.phpro.2016.08.092>.
- [147] V. Leskovšek, B. Suštaršič, G. Jutriša, The influence of austenitizing and tempering temperature on the hardness and fracture toughness of hot-worked H11 tool steel, *J. Mater. Process. Technol.* 178 (2006) 328–334, <https://doi.org/10.1016/j.jmatprotec.2006.04.016>.
- [148] R. Casati, M. Coduri, N. Lecis, C. Andrianopoli, M. Vedani, Microstructure and mechanical behavior of hot-work tool steels processed by Selective Laser Melting, *Mater Charact* 137 (2018) 50–57, <https://doi.org/10.1016/j.matchar.2018.01.015>.
- [149] O. Hentschel, L. Siegel, C. Scheitler, F. Huber, D. Junker, A. Gorunow, M. Schmidt, Processing of AISI H11 tool steel powder modified with carbon black nanoparticles for the additive manufacturing of forging tools with tailored mechanical properties by means of laser metal deposition (LMD), *Metals (basel)* 8 (2018), <https://doi.org/10.3390/met8090659>.
- [150] F. Lei, T. Wen, F. Yang, J. Wang, J. Fu, H. Yang, J. Wang, J. Ruan, S. Ji, Microstructures and mechanical properties of H13 tool steel fabricated by selective laser melting, *Materials* 15 (2022), <https://doi.org/10.3390/ma15072686>.
- [151] S. Li, S. Yang, Y. Zhao, Y. Dong, Z. Wang, 2 GPa H13 steels fabricated by laser powder bed fusion and tempering: microstructure, tensile property and strengthening mechanism, *Mater. Sci. Eng. A* 888 (2023) 145803, <https://doi.org/10.1016/j.msea.2023.145803>.
- [152] M. Wang, Y. Wu, Q. Wei, Y. Shi, Thermal fatigue properties of H13 hot-work tool steels processed by selective laser melting, *Metals (basel)* 10 (2020), <https://doi.org/10.3390/met10010116>.
- [153] J.A. Brooks, C.V. Robino, T.J. Headley, S.H. Goods, M.L. Griffith, Microstructure and Property Optimization of LENS Deposited H13 Tool Steel, in: *International Solid Freeform Fabrication Symposium, 1999*. <https://api.semanticscholar.org/CorpusID:149782403>.
- [154] F. Deirmina, N. Peghini, B. AlMangour, D. Grzesiak, M. Pellizzari, Heat treatment and properties of a hot work tool steel fabricated by additive manufacturing, *Mater. Sci. Eng. A* 753 (2019) 109–121, <https://doi.org/10.1016/j.msea.2019.03.027>.
- [155] M.J. Holzweissig, A. Taube, F. Brenne, M. Schaper, T. Niendorf, Microstructural characterization and mechanical performance of hot work tool steel processed by selective laser melting, *Metall. Mater. Trans. B* 46 (2015) 545–549, <https://doi.org/10.1007/s11663-014-0267-9>.
- [156] J. Krell, A. Röttger, K. Geenen, W. Theisen, General investigations on processing tool steel X40CrMoV5-1 with selective laser melting, *J. Mater. Process. Technol.* 255 (2018) 679–688, <https://doi.org/10.1016/j.jmatprotec.2018.01.012>.
- [157] R. Dörfert, J. Zhang, B. Clausen, H. Freife, J. Schumacher, F. Vollertsen, Comparison of the fatigue strength between additively and conventionally fabricated tool steel 1.2344, *Addit. Manuf.* 27 (2019) 217–223, <https://doi.org/10.1016/j.addma.2019.01.010>.
- [158] M. Katancik, S. Mirzababaei, M. Ghayoor, S. Pasebani, Selective laser melting and tempering of H13 tool steel for rapid tooling applications, *J. Alloys Compd.* 849 (2020) 156319, <https://doi.org/10.1016/j.jallcom.2020.156319>.

- [159] J. Šafka, M. Ackermann, L. Voleský, Structural properties of H13 tool steel parts produced with use of selective laser melting technology, *J. Phys. Conf. Ser.* 709 (2016) 012004, <https://doi.org/10.1088/1742-6596/709/1/012004>.
- [160] M. Mazur, M. Leary, M. McMillan, J. Elambasseril, M. Brandt, SLM additive manufacturing of H13 tool steel with conformal cooling and structural lattices, *Rapid Prototyp. J.* 22 (2016) 504–518, <https://doi.org/10.1108/RPJ-06-2014-0075>.
- [161] M. Mazur, P. Brincat, M. Leary, M. Brandt, Numerical and experimental evaluation of a conformally cooled H13 steel injection mould manufactured with selective laser melting, *Int. J. Adv. Manuf. Technol.* 93 (2017) 881–900, <https://doi.org/10.1007/s00170-017-0426-7>.
- [162] M. Ackermann, J. Šafka, L. Voleský, J. Bobek, J.R. Kondapally, Impact testing of H13 tool steel processed with use of selective laser melting technology, *Mater. Sci. Forum* 919 (2018) 43–51, <https://doi.org/10.4028/www.scientific.net/MSF.919.43>.
- [163] H. Zong, N. Kang, Z. Qin, M. El Mansori, A review on the multi-scaled structures and mechanical/thermal properties of tool steels fabricated by laser powder bed fusion additive manufacturing, *Int. J. Miner. Metall. Mater.* 31 (2024) 1048–1071, <https://doi.org/10.1007/s12613-023-2731-5>.
- [164] Z. Liu, C. Chua, K.F. Leong, K. Kempen, L. Thijs, E. Yasa, J. Van-Humbeek, J.-P. Kruth, A preliminary investigation on selective laser melting of M2 high speed steel, *In* (2011) 339–346, <https://doi.org/10.1201/b11341-54>.
- [165] T. Hermann Becker, D. Dimitrov, The achievable mechanical properties of SLM produced Maraging Steel 300 components, *Rapid Prototyp. J.* 22 (2016) 487–494, <https://doi.org/10.1108/RPJ-08-2014-0096>.
- [166] A.F. de Souza, K.S. Al-Rubaie, S. Marques, B. Zluhan, E.C. Santos, Effect of laser speed, layer thickness, and part position on the mechanical properties of maraging 300 parts manufactured by selective laser melting, *Mater. Sci. Eng. A* 767 (2019) 138425, <https://doi.org/10.1016/J.MSEA.2019.138425>.
- [167] P. Gao, G. Jing, X. Lan, S. Li, Y. Zhou, Y. Wang, H. Yang, K. Wei, Z. Wang, Effect of heat treatment on microstructure and mechanical properties of Fe–Cr–Ni–Co–Mo maraging stainless steel produced by selective laser melting, *Mater. Sci. Eng. A* 814 (2021) 141149, <https://doi.org/10.1016/J.MSEA.2021.141149>.
- [168] S. Yin, C. Chen, X. Yan, X. Feng, R. Jenkins, P. O'Reilly, M. Liu, H. Li, R. Lupoi, The influence of aging temperature and aging time on the mechanical and tribological properties of selective laser melted maraging 18Ni-300 steel, *Addit. Manuf.* 22 (2018) 592–600, <https://doi.org/10.1016/J.ADDMA.2018.06.005>.
- [169] Y. Hong, D.D. Dong, S.S. Lin, W. Wang, C.M. Tang, T.C. Kuang, M.J. Dai, Improving surface mechanical properties of the selective laser melted 18Ni300 maraging steel via plasma nitriding, *Surf. Coat. Technol.* 406 (2021) 126675, <https://doi.org/10.1016/J.SURFCOAT.2020.126675>.
- [170] J. Suryawanshi, K.G. Prashanth, O. Ramamurthy, Tensile, fracture, and fatigue crack growth properties of a 3D printed maraging steel through selective laser melting, *J. Alloys Compd.* 725 (2017) 355–364, <https://doi.org/10.1016/J.JALLCOM.2017.07.177>.
- [171] Q. Wang, Z. Zhang, X. Tong, S. Dong, Z. Cui, X. Wang, L. Ren, Effects of process parameters on the microstructure and mechanical properties of 24CrNiMo steel fabricated by selective laser melting, *Opt. Laser Technol.* 128 (2020) 106262, <https://doi.org/10.1016/J.OPTLASTEC.2020.106262>.
- [172] M.S. Kenevisi, F. Lin, Dissolution of Al₂Cu precipitate in Al2024 additively manufactured by electron beam melting, *Adv. Eng. Mater.* 23 (2021) 2100323, <https://doi.org/10.1002/adem.202100323>.
- [173] X. Yang, Y. Lai, Z. Zhang, T. Zhang, X. Yao, F. Song, Y. Hou, H. Qi, H. Tang, Microstructure evolution and mechanical properties of H13 steel produced by Selective Electron Beam Melting, *Mater. Charact.* 203 (2023) 113053, <https://doi.org/10.1016/J.MATCHAR.2023.113053>.
- [174] D. Cormier, O. Harrysson, H. West, Characterization of H13 steel produced via electron beam melting, *Rapid Prototyp. J.* 10 (2004) 35–41, <https://doi.org/10.1108/13552540410512516>.
- [175] Y. Wei, S. Qi, Y. Wang, X. Chu, Z. Sun, J. Wang, L. Zhang, W. Jia, X. Yang, S. Liu, Microstructural evolution and tribological properties of M2 high-speed steel fabricated under various selective electron beam melting processing parameters, *Tribol. Int.* 187 (2023) 108749, <https://doi.org/10.1016/J.TRIBOINT.2023.108749>.
- [176] K. Dalgarno, T. Stewart, Production tooling for polymer moulding using the RapidSteel process, *Rapid Prototyp. J.* 7 (2001) 173–179, <https://doi.org/10.1108/13552540110395600>.
- [177] D.I. Wimpenny, B. Bryden, I.R. Pashby, Rapid laminated tooling, *J. Mater. Process. Technol.* 138 (2003) 214–218, [https://doi.org/10.1016/S0924-0136\(03\)00074-8](https://doi.org/10.1016/S0924-0136(03)00074-8).
- [178] E. Sachs, E. Wylonis, S. Allen, M. Cima, H. Guo, Production of injection molding tooling with conformal cooling channels using the three dimensional printing process, *Polym. Eng. Sci.* 40 (2000) 1232–1247, <https://doi.org/10.1002/pen.11251>.
- [179] L. Rännar, A. Glad, C. Gustafson, Efficient cooling with tool inserts manufactured by electron beam melting, *Rapid Prototyp. J.* 13 (2007) 128–135, <https://doi.org/10.1108/13552540710750870>.
- [180] E.S. Gevorkyan, M. Rucki, V.P. Nerubatskyi, W. Żurowski, Z. Siemiątkowski, D. Morozow, A.G. Kharatyan, *Remanufacturing and Advanced Machining Processes for New Materials and Components*, 1st ed., Taylor & Francis, New York, 2022.
- [181] X. Zhang, W. Cui, W. Li, F. Liou, A hybrid process integrating reverse engineering, pre-repair processing, additive manufacturing, and material testing for component remanufacturing, *Materials* 12 (2019), <https://doi.org/10.3390/ma12121961>.
- [182] N. Asnafi, Tool and die making, surface treatment, and repair by laser-based additive processes, *BHM Berg- Und Hüttenmännische, Monatshefte* 166 (2021) 225–236, <https://doi.org/10.1007/s00501-021-01113-2>.
- [183] A. Pinkerton, W. Wang, L. Li, Component repair using laser direct metal deposition, *Proc. Inst. Mech. Eng B-J. Eng. MA* 222 (2008), <https://doi.org/10.1243/09544054JEM1008>.
- [184] J. Zhang, L. Yu, Y. Liu, Z. Ma, H. Li, C. Liu, J. Wu, J. Ma, Z. Li, Analysis of the effect of tungsten inert gas welding sequences on residual stress and distortion of CFETR vacuum vessel using finite element simulations, *Metals (base)* 8 (2018), <https://doi.org/10.3390/met8110912>.
- [185] C.Y. Su, C.P. Chou, B.C. Wu, W.C. Lih, Plasma transferred arc repair welding of the nickel-base superalloy IN-738LC, *J. Mater. Eng. Perform.* 6 (1997) 619–627, <https://doi.org/10.1007/s11665-997-0055-7>.
- [186] G. Bi, A. Gasser, Restoration of nickel-base turbine blade knife-edges with controlled laser aided additive manufacturing, *Phys. Procedia* 12 (2011) 402–409, <https://doi.org/10.1016/J.PHPRO.2011.03.051>.
- [187] P. Kattire, S. Paul, R. Singh, W. Yan, Experimental characterization of laser cladding of CPM 9V on H13 tool steel for die repair applications, *J. Manuf. Process.* 20 (2015) 492–499, <https://doi.org/10.1016/J.JMAPRO.2015.06.018>.
- [188] J. Leunda, C. Soriano, C. Sanz, V.G. Navas, Laser cladding of vanadium-carbide tool steels for die repair, *Phys. Procedia* 12 (2011) 345–352, <https://doi.org/10.1016/J.PHPRO.2011.03.044>.
- [189] J. Zeisig, N. Schädlich, L. Giebler, J. Sander, J. Eckert, U. Kühn, J. Hufenbach, Microstructure and abrasive wear behavior of a novel FeCrMoVC laser cladding alloy for high-performance tool steels, *Wear* 382–383 (2017) 107–112, <https://doi.org/10.1016/J.WEAR.2017.04.021>.
- [190] S. Jhavar, C.P. Paul, N.K. Jain, Micro-plasma transferred arc additive manufacturing for die and mold surface remanufacturing, *JOM* 68 (2016) 1801–1809, <https://doi.org/10.1007/s11837-016-1932-z>.
- [191] D.A. Rahito, A.H. Wahab, Azman, Additive manufacturing for repair and restoration in remanufacturing: an overview from object design and systems perspectives, *Processes* 7 (2019), <https://doi.org/10.3390/pr7110802>.
- [192] R.E. Petrusse, M.-C. Langa, Enhancing metal forging tools and moulds: advanced repairs and optimisation using directed energy deposition hybrid manufacturing, *Appl. Sci.* 14 (2024), <https://doi.org/10.3390/app14020567>.
- [193] J. Foster, C. Cullen, S. Fitzpatrick, G. Payne, L. Hall, J. Marashi, Remanufacture of hot forging tools and dies using laser metal deposition with powder and a hard-facing alloy Stellite 21®, *J. Remanuf.* 9 (2019) 189–203, <https://doi.org/10.1007/s13243-018-0063-9>.
- [194] J. Marashi, J. Foster, R. Zante, Defining a method of evaluating die life performance by using finite element models (FEM) and a practical open die hot forging method, *AIP Conf. Proc.* 1769 (2016) 130001, <https://doi.org/10.1063/1.4963520>.
- [195] J. Marashi, E. Yakushina, P. Xirouchakis, R. Zante, J. Foster, An evaluation of H13 tool steel deformation in hot forging conditions, *J. Mater. Process. Technol.* 246 (2017) 276–284, <https://doi.org/10.1016/J.JMATPROTEC.2017.03.026>.
- [196] W.T. Preciado, C.E.N. Bohorquez, Repair welding of polymer injection molds manufactured in AISI P20 and VP50IM steels, *J. Mater. Process. Technol.* 179 (2006) 244–250, <https://doi.org/10.1016/J.JMATPROTEC.2006.03.101>.
- [197] M.S. Kenevisi, Y. Yu, F. Lin, A review on additive manufacturing of Al–Cu (2xxx) aluminium alloys, processes and defects, *Mater. Sci. Technol.* 37 (2021) 805–829, <https://doi.org/10.1080/02670836.2021.1958487>.
- [198] M. Yuan, S. Karamchedu, Y. Fan, L. Liu, L. Nyborg, Y. Cao, Study of defects in directed energy deposited Vanadis 4 Extra tool steel, *J. Manuf. Process.* 76 (2022) 419–427, <https://doi.org/10.1016/J.JMAPRO.2022.02.014>.
- [199] X. Nie, F. Peng, Z. Hu, Y. Qi, H. Zhu, H. Zhang, The Effect of Thermal Cycle on Hot Cracking Evolution and Formation Mechanism in Thin Wall, Single Layer, and Cubic Samples of High-Strength Al-Cu-Mg-Mn Alloys Fabricated by Laser Powder Bed Fusion, *3D Print Addit Manuf* (2023). [10.1089/3dp.2023.0167](https://doi.org/10.1089/3dp.2023.0167).
- [200] A. Moradiani, F.M. Ghaini, Z.M. Beiranvand, R.M. Chandima Ratnayake, A. Aliabadi, Effect of laser pulse power on solidification cracking susceptibility in surface processing of a high carbon high chromium tool steel, *CIRP J. Manuf. Sci. Technol.* 38 (2022) 737–747, <https://doi.org/10.1016/J.CIRPJ.2022.06.005>.
- [201] N.A. Siddiqui, M. Muzamil, T. Jamil, G. Hussain, Heat sources in wire arc additive manufacturing and their impact on macro-microstructural characteristics and mechanical properties – an overview, *Smart Mater. Manuf.* 3 (2025) 100059, <https://doi.org/10.1016/J.SMMF.2024.100059>.
- [202] P. Jorge, Bártolo, *Innovative Developments in Virtual and Physical Prototyping*, 1st ed., CRC Press, 2011.
- [203] M.S. Kenevisi, S. Biamino, D. Ugues, A multivariate experimental design to investigate the effect of different heat treatment procedures and parameters' interactions on the hardness and retained austenite of K340 cold-work tool steel, *J. Mater. Eng. Perform.* (2024), <https://doi.org/10.1007/s11665-024-10486-7>.
- [204] N. Hantke, F. Großwendt, A. Strauch, R. Fechte-Heinen, A. Röttger, W. Theisen, S. Weber, J.T. Sehr, Processability of a hot work tool steel powder mixture in laser-based powder bed fusion, *Materials* 15 (2022), <https://doi.org/10.3390/ma15072658>.
- [205] M.L. Köhler, M. Norda, S. Herzog, A. Kaletsch, F. Petzoldt, C. Broeckmann, Towards carbide-rich tool steels in PBF-LB/M: TiC addition of AISI H13, *Addit. Manuf. Lett.* 6 (2023) 100143, <https://doi.org/10.1016/J.ADDLET.2023.100143>.
- [206] D.-G. Ahn, Direct metal additive manufacturing processes and their sustainable applications for green technology: a review, *Int. J. Precis. Eng. Manuf.-Green Technol.* 3 (2016) 381–395, <https://doi.org/10.1007/s40684-016-0048-9>.

- [207] W.R. Morrow, H. Qi, I. Kim, J. Mazumder, S.J. Skerlos, Environmental aspects of laser-based and conventional tool and die manufacturing, *J. Clean. Prod.* 15 (2007) 932–943, <https://doi.org/10.1016/J.JCLEPRO.2005.11.030>.
- [208] M. Leino, J. Pekkarinen, R. Soukka, The role of laser additive manufacturing methods of metals in repair, refurbishment and remanufacturing – enabling circular economy, *Phys. Procedia* 83 (2016) 752–760, <https://doi.org/10.1016/J.PHPRO.2016.08.077>.
- [209] J. Bennett, D. Garcia, M. Kendrick, T. Hartman, G. Hyatt, K. Ehmann, F. You, J. Cao, Repairing automotive dies with directed energy deposition: industrial application and life cycle analysis, *J. Manuf. Sci. Eng.* 141 (2018), <https://doi.org/10.1115/1.4042078>.
- [210] L. Ren, A.P. Padathu, J. Ruan, T. Sparks, F. Liou, Three dimensional die repair using a hybrid manufacturing system, 17th Solid Freeform Fabrication Symposium, SFF 2006 (2006) 51–59.
- [211] L. Zumofen, C. Beck, A. Kirchheim, H.-J. Dennig, Quality Related Effects of the Preheating Temperature on Laser Melted High Carbon Content Steels, 2018. 10.1007/978-3-319-66866-6_21.
- [212] The magazine for the metal additive manufacturing industry: Metal AM, 2018. <https://www.metal-am.com/> (accessed October 25, 2024).
- [213] B.M. Cortina, A Methodology for the Application of Hybrid Additive and Subtractive Machines for the Coating and Repair of Hot Stamping Tools, Universidad del Pais Vasco, 2020.
- [214] W. Jiang, P. Molian, Laser based flexible fabrication of functionally graded mould inserts, *Int. J. Adv. Manuf. Technol.* 19 (2002) 646–654, <https://doi.org/10.1007/s001700200109>.
- [215] J.D. Ayers, Wear behavior of carbide-injected titanium and aluminum alloys, *Wear* 97 (1984) 249–266, [https://doi.org/10.1016/0043-1648\(84\)90152-2](https://doi.org/10.1016/0043-1648(84)90152-2).
- [216] Y. Zhang, Z. Wei, L. Shi, M. Xi, Characterization of laser powder deposited Ti–TiC composites and functional gradient materials, *J. Mater. Process. Technol.* 206 (2008) 438–444, <https://doi.org/10.1016/j.jmatprotec.2007.12.055>.
- [217] W. Jiang, R. Nair, P. Molian, Functionally graded mold inserts by laser-based flexible fabrication: processing modeling, structural analysis, and performance evaluation, *J. Mater. Process. Technol.* 166 (2005) 286–293, <https://doi.org/10.1016/J.JMATPROTEC.2004.08.029>.
- [218] D.-G. Ahn, H.-W. Kim, Study on the manufacture of a thermal management mould with three different materials using a direct metal tooling rapid tooling process, *Proc. Inst. Mech. Eng. B J. Eng. Manuf.* 224 (2009) 385–402, <https://doi.org/10.1243/09544054JEM1523>.
- [219] F. Noecker, J. Dupont, Functionally Graded Copper – Steel Using Laser Engineered Net Shaping Process, ICALEO 2002 - 21st International Congress on Applications of Laser and Electro-Optics, Congress Proceedings (2002).
- [220] A. Nassehi, S. Newman, V. Dhokia, Z. Zhu, R.I. Asrai, Using formal methods to model hybrid manufacturing processes, in: H.A. ElMaraghy (Ed.), *Enabling Manufacturing Competitiveness and Economic Sustainability*, Springer Berlin Heidelberg, Berlin, Heidelberg, 2012, pp. 52–56.
- [221] P.C. Priarone, G. Campatelli, A.R. Catalano, F. Baffa, Life-cycle energy and carbon saving potential of Wire Arc Additive Manufacturing for the repair of mold inserts, *CIRP J. Manuf. Sci. Technol.* 35 (2021) 943–958, <https://doi.org/10.1016/J.CIRPJ.2021.10.007>.
- [222] G. Campatelli, G. Venturini, N. Grossi, F. Baffa, A. Scippa, K. Yamazaki, Design and testing of a WAAM retrofit kit for repairing operations on a milling machine, *Machines* 9 (2021), <https://doi.org/10.3390/machines9120322>.
- [223] F. Hou, G. Zhao, H. Zhang, H. Zhang, C. Huang, Evaluating the energy properties of the short-flow process based on the industrial metabolism: a case study on the metal 3D printing of hybrid deposition and micro rolling (HDMR), *J. Manuf. Process.* 97 (2023) 125–136, <https://doi.org/10.1016/J.JMAPRO.2023.04.061>.
- [224] Y. Xie, H. Zhang, F. Zhou, Improvement in geometrical accuracy and mechanical property for arc-based additive manufacturing using metamorphic rolling mechanism, *J. Manuf. Sci. Eng.* 138 (2016), <https://doi.org/10.1115/1.4032079>.
- [225] X. Zhou, H. Zhang, G. Wang, X. Bai, Y. Fu, J. Zhao, Simulation of microstructure evolution during hybrid deposition and micro-rolling process, *J. Mater. Sci.* 51 (2016) 6735–6749, <https://doi.org/10.1007/s10853-016-9961-0>.
- [226] H. Zhang, X. Wang, G. Wang, Y. Zhang, Hybrid direct manufacturing method of metallic parts using deposition and micro continuous rolling, *Rapid Prototyp. J.* 19 (2013) 387–394, <https://doi.org/10.1108/RPJ-01-2012-0006>.
- [227] H. Ko, S.K. Moon, J. Hwang, Design for additive manufacturing in customized products, *Int. J. Precis. Eng. Manuf.* 16 (2015) 2369–2375, <https://doi.org/10.1007/s12541-015-0305-9>.
- [228] R. Liu, Z. Wang, T. Sparks, F. Liou, J. Newkirk, Aerospace applications of laser additive manufacturing, *Laser Additive Manuf.: Mater., Des., Technol. Appl.* (2017) 351–371, <https://doi.org/10.1016/B978-0-08-100433-3.00013-0>.
- [229] N.C.Y. Yeo, H. Pepin, S.S. Yang, Revolutionizing technology adoption for the remanufacturing industry, *Procedia CIRP* 61 (2017) 17–21, <https://doi.org/10.1016/J.PROCIR.2016.11.262>.
- [230] P. Kashyap, Industrial applications of machine learning, in: P. Kashyap (Ed.), *Machine Learning for Decision Makers: Cognitive Computing Fundamentals for Better Decision Making*, Apress, Berkeley, CA, 2017, pp. 189–233, https://doi.org/10.1007/978-1-4842-2988-0_5.
- [231] R. French, M. Benakis, H. Marin-Reyes, Process monitoring and industrial informatics for online optimization of Welding Procedure specifications (WPS) in Gas Tungsten Arc Welding (GTAW) – Industry 4.0 for robotic additive remanufacturing of aeroengine components, in: In: 2018 3rd International Conference on Advanced Robotics and Mechatronics (ICARM), 2018, pp. 812–817, <https://doi.org/10.1109/ICARM.2018.8610808>.
- [232] J. Francis, L. Bian, Deep learning for distortion prediction in laser-based additive manufacturing using big data, *Manuf. Lett.* 20 (2019) 10–14, <https://doi.org/10.1016/J.MFGLT.2019.02.001>.